



저작자표시-비영리-변경금지 2.0 대한민국

이용자는 아래의 조건을 따르는 경우에 한하여 자유롭게

- 이 저작물을 복제, 배포, 전송, 전시, 공연 및 방송할 수 있습니다.

다음과 같은 조건을 따라야 합니다:



저작자표시. 귀하는 원저작자를 표시하여야 합니다.



비영리. 귀하는 이 저작물을 영리 목적으로 이용할 수 없습니다.



변경금지. 귀하는 이 저작물을 개작, 변형 또는 가공할 수 없습니다.

- 귀하는, 이 저작물의 재이용이나 배포의 경우, 이 저작물에 적용된 이용허락조건을 명확하게 나타내어야 합니다.
- 저작권자로부터 별도의 허가를 받으면 이러한 조건들은 적용되지 않습니다.

저작권법에 따른 이용자의 권리는 위의 내용에 의하여 영향을 받지 않습니다.

이것은 [이용허락규약\(Legal Code\)](#)을 이해하기 쉽게 요약한 것입니다.

[Disclaimer](#)

**Doctor of Philosophy**

**A study on controlled combustion strategies of Propane-Diesel dual fuel  
engine using rapid compression expansion machine**

**The Graduate School  
of the University of Ulsan  
Department of Mechanical Engineering  
Ardhika Setiawan**

**A study on controlled combustion strategies of Propane-Diesel dual fuel  
engine using rapid compression expansion machine**

**Supervisor: Prof. Ocktaeck Lim**

**A Dissertation**

**Submitted to**

**The Graduate School of the University of Ulsan**

**In partial Fulfillment of the Requirements**

**for the Degree of**

**Doctor of Philosophy**

**by**

**Ardhika Setiawan**


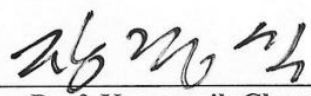
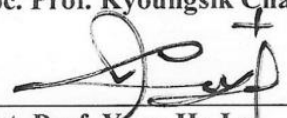
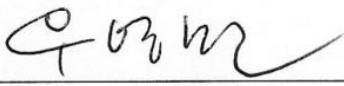

**Department of Mechanical Engineering**

**University of Ulsan, Republic of Korea**

**June 2024**

# A study on controlled combustion strategies of Propane-Diesel dual fuel engine using rapid compression expansion machine

This certifies that the dissertation of Ardhika Setiawan is approved.

Committee Chair	 Prof. Kyu Yeol Park
Committee Member	 Assoc. Prof. Kyoungsik Chang
Committee Member	 Assist. Prof. Yoon Ho Lee
Committee Member	 Dr. Youngmin Woo
Committee Member	 Prof. Ocktaeck Lim

Department of Mechanical Engineering  
University of Ulsan, Republic of Korea

June 2024

## ABSTRACT

### **A study on controlled combustion strategies of Propane-Diesel dual fuel engine using rapid compression expansion machine**

**Department of Mechanical Engineering  
Ardhika Setiawan**

A direct injection strategy on compression ignition is considered to achieve higher performance and produce lower pollutant emissions due to a higher volumetric efficiency compared to intake manifold injection. Applying the DI strategy on compressed gas fuel such as propane gives a better advantage due to the lower boiling temperature of the fuel, as it improves the atomization characteristics and reduces the possibility of pressure-temperature reduction compared to when the fuel is injected at the intake manifold. Propane itself is one of the promising alternative fuels for internal combustion engines as it contains a higher calorific value and produces cleaner combustion compared to diesel and gasoline. This characteristic of fuel makes it possible to apply lean combustion strategies where the excess of air in a lean-burn engine emits far fewer hydrocarbons. The experimental setup has been modified to be sufficient for dual direct injection; Propane and diesel as the ignition assistant. The validated model CFD was applied to study the combustion and emission of propane as well as the spatial distribution of propane in the research engine. The objective of this study was to analyze the combustion characteristics and emissions of Propane and find the optimum parameter to achieve the best emissions and performance. The results show that the reactive combustion state of propane increases the mean temperature in the premix combustion phase significantly. This phenomenon occurs due to the flame produced by propane developing much faster compared to diesel. Consequently, it increases the MPRR and peak pressure during combustion. However, it produces higher HRR at the mixing-controlled combustion phase as the fraction of the propane increases. It causes longer burn duration and reduces combustion efficiency. Compared to diesel, propane produces fewer particulates. The fluctuation of CO/CO<sub>2</sub> shows the indication of better combustion performance when propane up to 50% was applied. The lower CO<sub>2</sub> emission on the other propane energy fraction indicates the incapability to burn the fuel efficiently during the combustion process. An increase in the propane energy fraction indicates a rise in NO<sub>x</sub> when the LPG-Di was applied at CR 19. The auto-ignition resistance of propane makes a longer NO<sub>x</sub> formation compared to diesel. A higher propane energy fraction shows the indication of soot reduction. However, propane shows high auto-ignition resistance when 0° and 40°BTDC were applied. Consequently, significant soot emission was produced.

Keywords: RCEM; dual direct injection; compression ignition; in-cylinder performance; direct injection; propane; emission.

# TABLE OF CONTENT

ABSTRACT .....	iii
TABLE OF CONTENT.....	iv
LIST OF FIGURES .....	vii
LIST OF TABLES .....	x
ACKNOWLEDGEMENT .....	xi
NOMENCLATURES.....	xii
<b>1. INTRODUCTION</b> .....	<b>1</b>
<b>1.1 Background</b> .....	<b>1</b>
1.1.1 Compression ignition engine for lean injection strategy .....	1
1.1.2 Direct injection .....	2
1.1.3 Propane as a low-carbon Fuel.....	4
1.1.4 Propane economic value .....	5
<b>1.2 Challenge for propane auto ignition</b> .....	<b>6</b>
<b>1.3 Objective of the study</b> .....	<b>7</b>
<b>1.4 Scope of the study</b> .....	<b>8</b>
<b>1.5 Thesis outline</b> .....	<b>9</b>
<b>2. LITERATURE REVIEW</b> .....	<b>11</b>
<b>2.1 Low-carbon combustion of LPG as the alternative fuel</b> .....	<b>11</b>
<b>2.2 Propane direct injection strategy</b> .....	<b>12</b>
<b>2.3 Review of previous studies on in-cylinder performance, emission characteristics, and combustion operating parameter optimization</b> .....	<b>14</b>
2.3.1 Review of In-cylinder performance on LPG engine.....	15
2.3.2 Review of emission characteristics of LPG engine.....	16
2.3.3 Review of optimization application on internal combustion parameter .....	19
<b>2.4 Summary</b> .....	<b>22</b>
<b>3. RESEARCH METHODOLOGY</b> .....	<b>24</b>
<b>3.1 Experimental setup</b> .....	<b>24</b>
3.1.1 RCEM with a dual fuel direct injection system .....	24
3.1.2 Fuel system. ....	26

3.1.3	Fuel preparation.....	27
3.1.4	Accuracy of measurements and uncertainty .....	29
3.2	Governing equation .....	30
3.3	CFD modeling and simulation .....	31
3.4	Test procedure.....	35
3.5	Model validation.....	36
3.6	Summary.....	37
4.	<b>INVESTIGATION OF THE COMBUSTION CHARACTERISTICS OF A DUAL DIRECT INJECTION FUEL (DIESEL-PROPANE) STRATEGY ON A RAPID COMPRESSION EXPANSION MACHINE</b>	<b>38</b>
4.1	Combustion performance.....	38
4.1.1	Cycle Analysis.....	38
4.1.2	Combustion duration.....	48
4.2	In-cylinder Temperature distribution .....	51
4.3	Flow analysis.....	52
4.3.1	Turbulent kinetic energy.....	52
4.3.2	Turbulent kinetic viscosity .....	55
4.4	Conclusion	56
5.	<b>AN INVESTIGATION OF THE EFFECT OF PROPANE ENERGY FRACTION AND THE START OF INJECTION ON THE COMBUSTION AND EMISSIONS CHARACTERISTICS OF LOW CARBON HIGH-PRESSURE LPG DIRECT INJECTION ENGINE</b>	<b>58</b>
5.1	Validation of the CFD modeling on combustion characteristics .....	58
5.2	Effect of energy fraction and SOI of propane on the emissions of a CI engine ....	64
5.2.1	Carbon monoxide emissions (CO).....	64
5.2.2	Carbon dioxide emissions (CO <sub>2</sub> ) .....	67
5.2.3	Hydrocarbon emissions (HC).....	70
5.2.4	Nitrogen oxides emissions (NO <sub>x</sub> ) .....	71
5.2.5	Soot emissions.....	72
5.3	Conclusion. ....	73
6.	<b>Combustion characteristic prediction of dual direct injection fuel (diesel-propane) on RCEM based on an artificial neural network approach.</b>	<b>75</b>
6.1	CFD modeling and Artificial neural network construction .....	75

6.1.1	CFD modeling .....	75
6.1.2	ANN construction.....	77
<b>6.2</b>	<b>Data generation for artificial neural network optimized.....</b>	<b>83</b>
6.2.1	Regression modelling .....	83
<b>6.3</b>	<b>Input data parameter .....</b>	<b>85</b>
<b>6.4</b>	<b>Optimization of in-cylinder combustion, performance and emission using genetic algorithm .....</b>	<b>91</b>
6.4.1	Optimization of engine power based on the ITE and SoC .....	91
6.4.2	Optimization of engine power based on the ITE and CO .....	92
6.4.3	Optimization of engine power based on the CO and NO <sub>x</sub> .....	93
6.4.4	Optimization of ITE based on the burn duration and SOC .....	94
<b>6.5</b>	<b>Evaluation of ANN results.....</b>	<b>95</b>
<b>6.6</b>	<b>Comparing experimental result and discussion in ANN modeling .....</b>	<b>98</b>
6.5.1	In-cylinder pressure.....	98
6.5.2	In-cylinder temperature.....	99
<b>6.6</b>	<b>Conclusion. ....</b>	<b>103</b>
<b>7.</b>	<b>CONCLUSION AND CONTRIBUTION</b>	<b>105</b>
	<b>REFERENCES</b>	<b>108</b>



## LIST OF FIGURES

Figure 1.1	Comparison of BSFC between Base Models and Different Compression Ratio for CNG Direct Injection Engine [9].....	3
Figure 1.2	Flowcharts of the strategies to investigate the combustion and emission characteristics of dual direct injection fuel (diesel-propane) on compression ignition engine through experimental and simulation approach.....	8
Figure 2.1	PM and PN concentration from diesel and LPDi vehicle under WHVC mode [25].....	12
Figure 2.2	The direct injection setup for LPG fuel; a) spark ignition [34]. b) dual direct injection compression ignition [current study] .....	14
Figure 2.3	Covariance of indicated mean effective pressure ( $COV_{IMEP}$ ), maximum pressure rise rate (MPPR), ignition delay, and noise (left) and efficiency performances (right) for all test points. ....	16
Figure 2.4	Comparison of performance and emission results for GDI and LPG-DI at Lean Conditions [52] .....	18
Figure 2.5	Framework of research methodology in ANN genetic algorithm system [62]. ....	20
Figure 3.1	The schematic diagram of the RCEM.....	25
Figure 3.2	A schematic of the fuel system: a) diesel fuel system and b) propane fuel system. ....	27
Figure 3.3	The schematic of the fuel measuring system. ....	29
Figure 3.4	The schematic diagram of RCEM for CFD investigation. ....	33
Figure 3.5	Validation of CFD modeling based on in-cylinder pressure of RCEM.....	36
Figure 4.1	Identification of the combustion phase. ....	39
Figure 4.2	In-cylinder pressure for propane energy fractions of 10-100% for propane injection timings of 0o-40o BTDC and compression ratios of a) 17 and b) 19. ....	41
Figure 4.3	HRR under propane energy fractions of 10-100% for propane injection timings of 0°-40°BTDC and compression ratios of a) 17 and b) 19. ....	42
Figure 4.4	In-cylinder temperature under propane energy fractions of 10-100% for propane injection timings of 0°-40°BTDC and compression ratios of a) 17 and b) 19. ....	43
Figure 4.5	PRR under a propane energy fraction of 50% for propane injection timings of 0°-40°BTDC and compression ratios of a) 17 and b) 19.....	45
Figure 4.6	SoC of dual direct injection fuel under different propane energy fractions, SOI of propane, and CRs of a) 17 and b) 19.....	46
Figure 4.7	Torque, brake power, and indicated power. ....	47
Figure 4.8	Combustion duration. ....	48
Figure 4.9	Indicated thermal efficiency. ....	50
Figure 4.10	Temperature distribution. ....	51
Figure 4.11	Streamline flow visualization from the TKE flow pattern of dual direct injection fuel (diesel-propane) at CR 19, a propane energy fraction of 50%, and propane injection timings from 0°-40°BTDC. ....	54

Figure 4.12	Streamline flow visualization from the TKE flow pattern of dual direct injection fuel (diesel-propane) at CR 19, a propane energy fraction of 50%, and propane injection timings from 0°-40°BTDC. ....	54
Figure 4.13	Turbulent kinetic viscosity.....	55
Figure 5.1	In-cylinder pressure (a) and max in-cylinder pressure (b) of dual direct injection fuel (diesel-propane) under 10%-100% energy fraction and 0°-40°BTDC SOI of propane. ....	59
Figure 5.2	HRR of dual direct injection fuel (diesel-propane) under 10%-100% energy fraction and 0°-40°BTDC SOI of propane.....	61
Figure 5.3	Mean temperature (a) and max in-cylinder temperature (b) of dual direct injection fuel (diesel-propane) under 10%-100% energy fraction and 0°-40°BTDC SOI of propane. ....	63
Figure 5.4	Total CO emission (a) and CO emission (b) of dual direct injection fuel (diesel-propane) under 10%-100% energy fraction and 0°-40°BTDC SOI of propane. ....	65
Figure 5.5	OH formation at PD 50, SOI of propane 0° to 40° BTDC under dual direct injection fuel strategy. ....	66
Figure 5.6	Total CO <sub>2</sub> emission (a) and CO <sub>2</sub> emission (b) of dual direct injection fuel (diesel-propane) under 10%-100% energy fraction and 0°-40°BTDC SOI of propane. ....	67
Figure 5.7	O <sub>2</sub> consumption at PD 50, SOI of propane 0° to 40° BTDC under dual direct injection fuel strategy. ....	68
Figure 5.8	Total HC emission (a) and HC emission (b) of dual direct injection fuel (diesel-propane) under 10%-100% energy fraction and 0°-40°BTDC SOI of propane. ....	70
Figure 5.9	Total NO <sub>x</sub> emission (a) and NO <sub>x</sub> emission (b) of dual direct injection fuel (diesel-propane) under 10%-100% energy fraction and 0°-40°BTDC SOI of propane. ....	71
Figure 5.10	Total soot emission (a) and soot emission (b) of dual direct injection fuel (diesel-propane) under 10%-100% energy fraction and 0°-40°BTDC SOI of propane. ....	72
Figure 6.1	Schematic Diagram of RCEM for CFD investigation .....	76
Figure 6.2	Flow chart of the study.....	78
Figure 6.3	Representation of a model neuron.....	80
Figure 6.4	Artificial neural network structure for RCEM.....	81
Figure 6.5	In-cylinder pressure under propane energy fraction 10-100%, Propane injection timing 0o-40o BTDC and compression ratio of: a) 17 and b) 19.....	85
Figure 6.6	In-cylinder temperature under propane energy fraction 10-100%, propane injection timing 0o-40o BTDC and compression ratio of: a) 17 and b) 19.....	86
Figure 6.7	TKE flow pattern of dual direct injection fuel (diesel-propane) at CR 19, propane energy fraction 50% and propane injection timing 0°-40°BTDC. ....	88
Figure 6.8	Power of RCEM for variations in CR, propane energy fraction, and SOI of propane. ....	89
Figure 6.9	Thermal efficiency of RCEM under variation of CR, propane energy fraction and SOI of propane. ....	90
Figure 6.10	Pareto front for optimization considering SoC and ITE .....	92
Figure 6.11	Pareto front for optimization considering ITE and CO .....	93

<b>Figure 6.12</b>	<b>Pareto front for optimization considering CO and NO<sub>x</sub>.....</b>	<b>94</b>
<b>Figure 6.13</b>	<b>Validation MSE and R values for different neuron numbers in the hidden layer. ....</b>	<b>96</b>
<b>Figure 6.14</b>	<b>Plot of regression value of ANN performance for testing data prediction in 5 representative parameters.....</b>	<b>97</b>
<b>Figure 6.15</b>	<b>Plot of in-cylinder temperature of experiment, simulation and ANN prediction. ....</b>	<b>99</b>
<b>Figure 6.16</b>	<b>Plot of in-cylinder temperature of RCEM's experiment, simulation and ANN prediction data. ....</b>	<b>100</b>
<b>Figure 6.17</b>	<b>Plot of power of RCEM experiments, simulation and ANN prediction data. ....</b>	<b>101</b>
<b>Figure 6.18</b>	<b>Plot of ITE of RCEM for experiment, simulation and ANN prediction data.....</b>	<b>102</b>
<b>Figure 6.19</b>	<b>Plot of TKE of RCEM's experiment, simulations, and ANN prediction data. ....</b>	<b>103</b>

## LIST OF TABLES

Table 1.1 Energy-related parameters. LPG: Liquefied Petroleum Gas [27].	4
Table 1.2 The average cost of fuel per 100km by European country (2022 1st quarter) [31]	5
Table 1.3 Thesis Outline	10
Table 2.1 Various ANN method for CI engine responses prediction	21
Table 3.1 Engine specification	26
Table 3.2 Properties of fuels [23]	28
Table 3.3 Uncertainty of measured parameters	30
Table 3.4 CONVERGE modeling used in this study	33
Table 3.5 Simulation initial and boundary conditions	34
Table 3.6 Experimental conditions	36
Table 6.1 CFD parameter input	77
Table 6.2 Particulars of the neural network [39].	82
Table 6.3 Symbol used in modelling for the variables in the regression formulas	84
Table 6.4. Regression model	84
Table 6.5 Properties of GA algorithm in Matlab	91
Table 6.6 optimum combination of selected operating parameters	95

## ACKNOWLEDGEMENT

I am sincerely grateful to my advisor, Professor Lim Ocktaeck for giving me the opportunity to study in the Smart Powertrain Laboratory and for his continuous guidance on my research. And also, for his patience, motivations and insightful feedback to help me sharpen my thinking and take my work to the next level. Without his support and encouragement, I would not have been able to complete this dissertation. I would like to express my gratitude to the Graduate School of Mechanical and Automotive Engineering, University of Ulsan and Ministry of Manpower of the Republic of Indonesia for providing me the opportunity, approval, and support to pursue my Ph.D. program.

I feel very fortunate to be a member of the Smart Powertrain Laboratory at University of Ulsan. I would like to thank all my current and former colleagues – Dr. Bambang Wahono, Dr. Yanuandri Putrasari, Dr. M.K Aditya Wardana, and Dr. Windarto, and all laboratory members for the many fond memories we have spent together and their valuable support during my research. This work could only be realized thanks to their unconditional help and honest feedback.

I would like to thank the sponsors of the research: National Research Foundation of Korea, Regional Innovation Strategy (RIS), Hyundai Heavy Industries Co., Ltd., and the University of Ulsan.

My special thanks go to my lovely mother, my wife Mentari Mekar Sari, and my daughters, Aileen and Arsy. Without their unwavering support, I would not have been able to complete this important journey in my life. This dissertation is dedicated to them.

Finally, I would like to thank the members of my dissertation committee for their time and valuable comments to improve the quality of this work.

This dissertation contains all of the research conducted during the doctoral studies. The entire content of this thesis was written to partially fulfill the requirements of the PhD of Science in Mechanical and Automotive Engineering at the University of Ulsan.

## NOMENCLATURES

SI-engine	: Spark ignition engine
CI-engine	: Combustion ignition engine
TDC	: Top dead center
BTDC	: Before top dead center
ATDC	: After top dead center
ITE	: Indicated thermal efficiency, (%)
HRR	: Heat release rate, (j/deg)
HC	: Hydrocarbon
PM	: Particulate matter
THC	: Total hydrocarbon emissions
CA	: Crank angle, deg
$Q_h$	: Total fuel heat input ,(W)
SOI	: Start of injection
$\phi$	: Equivalence ratio
$\alpha$	: Crank angle, (deg)
$\alpha_0$	: Start of combustion, (deg)
$\Delta\alpha_c$	: Combustion duration, (deg)
$T_c$	: Combustion gas temperature, (K)

$K$	: Ratio of specific heats (-)
$Q_{\text{released, eff}}$	: Effective release energy (kJ)
$Q_{\text{released}}$	: Release energy (kJ)
$V_D$	: Displacement volume, ( $\text{m}^3$ )
$r$	: Compression ratio (-)
$P_c$	: Cylinder pressure (Pa)
$R$	: Gas constant ( $\text{J}/(\text{kmol}\cdot\text{K})$ )
$m_{\text{air}}$	: Air mass flow [ $\text{kg}/\text{s}$ ]
AFR	: Air-fuel ratio (-)
$n$	: Engine speed (rpm)
$T_{\text{eff}}$	: Engine effective torque, (Nm)

# 1. INTRODUCTION

## 1.1 Background

### 1.1.1 Compression ignition engine for lean injection strategy

Concerns about environmental pollution arising from the use of petroleum-based fuels in automobiles, and moving to alternative fuels will become necessary as petroleum-based fuels become less readily available in the future [1]. The reserves are being depleted and air pollution has increased as a result of excessive use of fossil fuels. These issues raise awareness of the efficient use of current resources and the gradual transition to environmentally friendly alternative fuels [2]. Utilizing gaseous fuels in the compression ignition (CI) engine in addition to liquid diesel is one approach to address these issues. The CI engine heats the air in the engine cylinder more efficiently than a dual spark injection (SI) engine because of its higher compression ratio [3][4][5]. Worldwide, CI engines, which are mainly found in trucks and buses, are the primary means of moving freight. However, because diesel is the primary fuel, it is well known for producing air pollution due to its high levels of nitrogen oxides (NO<sub>x</sub>) and suspended particulate matter (SPM). Both acute and long-term health issues are brought on by these air pollutants. By 2040, the worldwide abolition of emissions linked to diesel-related air pollutants may avert roughly 174,000 premature deaths [5]. As a matter of fact, on-road diesel vehicles emit a variety of air pollutants; NO<sub>x</sub>, for instance, makes up 20% of anthropogenic emissions [6]. It should come as no surprise that diesel car air pollution is worse in cities with heavy traffic.

In the pursuit of cleaner and more efficient combustion engines, researchers and engineers are exploring innovative strategies to improve the performance of compression ignition engines. One such approach gaining traction is lean combustion, which involves burning fuel with an excess of air [7]. Lean combustion entails operating an engine with a higher air-to-fuel ratio than stoichiometric combustion, where the air-fuel mixture contains exactly enough oxygen for complete combustion. By introducing excess air, lean combustion promotes more complete fuel oxidation, leading to reduced emissions of pollutants such as nitrogen oxides (NO<sub>x</sub>) and particulate matter (PM). Lean combustion significantly decreases NO<sub>x</sub> emissions due to lower combustion temperatures and reduces PM emissions by promoting more complete combustion. The leaner air-fuel mixture in compression ignition engines can enhance thermal efficiency by optimizing combustion characteristics and reducing heat losses. Finally, it allows for greater flexibility in fuel

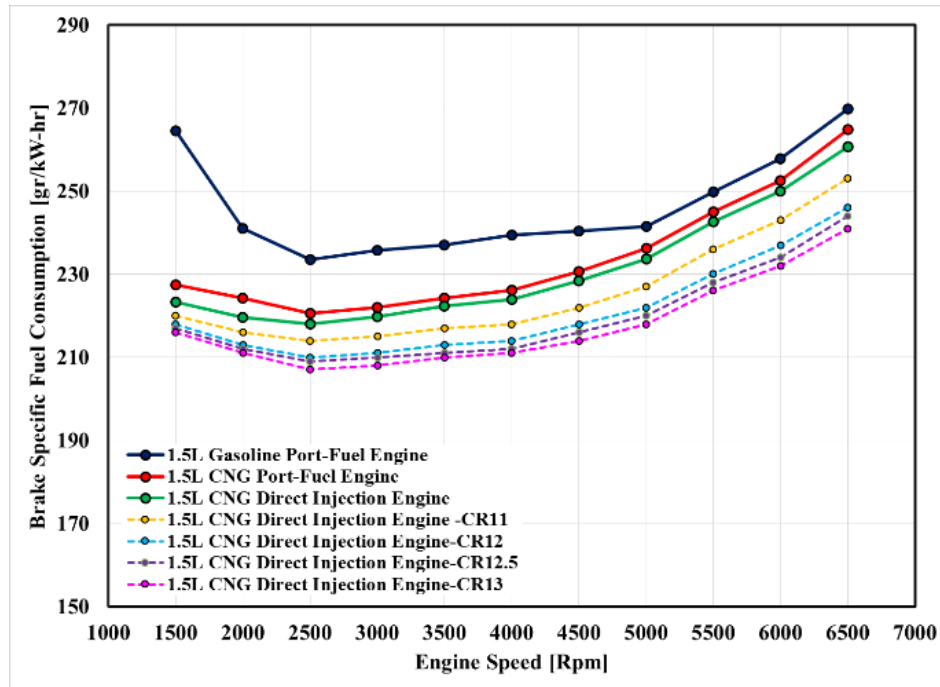


selection, enabling the use of alternative fuels with varying properties, such as natural gas, hydrogen, and biofuels [8]. While lean combustion offers several advantages, its implementation in compression ignition engines presents certain challenges. Lean mixtures can be prone to combustion instability, leading to issues such as misfires and combustion knock, increasing the risk of engine damage, particularly to components such as exhaust after-treatment systems and turbochargers. Controlling emissions of nitrogen oxides (NO<sub>x</sub>) and unburned hydrocarbons (UHC) remains challenging under lean combustion conditions, necessitating advanced after-treatment technologies [8].

### **1.1.2 Direct injection**

Direct injection (DI) and intake manifold injection (IMI) are two primary fuel delivery systems used in internal combustion engines, each with its own set of advantages and limitations. In recent years, direct injection has gained prominence due to its superior performance and efficiency compared to intake manifold injection. Direct injection offers superior combustion efficiency and fuel consumption [9] by precisely delivering fuel directly into the combustion chamber. This allows for better fuel atomization and mixing with air, resulting in more complete combustion [10]. Research by Zhang et al. (2020) demonstrated that direct injection strategies improve combustion efficiency in compression ignition engines, leading to enhanced fuel economy and reduced emissions [11]. One of the key advantages of direct injection is its ability to control injection timing and fuel stratification within the combustion chamber. This enables optimized combustion processes tailored to specific operating conditions, such as load and speed [12]. Peng et al. (2022) found that direct injection strategies offer greater flexibility in adjusting fuel-air mixture properties, resulting in improved thermal efficiency and reduced emissions [13]. Direct injection minimizes heat losses associated with fuel vaporization on intake valves and cylinder walls, leading to improved overall engine efficiency [14]. Hariram et al. (2015) investigated the impact of direct injection on heat transfer in compression ignition engines and concluded that direct injection reduces heat losses compared to intake manifold injection, resulting in higher thermal efficiency [15]. Direct injection contributes to lower emissions of pollutants such as nitrogen oxides (NO<sub>x</sub>) and particulate matter (PM) by promoting more complete combustion and minimizing fuel-rich zones within the combustion chamber [16]. Tan et al. (2023) conducted a study on the emissions

reduction potential of direct injection in compression ignition engines and found significant reductions in NO<sub>x</sub> and PM emissions compared to intake manifold injection [17].



**Figure 1.1** Comparison of BSFC between Base Models and Different Compression Ratio for CNG Direct Injection Engine [9].

Numerous studies have shown that using LPG as an alternative fuel produces positive emissions results. Compared to vehicles powered by conventional fuel, LPG vehicles have substantially fewer emissions [18]. According to Snelgrove et al. [19] an LPG-operated vehicle reported 40% lower hydrocarbon (HC), 60% lower carbon monoxide (CO), and substantially reduced carbon dioxide (CO<sub>2</sub>) emissions over the European Test Cycle at 25°C. Furthermore, due to its lower carbon content compared to gasoline, LPG emits almost no particulate matter and very little NO<sub>x</sub> [20]. Keunsoo Kim et al. investigate the emission of LPG using a direct injection strategy on an SI engine. They found that a significant reduction of particulate matter emissions by the spray-guided LPG homogeneous stoichiometric combustion was achieved for all engine conditions. LPG reduced particulate matter emissions due to its simple molecular structure and low carbon contents with stoichiometric combustion [21]. Sungha Baek et al. compared diesel applied to a CI engine to LPG-DI on an SI engine. They claimed that diesel emits 3.6 times as much CO<sub>2</sub>-equivalent N<sub>2</sub>O and CH<sub>4</sub> emissions compared to the LPG [22]. Windarto et al. applied

100% propane DI on an SI engine compared to diesel. In his investigation, he found that propane produces lower HC, CO, CO<sub>2</sub>, and NO<sub>x</sub> than diesel. However, diesel has a thermal efficiency 14.26% higher than propane. The propane fuel achieved an improved engine-indicated thermal efficiency and slightly higher brake-specific fuel consumption with the advancing of spark duration [23]. Numerous researchers have examined the effects of LPG-DI on SI engines. However, the investigation of LPG-DI on CI engines is very rare to be found.

### 1.1.3 Propane as a low-carbon Fuel

Earth gets warmer due to greenhouse gas trapping heat. Almost all of the rise in greenhouse gases in the atmosphere over the past 150 years is attributable to human activity [24]. Burning fossil fuels for transportation, heat, and electricity is the main human activity-related source of greenhouse gas emissions in the United States. The main human activity contributing to climate change is the burning of carbon-based fuels, which mainly include coal, oil, natural gas, and so forth [25]. The hydrocarbons propane (C<sub>3</sub>H<sub>8</sub>) and butane (C<sub>4</sub>H<sub>10</sub>) make up the majority of the light hydrocarbon mixture in LPG, which is significantly less carbon content than that of petrol (C<sub>8</sub>H<sub>18</sub>) and diesel fuel (C<sub>10</sub>H<sub>20</sub> to C<sub>15</sub>H<sub>28</sub>). When LPG is burned, a gallon produces 12.52 pounds (5,680 grams) of CO<sub>2</sub>, while a mile driven on average produces 319 grams of CO<sub>2</sub>. It has many positive environmental effects and fights climate change, but its source needs to be taken into account. LPG cars release fewer nitrogen oxides, which are a major cause of smog, than diesel and gasoline cars [26].

**Table 1.1** Energy-related parameters. LPG: Liquefied Petroleum Gas [27].

Energy Source	Average Low Calorific Value (KJ/kg, KJ/m <sup>3</sup> )	Carbon Emission Coefficient (kgC/GJ)	Carbon Oxidation Factor
Coal	20,908.00	26.36	0.93
Petrol	43,070.00	18.90	0.98
Kerosene	43,070.00	19.60	0.98

<b>Energy Source</b>	<b>Average Low Calorific Value (KJ/kg, KJ/m<sup>3</sup>)</b>	<b>Carbon Emission Coefficient (kgC/GJ)</b>	<b>Carbon Oxidation Factor</b>
Diesel	42,652.00	20.20	0.98
Fuel Oil	41,816.00	21.10	0.98
LPG	50,179.00	17.20	0.98
Natural Gas	38,931.00	15.30	0.99

#### 1.1.4 Propane economic value

The best option for medium- to large-sized ships right now is LNG, which may also help with the transition to commercialized zero-carbon ships given the current state of economic viability, legal and regulatory frameworks, and technology. LNG is the alternative shipping fuel that has received the most research attention and has seen a significant increase in use in recent years [28]. In contrast, liquefied petroleum gas (LPG) was discovered to be at least as appealing as LNG due to its reduced investment costs, shorter payback periods, and decreased susceptibility to changes in fuel prices [29]. Furthermore, unlike modern shipping fuels like heavy fuel oil (HFO), LPG has very similar emission advantages to LNG without imposing size restrictions on ships, and it doesn't produce marine pollutants when it leaks. [30]. In contrast to other traditional petroleum fuels, LPG is regarded as a more affordable and superior energy substitute. In the meantime, hydrogen, an alternative fuel, is twice as expensive as LPG while having a higher energy content. Table 1 shows the comparison of fuel in the Europe country in 2022.

**Table 1.2** The average cost of fuel per 100km by European country (2022 1st quarter) [31]

<b>Member State</b>	<b>Electricity</b>	<b>Petrol 95 E10</b>	<b>Diesel B7</b>	<b>CNG</b>	<b>LPG</b>	<b>Hydrogen</b>
Belgium	4.60 €	10.10 €	8.80 €	6.40 €	4.90 €	9.00 €

Cyprus	3.83 €	9.88 €	8.58 €	n.a.	n.a.	n.a.
Denmark	8.59 €	10.76 €	8.27 €	n.a.	n.a.	13.45 €
Finland	3.96 €	10.75 €	10.90 €	7.21 €	6.48 €*	n.a.
France	2.90 €	9.30 €	7.00 €	6.00 €	6.60 €	11.30 €
Germany	5.84 €	11.74 €	9.05 €	6.48 €	6.63 €	7.6 €
Italy	n.a.	10.66 €	7.91 €	7.46 €	6.10 €	n.a.
Luxembourg	3.12 €	9.76 €	8.78 €	6.31 €	6.28 €	n.a.
Netherlands	5.31 €	12.32 €	8.66 €	7.52 €	7.78 €	10.89 €
Norway	n.a.	12.86 €	9.70 €	n.a.	n.a.	n.a.
Poland	5.31 €	8.63 €	6.71 €	5.23 €	4.70 €	n.a.
Sweden	3.48 €	12.54 €	13.06 €	12.51 €	n.a.	15.06 €

## 1.2 Challenge for propane auto ignition

The utilization of propane as an alternative fuel in compression ignition engines presents promising opportunities for reducing emissions and diversifying the energy sources in the transportation sector. However, several challenges need to be addressed to realize the full potential of propane in compression ignition engines. Propane has different autoignition characteristics compared to diesel fuel, including higher octane rating and lower cetane number. These differences can pose challenges in achieving optimal combustion timing and stability in compression ignition engines [32]. Adapting the fuel injection system of compression ignition engines to accommodate propane presents technical challenges. Propane requires different injection strategies, injector designs, and fuel delivery systems compared to diesel fuel, necessitating modifications to existing engine components [33]. Achieving stable combustion with propane in compression ignition engines can be challenging due to its lower energy density and slower combustion rate compared

to diesel fuel. Maintaining proper air-fuel mixing and ignition timing is crucial to prevent issues such as incomplete combustion, misfires, and combustion instability [34]. Cold starting presents challenges for propane compression ignition engines, particularly in cold climates. Propane's lower vapor pressure at low temperatures can hinder fuel atomization and combustion efficiency during engine startup, leading to prolonged cranking times and increased emissions [35].

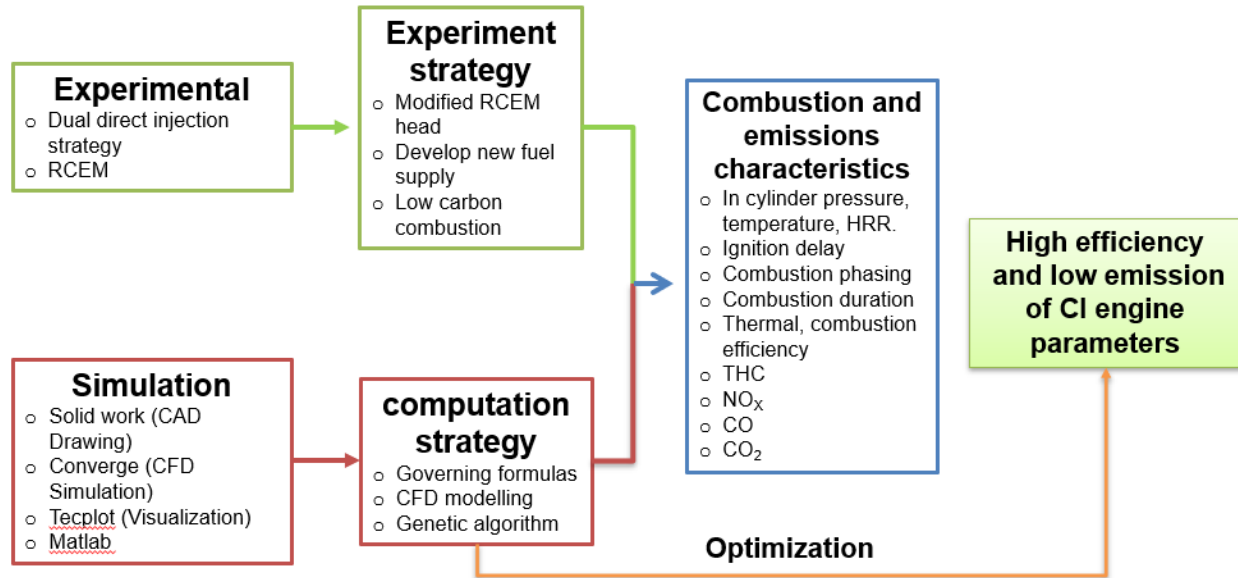
### **1.3 Objective of the study**

This study focuses on the combination of experimental and simulation methods to investigate the effect of compression ratio, energy fraction, and Start of injection (SOI) of propane applied on dual direct injection engine on the compression ignition engine performance and emission characteristics on propane fuel combustion.

The objectives of this study are given below:

- (i) Set up an experimental system to provide the basic information to validate the simulation model. The basic data are in-cylinder pressure, heat release rate, mean and maximum in-cylinder temperature, and efficiency.
- (ii) Setup a simulation model base on Converge software to estimate the engine performance and engine emission characteristics with the various energy fractions, SOI of propane, and engine compression ratio.
- (iii) To study the fundamental propane injection auto-ignition characteristics and the effect of propane direct injection on the diesel auto ignition performance
- (iv) To develop a better understanding of the energy fraction, SOI of propane and compression ratio to achieve the optimum performance.
- (v) To optimize the operating parameter of compression ratio, energy fraction and SOI of propane on the performance and emission characteristics.

To obtain the above targets, the brief explanation in the effect flowchart as seen in Figure 1.2.



**Figure 1.2** Flowcharts of the strategies to investigate the combustion and emission characteristics of dual direct injection fuel (diesel-propane) on compression ignition engine through experimental and simulation approach

### 1.4 Scope of the study

In the efforts to provide a good accuracy method to control combustion duration, prediction of exhaust residual gas and to determine optimal parameters to improve engine efficiency and engine emission. This method also helps to eliminate the drawback of the experimental method in the scope of research on engine hardware and software optimization.

The scopes of the study include:

- a. Modify the cylinder head of the rapid compression and expansion machine to be sufficient for dual direct injection mechanisms.
- b. Develop a high-pressure propane fuel system for the direct injection requirement.
- c. Injection quantity test comparison between diesel and propane by using different injection timing, duration, and pressure.
- d. RCEM research engine experimental under different operating conditions such as propane energy fraction, start of injection, and compression ratio.

- e. Combustion analysis for experimental works is based on cylinder pressure trace and its derivative parameters, while thermal efficiency was calculated based on fuel consumed during the combustion process.
- f. The simulation validation is taken from the experiments results from rapid compression and expansion machine research engine.
- g. The multi-functions of the simulation model are using CFD Converge version 3.0.
- h. Analysis of regular exhaust emissions such as CO, HC, NO<sub>x</sub>, soot, and CO<sub>2</sub>.
- i. The NO<sub>x</sub>, CO, CO<sub>2</sub>, soot, and HC emissions are used to estimate the engine emission characteristics.
- j. The obtained results may only be valid for the engine used in this study.

## 1.5 Thesis outline

The thesis consists of seven chapters, which are organized into five main sections, as illustrated in Table 1.3. The first section consists of Chapter 1 and Chapter 2. Chapter 1 gives a briefly introduction of thesis general topic area of dual direct injection fuel(diesel-propane) strategy to improve compression ignition engine performance and emission characteristics, explanation how important SOI and propane energy fraction on in-cylinder performance and emission, brief introduction the effective solution which research specific aims and scope of the research. Meanwhile, chapter 2 gives a briefly literature review of the research object most closely related to the work such as: low-carbon combustion of direct-injection propane, dual direct injection fuel (diesel-propane) strategy, in-cylinder performance and emission. A briefly review of familiar previous research that has been done in this area. Highlight the gap of the research on engine optimization that has not been well researched or solved. This gap will be filling up by this thesis work.

The second section is chapter 3, in which detailed descriptions of the research methodology, engine specification, experimental system and simulation model.

The third section consists of chapter 4 and chapter 5. Chapter 4 presents the experiment and simulation results and discussion in detail of engine performance and emission of compression ignition direct injection engines. The SOI and propane energy fraction effect, velocity distribution flow trend, combustion performance will be completely studied. In Chapter 5, the experiment and simulation results and discussion of SOI and propane energy fraction effect on low-carbon



combustion are explored and explained based on the effect of SOI of propane on combustion performance and emissions of CI engines.

The fourth section is chapter 6, which presents the optimization operating parameter of SOI and propane energy fraction effect on the in-cylinder performance and emission.

The final section of this thesis is chapter 7, which comprises the summary of this research, and recommendations to future work research outcomes, along with the additional information in the references and appendices

**Table 1.3** Thesis Outline

Research objectives and literature review	<p><b>Chapter 1. INTRODUCTION</b> Key point: background, challenge, objective, and scope</p> <p><b>Chapter 2. LITERATURE REVIEW</b> Key point: Low carbon fuel, auto ignition characteristics, review on previous study</p>
Research platform	<p><b>Chapter 3. RESEARCH METHODOLOGY</b> Key point: experimental setup and CFD modeling</p>
Research on combustion end emission characteristics	<p><b>Chapter 4. INVESTIGATION OF THE COMBUSTION CHARACTERISTICS OF A DUAL DIRECT INJECTION FUEL (DIESEL-PROPANE) STRATEGY ON A RAPID COMPRESSION EXPANSION MACHINE</b> Key point: compression ratio, SOI, and propane energy fraction on combustion characteristics</p> <p><b>Chapter 5. AN INVESTIGATION OF THE EFFECT OF PROPANE ENERGY FRACTION AND THE START OF INJECTION ON THE COMBUSTION AND EMISSIONS CHARACTERISTICS ON LOW CARBON HIGH-PRESSURE LPG DIRECT INJECTION ENGINE</b> Key point: : compression ratio, SOI, and propane energy fraction on emissions</p>
Research on optimization parameter	<p><b>Chapter 6. OPTIMIZATION OF OPERATING CONDITION OF DUAL DIRECT INJECTION FUEL (DIESEL-PROPANE) ENGINE ON THE PERFORMANCE AND EMISSIONS CHARACTERISTICS</b> Key point: ANN, optimization, validation</p>
Research outcome	<p><b>Chapter 7. SUMMARY AND CONCLUSIONS</b> Key point: Summary and future work</p>

## 2. LITERATURE REVIEW

### 2.1 Low-carbon combustion of LPG as the alternative fuel

Studies of substitute fuels have been conducted as the demands for efficient operation of internal combustion engines [36] and reduction of net CO<sub>2</sub> emissions [37] has increased during the past decade. Various works that involve compression ignition (CI) engines have tested alternative fuels, such as biodiesel [38], liquefied petroleum gas (LPG) [39], ammonia [40], and methanol [41]. Liquefied petroleum gas (LPG) and, more specifically, propane are an attractive substitute fuel for CI machines to reduce carbon emissions due to their lower carbon content than conventional diesel fuels, especially for heavy-duty vehicle applications. Propane is a favorable and environmentally friendly source of energy due to its high octane number [42], sensitivity [43], high compression ratio and boost operation [44], liquid state at low pressure [45], lower fuel cost [46], allowed use of current fuel production and delivery systems [47], lower carbon content [48], and higher H/C ratio than conventional fuels [49]. Propane, ethane, n-butane, propene, isobutane, butene, and a small amount of methane are most of the components of LPG fuel [50]. Typically, LPG is derived from natural gas streams either from oil and gas sources or as a byproduct of processing crude oil at refineries. The extraction location, time of year, and processing method all have a substantial impact on the species composition in LPG fuels. When used as a vehicle fuel, its composition varies greatly from nation to nation, with propane concentrations ranging from over 100% to as low as 50% [46].

In a series of experimental works [51], [52], [53], [54], the use of propane as a fuel leads to a significant reduction in emissions, while the engine performance is comparable to that of diesel. An earlier study by the authors [55] showed the possibilities of deploying propane in high-performance compression ignition machines. Using a single-cylinder research engine, Hodges et al., [56] investigated the impacts of propane energy substitution percentage on diesel-ignited propane dual-fuel low-temperature combustion (DPDFLTC). They found that the maximum propane energy fraction was capped at 90% as a result of excessive cyclic combustion variability ( $COV_{IMEP} \sim 11\%$ ) and the minimum propane energy fraction was capped to 53% due to the onset of engine knock

(MPRR~10.5 bar/deg.). According to Elnajjar et al. [57], engine parameters (maximum in-cylinder pressure, thermal efficiency, maximum rate of pressure rise, and indicated mean effective pressure) play an important role in engine performance. However, different LPG fuel compositions had a direct impact on the combustion noise produced by the engine but little to no impact on its efficiency. Using liquefied petroleum gas in diesel operation, Chakraborty et al. [58] showed how different parametric combinations of input factors strongly influence the combustion parameter (ignition delay), power output, and emissions. Aydin et al. [59] observed how LPG direct injection affected engine emissions and performance parameters towards the end of the air intake phase. Diesel engines can run on liquid or gaseous LPG fuel. It is produced in the intake manifold and atomized in the intake air during the gas phase. The high-pressure pump pressurizes liquefied LPG before it is delivered to the injection nozzle. Comparable PM and PN emissions were emitted with two fueled vehicles, as shown in Figure 2.1. The gravimetric PM emissions were 0.0119 g/km (diesel) and 0.0078 g/km (LPG) [22]. Propane fuel was shown to prolong combustion at low temperatures and to reduce cyclic fluctuations and HC and CO emissions compared to diesel. Consequently, it is crucial to investigate how the use of propane in high-pressure direct-injection engines affects combustion, in-cylinder performance, and emissions.

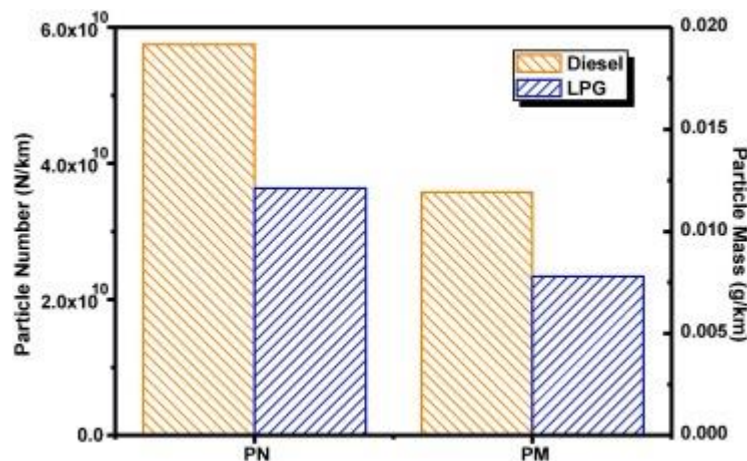
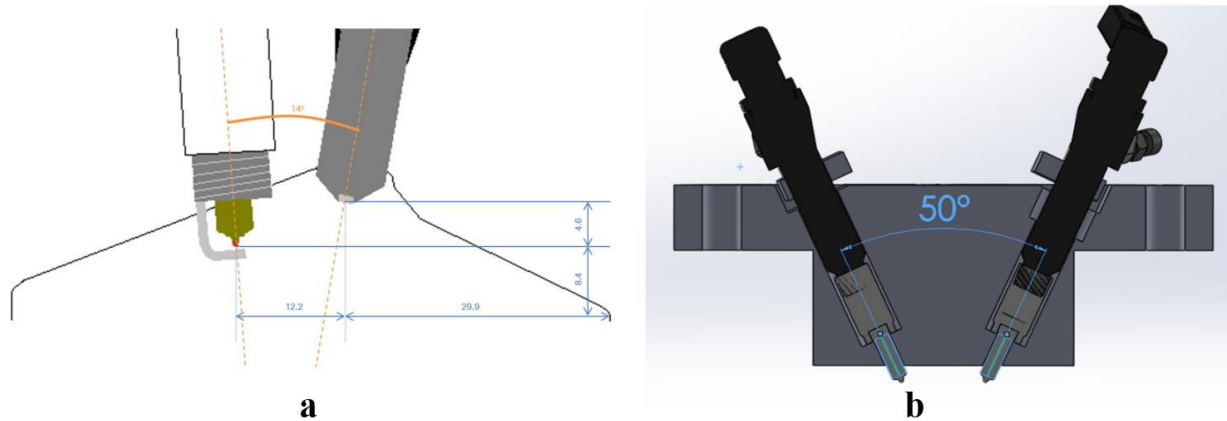


Figure 2.1 PM and PN concentration from diesel and LPDi vehicle under WHVC mode [22].

## 2.2 Propane direct injection strategy

Various kinds of combustion strategies have been proposed to meet the demand for emission regulations and fuel economy. Among them, direct injection that fuel is directly injected into the in-cylinder by high-pressure fuel supply systems, has gained wide attention [60]. Direct-injected fuel can be easily vaporized and then decreased the combustion chamber temperature. This leads to improved volumetric efficiency by increasing the charge density. In this study, the spray-guided injection system was selected. It uses a high-pressure fuel injection positioned near the spark plug, with improved fuel wall-wetting characteristics that exceed all other direct injection methods (e.g., wall-guided, air-guided). The spray-guided direct injection system also enables a well-established air-fuel mixture independent of the surrounding in-cylinder airflow [61]. The gasoline direct injection (GDI) engine test results have been published by several companies and research institutes. The GDI combustion strategies exhibited particulate emissions during operation, making it a challenge for these strategies to meet further future regulations. Therefore, several studies have focused on the reduction of particulate emissions from direct injection engines [62][63][64]. The performance shortcomings of the LPG-PFI system can be substantially measured by the adoption of the state-of-the-art LPG direct injection (LPG-DI) technology. In an LPG-DI engine, as the liquid LPG fuel vaporizes in a very short length of time during the intake stroke, the amount of the homogeneous mixture in the combustion chamber is substantially increased. Therefore, an LPG-DI engine has a better cold start performance than a GDI engine because it does not need excessive enrichment of the air-fuel ratio (A/F) at low coolant temperatures, which plays a key role in limiting the amount of particle formation for the gaseous fuels [65][66][62]. However, there are some technical problems associated with the handling of high pressure LPG over 150 bars in a direct injection system combined with the development of a dedicated engine hardware and engine control unit (ECU) for LPG fuel [67]. Moreover, the high octane number of LPG makes it difficult to apply it on CI mechanism due to the high auto-ignition resistance. For that reason, many researchers use spark plugs to ignite the fuel. However, in the current study, LPG was applied to the CI engine and used diesel as the auto-ignition initiator.



**Figure 2.2** The direct injection setup for LPG fuel; a) spark ignition [21]. b) dual direct injection compression ignition [current study]

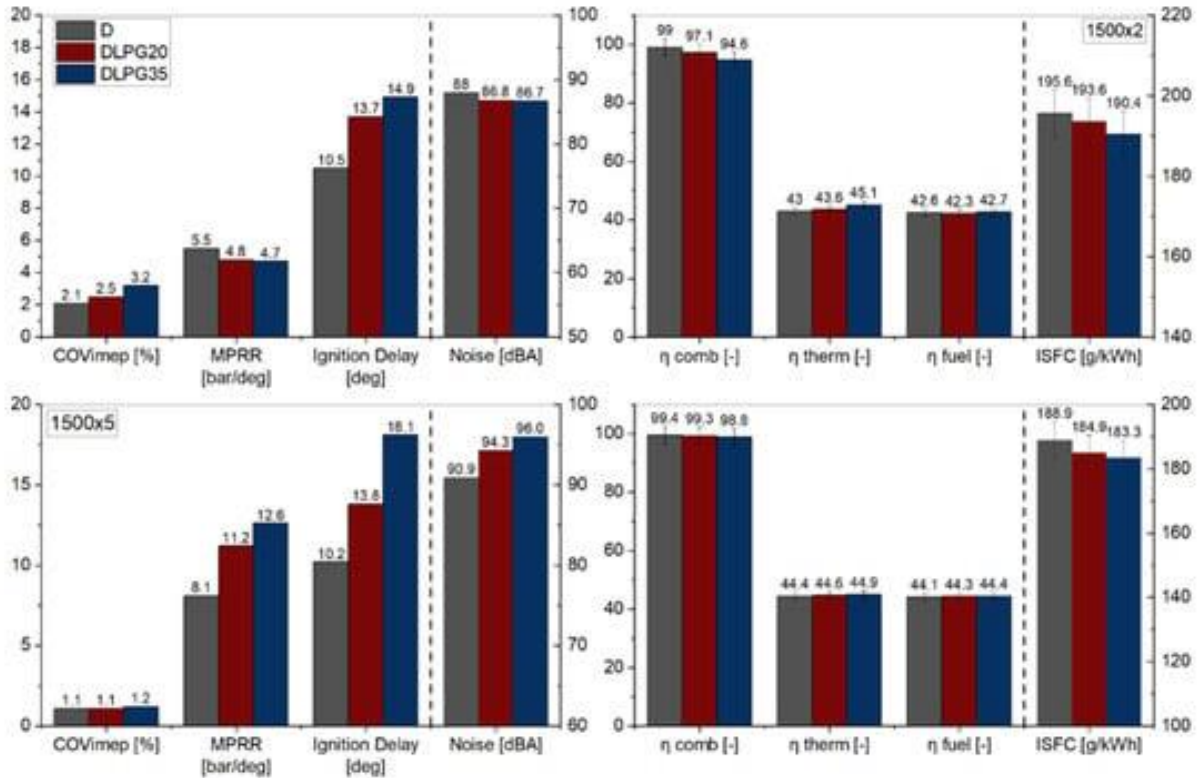
Research by Hashem et al. (2023) demonstrated that direct injection of LPG results in improved combustion efficiency compared to traditional port fuel injection (PFI) systems. The precise control over fuel delivery achieved with direct injection enhances fuel-air mixing and combustion stability, leading to higher thermal efficiency [68]. Investigations conducted by Kim et al. (2017) revealed that direct injection of LPG leads to reduced emissions of pollutants such as nitrogen oxides (NO<sub>x</sub>), particulate matter (PM), and unburned hydrocarbons (UHC) compared to PFI systems. The stratified charge combustion enabled by direct injection minimizes fuel-rich zones and promotes more complete combustion, resulting in cleaner exhaust emissions [69]. Research conducted by Li et al. (2009) evaluated the cold start performance of direct injection LPG systems and found them to be comparable or superior to PFI systems. The ability to deliver precise amounts of fuel directly into the combustion chamber enables faster warm-up times and reduced emissions during cold starts [70]. Investigations into injection system optimization for direct injection LPG engines, such as the work by Woo et al. (2023), have led to improvements in combustion stability, emissions control, and overall engine performance. Research focused on injector design, fuel atomization, and injection timing has resulted in enhanced combustion characteristics and efficiency [71]

### **2.3 Review of previous studies on in-cylinder performance, emission characteristics, and combustion operating parameter optimization**

This part presents a review of familiar previous research that has been done in this area. The previous results of study the effect of combustion duration, bore-stroke ratio, valve port diameter – bore ratio, exhaust valve closing timing and residual gas on engine performance and emission characteristics will be shown. The drawback of those research also are pointed out and will be solved.

### **2.3.1 Review of In-cylinder performance on LPG engine**

For various reasons, CI machines outperform SI engines in terms of efficiency. For instance, CI machine can serve at aspect load by lowering the number of injected fuel, and due to the compression stroke only compressing air in a CI machine instead of a fuel-air blend, the achievement is somewhat close to the ideal cycle efficiency [72]. CI machines also do not get knocking at high loads, allowing them to reach greater compression ratios than SI machines. Theoretically, the propane is suitable for usage in greater compression ratio CI machines due to its greater octane value (which corresponds to a low cetane number) [73]. Compression-ignition (CI) engines produce relatively low levels of CO and THC emissions [74] and fuel-lean equivalency ratios because they use compressed air rather than an electrical spark to start combustion [75], [76]. Propane in diesel engines produce a better thermal efficiency and high output torque due to a larger lower heating value [59]. It also contributes to lower NO<sub>x</sub> pollutants by lowering the charge temperature, which reduces NO<sub>x</sub> forming [77]. Ianniello et al. [78] studied a single-cylinder engine for two fuels: diesel and LPG, in volume ratios of 20/80 and 35/65 operating at 1200 rpm per 2 bar and 1500 rpm per 5 bar, respectively, to achieve a constant NO<sub>x</sub> target. They reported that the engine load increase resulted in an increase in the peak combustion duration due to the cooling effect on the in-cylinder charge, which improves the premixed combustion before the main combustion (mixing controlled combustion) phase as shown in Figure 2.3



**Figure 2.3** Covariance of indicated mean effective pressure ( $COV_{IMEP}$ ), maximum pressure rise rate (MPPR), ignition delay, and noise (left) and efficiency performances (right) for all test points.

Propane has a desirable calorific value, but it has a lower knock resistance. The functioning range of the machine (workable loads and speeds) may be constrained by early propane autoignition or later part knock, despite the fact that propane's increased reactivity leads in quicker burn rates and perhaps greater brake thermal efficiencies [79]. Since propane has a very limited cetane number [80], reliable ignition requires the use of spark ignition. Based on these facts, it is necessary to develop an innovative combustion strategy to accomplish high efficiency comparable to a diesel engine while forming low emissions comparable to a propane engine. The combustion and performance of a diesel machine running with diesel fuel only, referred to as the diesel baseline, and running with propane are compared in order to analyze the influence of the spark released energy of CI engines fuelled with propane. This comparison is done using experimental and computational fluid dynamics modelling simultaneously.

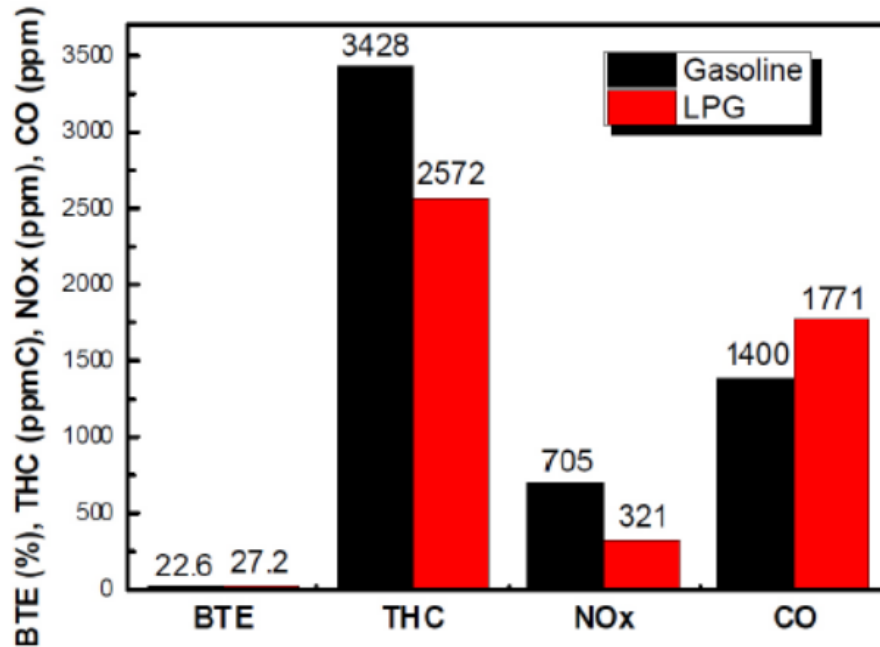
### 2.3.2 Review of emission characteristics of LPG engine



Different types of combustion techniques have been developed to meet pollution and fuel efficiency requirements. Direct injection, in which a high-pressure fuel delivery system injects fuel directly into the cylinder, is one such technique that has attracted much attention [71]. The temperature in the combustion chamber can be easily lowered by evaporating the directly injected fuel [81]. Increasing the charge density leads to better volumetric efficiency [82]. Propane is considered a viable option for reducing particulate emissions and ultimately NO<sub>x</sub> emissions [26] when used with diesel engines [51]. Ryskamp provided a visual explanation of the high standard deviation and coefficient of variation for LPG for a specific vehicle or engine. From the available results of Atlantic Consulting's survey, DI with LPG unanimously produced less CO<sub>2</sub>, PM, PN, and CO emissions compared to GDI. These results are intuitive based on the lower H:C ratio of LPG benefitting CO<sub>2</sub>, CO, and PM/PN as well as the superior vaporization properties of LPG benefitting PM/PN and CO on the basis of a more homogeneous air and fuel mixture. Results for NO<sub>x</sub> and HC emissions were more difficult to evaluate noting that there was limited data (only provided for 3 studies) for NO<sub>x</sub> and HC emissions. Furthermore, the data that was available ranged from reductions to increases in NO<sub>x</sub> and HC emissions from DI LPG versus GDI.

A study by Park et al. titled "Emission Characteristics of Gasoline and LPG in a Spray-Guided Type Direct Injection Engine" provided laboratory based research results [83]. Results from that study for LPG DI versus GDI for a single-cylinder research engine at each fuel's best operating point are presented in Figure 2.4. As shown in Figure 2.4, a lower THC and NO<sub>x</sub> emissions, while the CO emissions are higher for LPG-DI operation. However, it is important to note that these were engine-out emissions while much of the other emissions data analyzed for this composition were measured downstream of a TWC. As previously mentioned efficient TWC operation relies on tightly controlling the A:F ratio of the engine to balance CO and THC mitigation versus NO<sub>x</sub> reduction.





**Figure 2.4** Comparison of performance and emission results for GDI and LPG-DI at Lean Conditions [84]

Another study by Walls et al. titled “Impact of the Direct Injection of Liquid Propane on the Efficiency of a Light-Duty, Spark-Ignited Engine” examined 11 different speed and load operating points for LPG DI versus GDI on a 3.5 L Ford EcoBoost engine [84]. The authors reported that engine out emissions of CO and HC were lower for the majority of modes tested while NOX emissions were higher for the majority of modes tested for LPG DI operation versus GDI operation. Again, this doesn’t include emissions measurements downstream of a TWC which would be an integral part of examining a modern vehicle’s emissions. PM emissions from that study also agreed with the review performed by Atlantic Consulting. In essence, PM emissions from LPG DI operation were negligible compared to GDI operation. The ability of LPG to produce such low PM emissions in DI engines could eliminate the need for particulate filters which are poised to become commonplace on GDI engines due to increasing scrutiny from regulators. Contrary to LPG PFI, LPG DI operation doesn’t reduce the volumetric efficiency of the engine, essentially allowing LPG to provide similar if not better fuel consumption compared to GDI operation. Emissions certification results from 3 vehicles equipped with a Prins LiquiMax DI LPG system installed on OEM GDI platforms were also examined [85]. The three vehicles were a Kia Ceed 1.6 L, a Mercedes E-Class 2.0 L, and a Mazda CX-5 2.5 L all pursuant to Euro 6a emissions regulations.

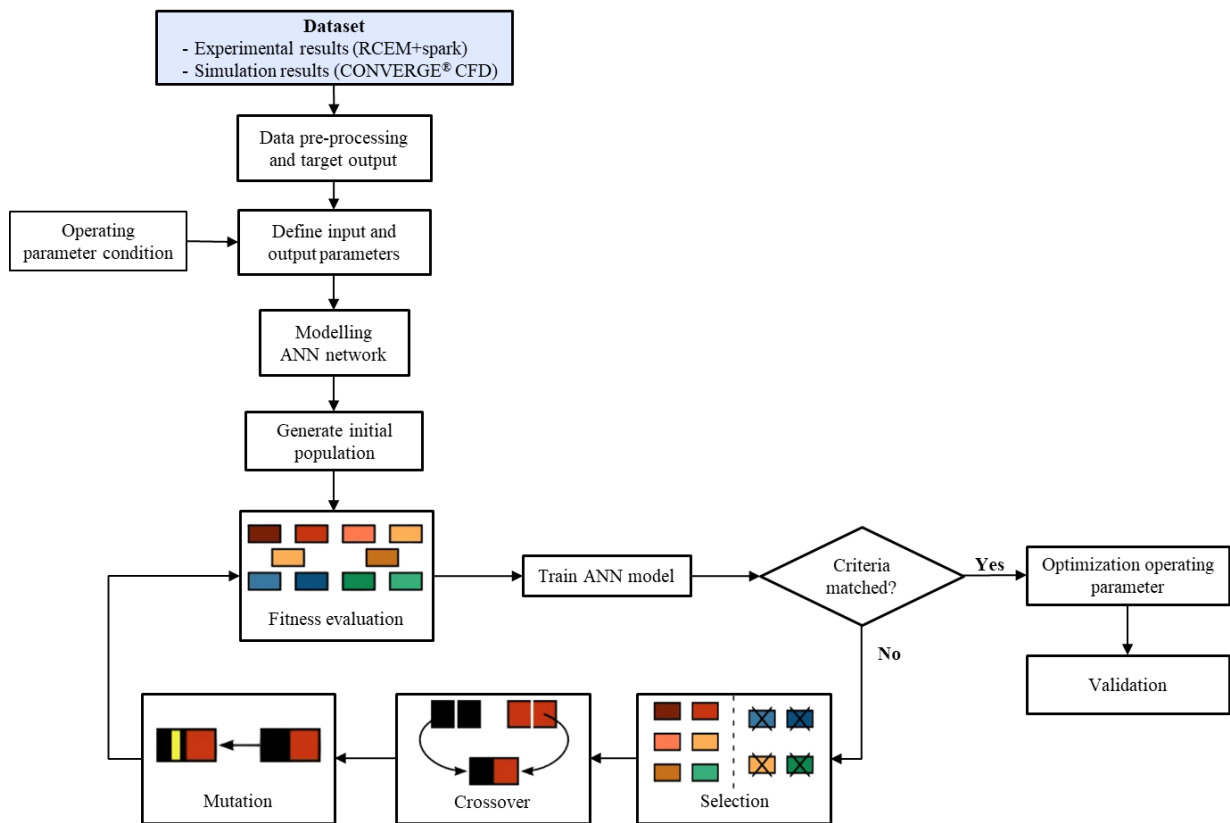
All vehicles resulted in over 90 percent reduction of PN emissions while achieving similar CO, HC, and NOX emissions compared to GDI operation that was well below the Euro 6a standards.

### **2.3.3 Review of optimization application on internal combustion parameter**

Various combustion strategies have been developed to fulfil environmental and fuel efficiency standards. One of these, known as direct injection, has attracted a lot of interest [71]. It involves injecting gasoline directly into the cylinder via a high-pressure fuel delivery system. Evaporating the directly injected fuel is a simple way to reduce the temperature in the combustion chamber [81]. This improves volumetric efficiency by raising the charge density [82]. When utilised with diesel engines, propane is seen to be a practical choice for lowering particle emissions and eventually NO<sub>x</sub> emissions [51]. Although it is difficult to employ propane in compression-ignition engines due to its low cetane number [80] and poor auto-ignition behaviour [32], these factors are its principal drawbacks.. In order to obtain great efficiency, equal to that of a diesel engine, but generating little pollution, a special combustion technique must be created. Increased spark energy has been found to be advantageous for the formation of flames in earlier studies [86], [87], [88], and [89]. However, there hasn't been a full investigation of how spark discharge time affects combustion, in-cylinder performance, and emissions from low-temperature direct-injection propane combustion. The two goals of achieving fewer exhaust pollutants and improved engine effectiveness are incompatible. There is no quick cut to figuring out the optimum operational parameter values because the emission and performance of engines are regulated by several operational parameters. It can be accomplished by extensive experimental experiments, but both time and money are expended on this [90]. Therefore, optimisation is undoubtedly required to obtain the best possible combinations of operating parameters such compression ratio, start of injection, load, and equivalency ratio in propane in order to meet goals.

The artificial neural network model used the compression ratio, equivalency ratio, mix percentage, and engine workload as input parameters. As output parameters, engine performance and emissions were calculated, including BTE, BSFC, CO, unburned HC, and NO<sub>x</sub>. By using a genetic algorithm, Liu et al. [91] chose to concurrently optimise a diesel/natural gas-fueled dual fuel engine's fuel consumption, NO<sub>x</sub> emissions, and CH<sub>4</sub>

emissions. By using an artificial neural network (ANN) in conjunction with a genetic algorithm (GA), Li et al. [92] discovered a better way to increase fuel economy and reduce nitrogen oxide (NO<sub>x</sub>) emissions with less computing time. Through performing RCM simulations and comparing the results to two different sets of published literature ignition delay durations for propane, DelVescovo et al. [50] used a genetic algorithm technique to optimise the six reaction rate parameters within defined uncertainty ranges. Numerous studies have predicted ANN output values and compared them to experimental values, highlighting how well the projected values resemble the values obtained through experimentation. The process of creating the ANN model was mostly based on the neural network toolbox of MATLAB R2017b, and the learning rate and training epochs of ANN model were set to 0.001 and 1000, respectively. Figure 2.5 shows the schematic representation process flow of the ANN approach for prediction and training for the spark discharge energy impacts on in-cylinder performance of a large bore compression ignition engine.



**Figure 2.5** Framework of research methodology in ANN genetic algorithm system [93].

Table 2.1 shows selected studies on artificial neural networks to make prediction of the necessary parameters of the compression ignition engine. Input parameters covering the entire problem domain under study provide effective predictions. To make sure that each input contributes equally to the ANN, within the first and second hidden layers, there are, respectively, selected number of neurons. In the hidden layer of the network, the activation function was tan sigmoid, while in the output layer, it was linear. The network has been trained using a common back-propagation approach. Levenberg-Marquardt method, a feedforward network training technique, is used because it can train small and medium-sized networks and cope with non-linear issues.

**Table 2.1** Various ANN method for CI engine responses prediction

Author	ANN Method (algorithm)	Input parameters	Output parameters	Main finding
Mebin et al. [94]	Feed-Forward Backpropagation	Load, DTBP, RH, Water	BSFC, BTE, CO, HC, NO <sub>x</sub> , and Smoke	The use of ANN to predict multi-component fuel mixtures improves in reducing the quantity of experimental work required to determine engine output characteristics.
Channapattana et al. [90]	Levenberg-Marquardt back propagation	CR, SIT, FIP, Load, Blend	BTE, BSEC, EGT, CO, CO <sub>2</sub> , NO <sub>x</sub> , HC, Smoke	The ANN model can forecast engine combustion and emission behaviour under various operating situations.
Babu et al. [95]	Back-propagation multilayer perceptron feed-forward neural network (BPNN) - Levenberg-Marquardt	PrIT, MIT, PIT, Test fuels	BSEC, BTE, ID, CD, CPP, CO, CO <sub>2</sub> , UBHC, NO, Smoke	To forecast the output more accurately, an artificial neural network is recommended above other theoretical and empirical models.
Seo et al. [96]	Multi-layer, feedforward neural network	vehicle specific power, velocity, engine speed, engine coolant temperature and engine torque	CO <sub>2</sub> , NO <sub>x</sub> , HC total, and CO emissions	During the cold start period, the suggested ANN models correctly anticipated fast increases in carbon monoxide, hydrocarbons, and nitrogen oxides.
Hoang et al. [97]	ANN	Load, Fuel blend, Injection	BTE, EGT	The ANN model may be capable of accurately predicting engine behaviour to a level over 95%.
Foroutani et al. [98]	Standard back-propagation learning algorithm	Injection timing, fuel type, fuel consumption	Indicated power, thermal efficiency, NO <sub>x</sub> , PM, CO, CO <sub>2</sub>	The findings for the best ANN model demonstrated that the built model accurately predicted the operation and pollutants of the CI diesel engine.
Farzad et al. [99]	The back propagation learning algorithm	Percentage of biodiesel, engine speed, engine load	$T_{exhaust}$ , SFC, Power, Torque, CO, CO <sub>2</sub> , HC, NO <sub>x</sub>	With determination coefficient ( $R^2$ ) values quite closer to 1, the ANN estimated data closely matched the experimental results overall, demonstrating great accuracy.
Fang et al. [100]	Levenberg–Marquardt algorithm	Speed/load condition, exhaust back-pressure, boost pressure, inlet Temperature, and , rail pressure	IMEP, NO <sub>x</sub> , volumetric efficiency, brake power	The ability of ANN to forecast pollutants outside of its training variety with a high degree of precision makes it a valuable tool for directing future experimental and numerical research on NO <sub>x</sub> emissions.
El-Shafay et al. [101]	Feed-forward back propagation	Engine speed, load, fuel-blend ratio	BSFC, BTE, $T_{exh}$ , AF equivalence ratio, HC, CO, NO <sub>x</sub> , smoke, ID	When contrasted with diesel powered by Palm biodiesel mixes, ANN is an efficient modelling technique with great accuracy in engine performance, combustion, and emission cuts.
Niu et al. [102]	Support Vector Machine (SVM)	Pressure, injection timing, temperature	Engine response	The comparative study of ANN and SVM shows that ANN may converge to local minima and encounter an overfitting issue, but SVM can discover the best

				global solution with less experimental data and has strong generalisation and prediction accuracy capabilities.
Taghavifar et al. [103]	Levenburg-Marquardt	Crank angle, heat release rate, SMD, NO <sub>x</sub> , pressure	Chemical availability, thermos-mechanical, irreversibility rate	Neural network-based data analytics can offer a suitable method in diesel engines for increasing energy efficiency and lowering pollutants.

## 2.4 Summary

This chapter gives an introduction of research engine and a literature review about the effect the spark discharge effect on ignition and emission characteristics of LPG engine using RCEM. All previous studies have focused on the behavior of dual fuel combustion using propane and diesel in various CI engines.

The adaptation of the propane direct injection system and the potential benefits combining with spark application, in terms of engine performances, motivate the use of propane direct injection strategies is performed. These facts make it necessary to develop a combustion strategy in order to gain high efficiency comparable to a diesel machine while forming low emissions comparable to a propane engine. Spark timing and discharge current both have an implication on how much discharge energy is transmitted to the spark plug in a spark ignition system. Previous research has shown that increased spark energy is beneficial for producing flames, and that the flow that forms vortices close to the spark plug also plays a role in this. Because spark energy is the integration of discharge current and voltage, both of them have an influence on the number of energies transferred to the spark electrode. It has not yet been thoroughly investigated how the discharge energy and discharge duration affect the RCEM's in-cylinder pressure when it is powered by propane. The goal of this study is to explore the impact of the released energy and spark period during the beginning phase of combustion cycle. The combustion efficiency of a RCEM modified with spark and direct injection of propane is contrasted, as well as the implications of the spark released energy on the ignition schema as well as the interactional correlation between the spark released energy and streamflow characteristics, using both experimental and computational fluid dynamics simulation. We investigated how the multi-coil spark affects the in-cylinder work on RCEM with a spark and fueled with liquid direct fuel injection of propane method and how far the

in-cylinder stream field impacts to the spark flame that use experimental and CFD simulation to determine the optimal interactions throughout ignition strategies.

Thus, to understand the fundamentals of the emission processes at different spark discharge durations, the test engine was numerically represented as a three-dimensional (3D) computational fluid dynamics (CFD) model. Both experimental and computational fluid dynamics models were used for analysis. The novelty of this study is creation of an internal prototype of an RCEM modified with spark discharge and equipped with a high-pressure direct propane injection employing a common rail injection control mechanism. With these features, the current study and its difference from the studies in the literature are emphasized on the behavior of propane in compression ignition engine and spark duration effects in terms of in-cylinder combustion, performance, and emissions in RCEM research engine were investigated comparatively

### 3. RESEARCH METHODOLOGY

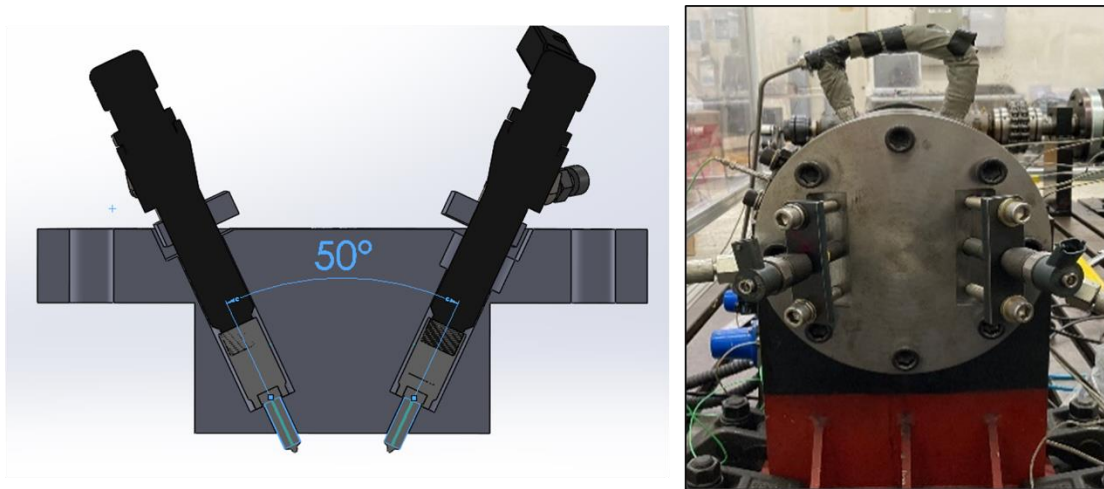
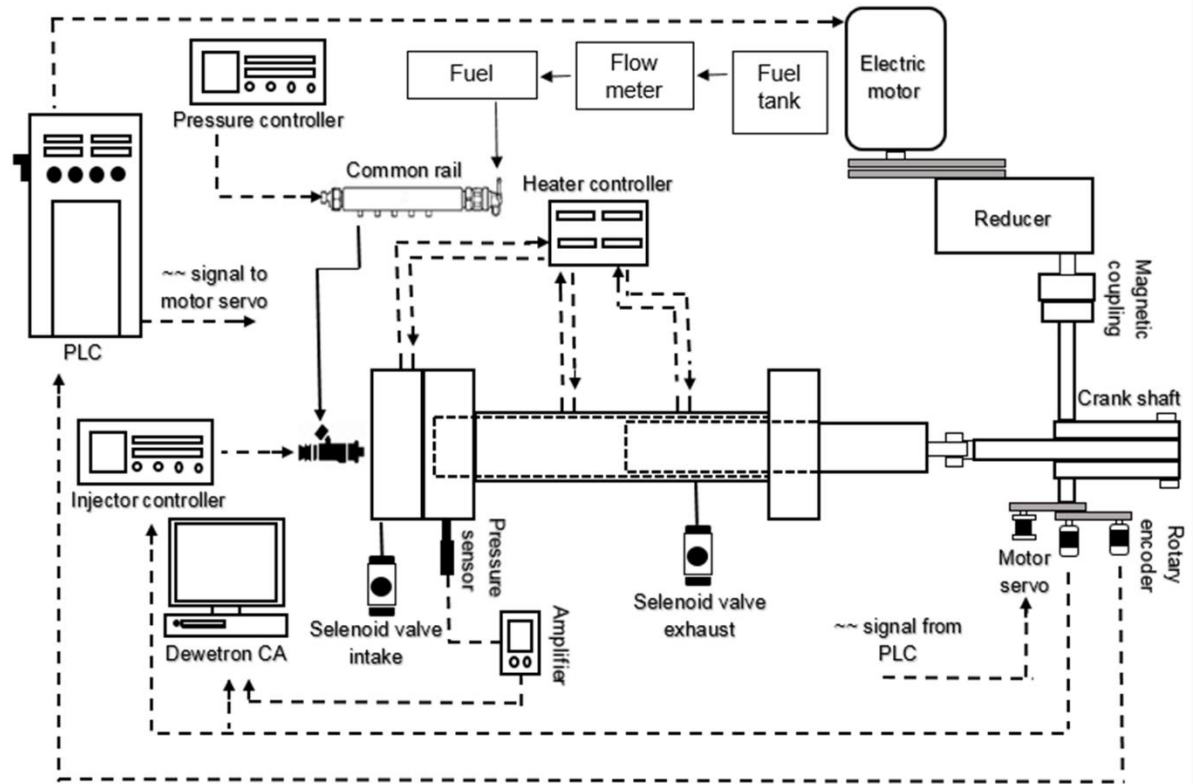
This chapter details the research platforms of experiment and simulation used for the empirical study. Three types of experiment platforms are employed: (1) a set dual direct injection fuel (diesel-propane) platform; (2) a build a high pressure LPG fuel system; and (3) a rapid compression and expansion research engine modified with dual injector. Meanwhile, a simulation platform is employed using CFD Converge.

#### 3.1 Experimental setup

##### 3.1.1 RCEM with a dual fuel direct injection system

Using a hydraulically and electrically controlled driving system, the rapid compression-expansion machine (RCEM) is a highly developed device that replicates a similar combustion mechanism in a diesel cycle [104]. The single cycle, rapid compression stage of a test fuel can be analyzed in an RCM/RCEM under precisely defined and controlled conditions without the complicated fluid dynamics characteristics of an internal combustion engine mechanism [105]. The ignition strategy can be modified by changing the cylinder head to satisfy the requirement of a compression ignition or dual direct injection ignition engine. For the current study, the cylinder head was modified to fit the two direct injection strategy using diesel and LPG as fuel. The schematic of the RCEM is shown in Figure 3.1 . With a 100 mm bore and 450 mm stroke, it has a single-cylinder engine coupled to a 22 kW electric motor. The electric motor is able to run 1,200 RPM at full power. The motor is coupled to a gearbox to reduce the rotation of RCEM to 240 RPM coupled with a magnetic clutch to transfer sudden energy to the crankshaft. The crankshaft's base contains a screw that can be turned to alter the compression ratio, which is adjustable from 10 to 27.





**Figure 3.1** The schematic diagram of the RCCEM.

Temperature sensors and controls were attached in the body, top dead center (TDC), and bottom dead center (BDC) to maintain the temperature consistency, which could reach a maximum of 393 K. A Kistler 5018 amplifier and a Kistler 6052CU20 pressure transducer were used to monitoring the engine pressure. Table 3.1 displays the engine specifications. A piezoelectric pressure transducer (Kistler type 6052CU20) with a reading accuracy of 0.005 and an amplifier



(Kistler type 5018) were used to measure the in-cylinder pressure. An Autonics rotary encoder with a crank angle resolution of 0.1 degrees was installed to measure the crank angle. For the acquisition of data, the sensors were connected to a Dewetron type DEWE800-CA acquisition device.

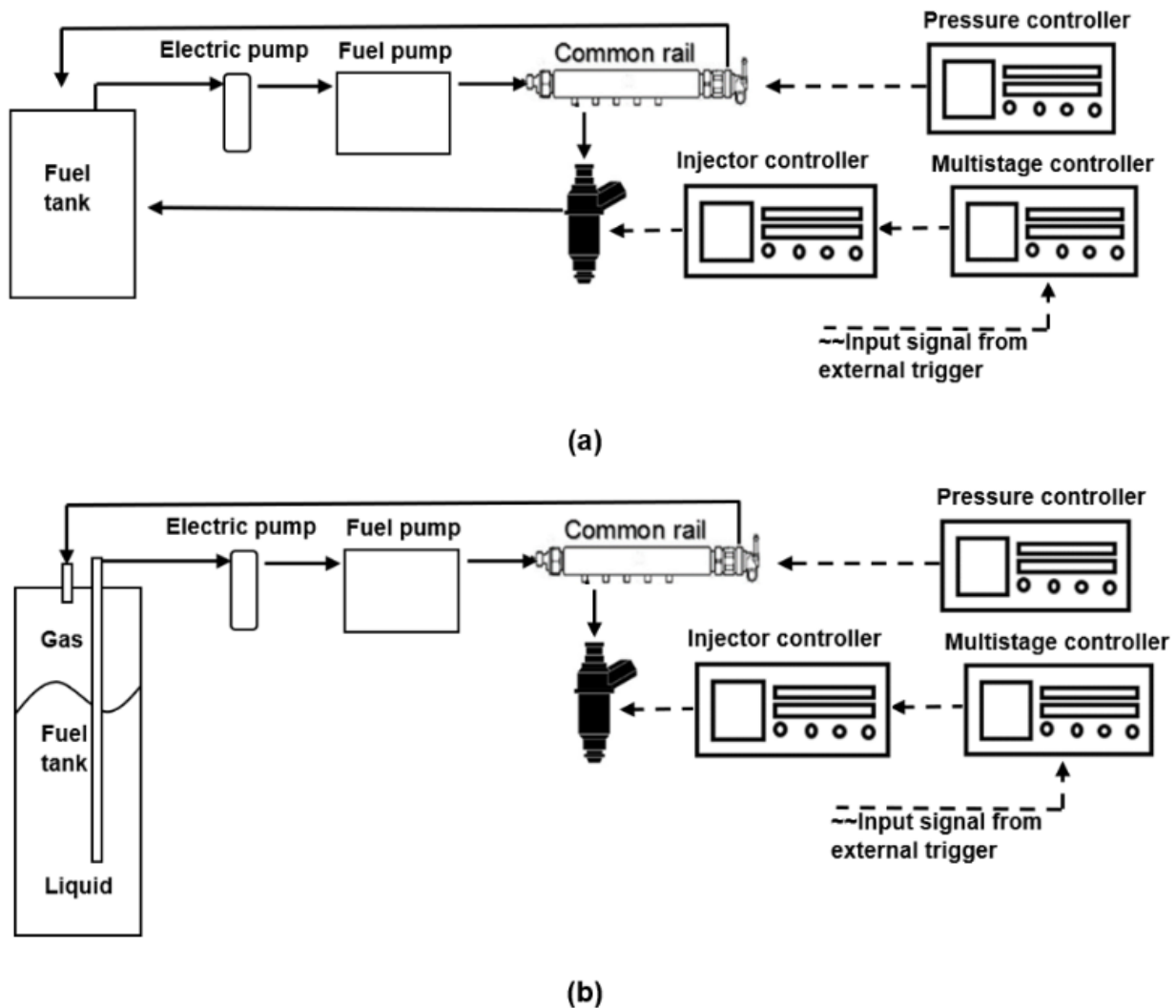
**Table 3.1** Engine specification

Bore x stroke	100x450mm
Connecting road	900mm
Compression ratio	10:1 – 27:1
Number of nozzle holes	7
Injector Diesel	A Bosch 0445110327
Injector Propane	Denso 0221
Motor speed	1200 rpm
Crank shaft speed	240 rpm
Temperature control	323.15 – 413.15 K
Fuel injection system	Common rail direct injection (CRDI)

### 3.1.2 Fuel system.

Two common rail fuel systems were manufactured in order to sufficiently apply the current fuel parameters. The diesel fuel system utilizes a BOSCH CP3.3 pump. However, due to the lack of lubrication properties of LPG, a different fuel pump with an initial lubrication system was employed. For the LPG fuel direct injection system, a four-piston pump was used to deliver LPG in the liquid phase to the common rail. At 20°C, propane gas vapor requires about 836 kPa of pressure to liquefy and at 50°C, it requires about 1,713 kPa of pressure. The electric fuel pump was used to deliver the LPG from the fuel tank to the fuel pump considering the liquid pressure condition requirements of LPG. A pressure gauge and thermocouple were installed between the two fuel pumps to monitor the phase of the fuel. The schematic of the fuel system is shown in Figure 3.2. Up to five injections can be made per cycle when the production ECU and ETAS INCA calibration software are used. For diesel, an experimental 7 x 1550 minisac nozzle tip with a flow

rate of 440 cc/30 s and a 7 x 1550 Denso 0221 nozzle tip were used with a production CRIP2-MI injector. An Autonics E40S8-1800-3-T-24 rotary encoder was used to measure the crank angle position. To record the data, a Dewetron data acquisition device (DEWE-800-CA) was connected to each sensor. The fuel injectors were coupled with a common rail solenoid injector peak and an injector controller (Zenobalti ZB-8035 multi-stage injection device). To control the injection timing and duration, the fuel injector was outfitted with a Zenobalti type ZB-5100 common rail driver solenoid injector and a Zenobalti type ZB-8035 multi-stage injection mechanism.



**Figure 3.2** A schematic of the fuel system: a) diesel fuel system and b) propane fuel system.

### 3.1.3 Fuel preparation.

The main fuel used in this investigation was LPG which consists of 99.99% propane and conventional diesel that was obtained from a local fuel station in Korea. The physical properties of the fuels are shown in Table 3.2 [106]. The fuel is identified as "DP10 to P100" to represent the propane and diesel energy composition, where "P" represents propane, "D" represents diesel, and the number in the last digit represents the percentage of propane energy. The injection rate test was performed on the fuel injection rate device depicted in Figure 3.3 to verify the volume of fuel injected into the chamber. The rate of injection flow was calculated using a Bosch 7-hole injector (0445110 327) and a Denso 0221 connected to the fuel injection rate device. A Zenobalti multistage injection controller (ZB-8035), in conjunction with a common rail solenoid injector peak and hold driver of type ZB-5100, internally activated the injector solenoid to control the SOI timing. A PCV driver (ZB-1100) for a common rail and an electric motor controller both kept the injection pressures at 30 bar by controlling them with common rail controllers and high-pressure injection pumps, respectively. A 500 cycle injection rate test was performed beforehand to obtain the same amount of energy from fuel with 0.5 of an equivalence ratio. The propane energy fraction (%P), Eq. (1), is the fraction of energy from propane in the total fuel energy input to the system.

$$\%P = \frac{\dot{m}_P LHV_P}{\dot{m}_P LHV_P + \dot{m}_D LHV_D} \times 100 \quad (1)$$

Here,  $\dot{m}$  is the mass of the fuel and LHV is the low heating value.

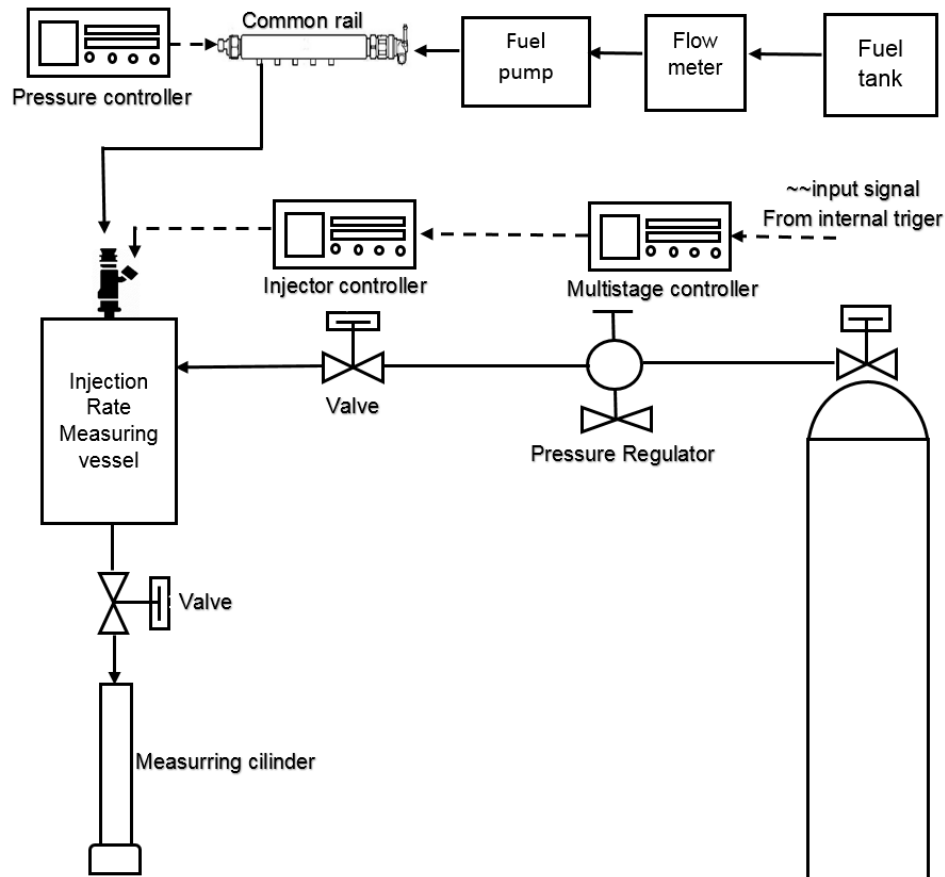
The equivalence ratio of the DP mixture can be calculated using Equation (2).

$$\phi_{DP} = \frac{\dot{m}_P AFR_{St,P} + \dot{m}_D AFR_{St,D}}{\dot{m}_{Air}} \quad (2)$$

Here, AFR indicates the air fuel ratio and  $\dot{m}_{air}$  is the mass of air inside the cylinder.

**Table 3.2** Properties of fuels [106]

Properties	Propane	Diesel
Molecule formula	C <sub>3</sub> H <sub>8</sub>	C <sub>n</sub> H <sub>1.8n</sub>
Boiling point (°C)	-42.1	180-370
Stoichiometric A/F	15.71	14.6
Auto ignition temperature (°C)	481	250
Lower heating value (MJ/kg)	46.34	42.5



**Figure 3.3** The schematic of the fuel measuring system.

### 3.1.4 Accuracy of measurements and uncertainty

Every item of equipment was calibrated within a predetermined time frame to guarantee the dependability of measurement tools. Prior to the subsequent measurement cycle, all electric equipment is purged and calibrated after each measurement. To eliminate reading uncertainty, each set of test conditions was repeatedly measured three times. Based on the certainty of the instrument used and the measured rate, a thorough uncertainty analysis is carried out to predict the limiting

inaccuracy connected with every calculated parameter [107]. Table 3.3 summarizes the uncertainty range of the measured parameters [108].

**Table 3.3** Uncertainty of measured parameters

Measured parameter	Uncertainty (%)
Pressure	<2
Temperature	<2
Fuel rate	<1
Research engine crank angle	<1
Research engine speed	<1

### 3.2 Governing equation

Using information of the cylinder pressure, it is possible to calculate the work transferred from the gas to the piston. Due to its independence from the engine speed, cylinder count, and piston displacement, the result serves as a fundamental parameter for assessing engine efficiency. A P-V graph displays the pressure against cylinder volume, where the work is the following.

$$w_i = \int P dV \quad (3)$$

The pressure results of combustion inside the cylinder reveals the thermodynamic state. The first law of thermodynamics can be used to calculate the percentage of combustion with a few basic assumptions. The following equation can be used to determine the rate of heat release:

$$\frac{dQ}{d\theta} = \frac{\gamma}{\gamma-1} p \frac{dV}{d\theta} + \frac{1}{\gamma-1} V \frac{dp}{d\theta} \quad (4)$$

Where  $p$  is the internal cylinder pressure,  $\gamma$  is the specific heat ratio, and  $V$  is the volume of combustion chamber. For a CI engine, the appropriate specific heat ratio value is 1.3. The ideal gas law can be used to measure the in-cylinder temperature using the in-cylinder pressure and volume using the equation below.

$$T = \frac{p \cdot V}{n \cdot R} \quad (5)$$

Here,  $n$  and  $R$  are the quantity of substance and gas constant, respectively, and  $p$  and  $V$  are the pressure and volume, respectively.

The performance of an internal combustion engine is greatly influenced by its power output. Indicated power and brake horsepower are two of the most popular ways to gauge this output of power. The indicated power is the total power generated inside the cylinder during one full cycle, excluding any losses.

$$I. P. = \frac{kP_{mi}LAN}{60000} \quad (6)$$

Here,  $k$  is the number of cylinders,  $P_{mi}$  is the indicated mean effective pressure,  $L$  is the length of stroke,  $A$  is the area of a piston, and  $n$  is the number of ignitions per minute.

The amount of power available at the power produced by an engine at the output shaft is called brake power.

$$B. P. = \frac{2\pi NT}{60000} \quad (7)$$

Here,  $T$  is the torque and  $N$  is engine speed.

The calculated indicated fuel efficiency is calculated as the indicated power divided by the energy input per cycle. Eq. (8) provides the following as the indicated thermal efficiency formula:

$$\eta_t = \frac{P_i}{Q_{in}} \times 100 \quad (8)$$

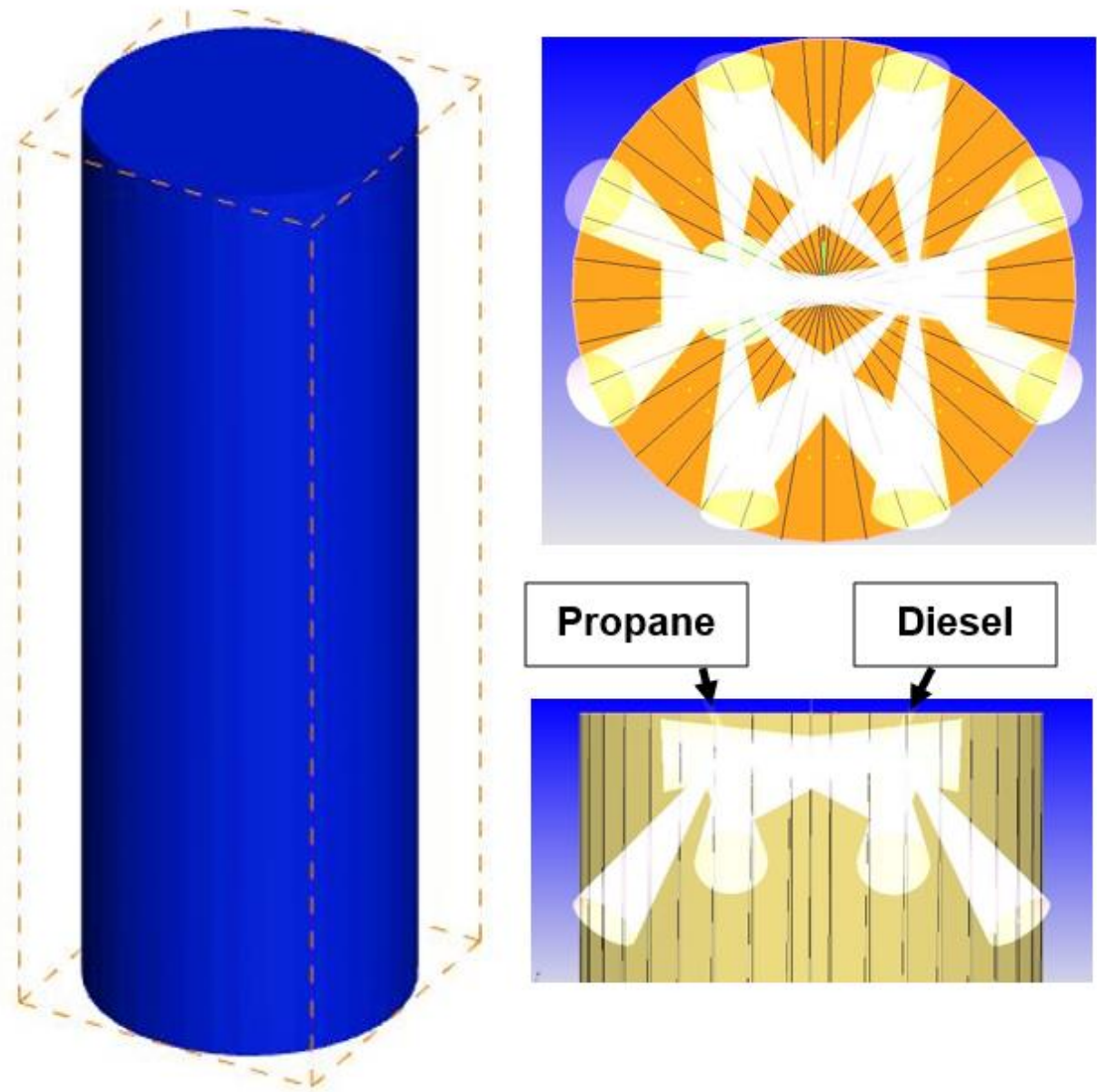
where  $\eta_t$  is the thermal efficiency [%],  $P_i$  is the work/power [J/cycle], and  $Q_{in}$  is the input energy [J/cycle].

### 3.3 CFD modeling and simulation

CONVERGE CFD software was used in this study to simulate internal combustion engine processes. Advanced numerical methods and physical models of the spray, turbulence, and combustion processes, as well as their nonlinear interactions, are included in CONVERGE. To better understand the behavior of combustion in dual fuel engines, the dual fuel combustion was

modelled. In addition to experimental research on an RCEM, modelling was also carried out. Surfaces for the geometry were produced both before and after simulation using a full mesh construction method. Using the methods of fixed embedding and adaptive mesh refinement subdivision (AMR) as well as the basic grid size, users can modify the grid size and the total number of grid cells.

CONVERGE CFD 3.0 was used for the computational analyses. Using the combustion chamber's full sector geometry, closed cycle simulations were carried out. A turbulence model must be used to obtain accurate CFD simulation results because turbulence has a significant impact on the rate at which momentum, energy, and species mix. The Renormalization Group (RNG)  $k-\epsilon$  turbulence model [109] performs better than the standard  $k$ -turbulence model at describing anisotropic and non-equilibrium effects. In order to use the discretized Navier-Stokes equation on the Cartesian grid, a finite volume indirect discretization method was selected. To save time, the computer simulates all three processes: combustion, compression, and expansion. Utilizing the information gleaned from experimental observations, the initial fuel, ambient temperature, and air conditions were specified. The initial fields of temperature, flow velocity, and pressure were generated until the motoring pressure from the experiments is met.



**Figure 3.4** The schematic diagram of RCEM for CFD investigation.

**Table 3.4** CONVERGE modeling used in this study

Phenomenon	Model
Turbulence flow	RNG k- $\epsilon$ [109]
Drop drag	Dynamic drop drag [110]
Break-up	KH-RT[111]
Drop collision	NTC[112]



Drop evaporation	Frossling[113]
Drop turbulent dispersion	TKE preserving[110]
Chemistry solver	SAGE [114]

---

N-Heptane (C<sub>7</sub>H<sub>16</sub>) was used as a representation for diesel fuel. Because of its resemblance to diesel in terms of heat release rate (HRR) and the ignition delay behavior in engines, straight-chain n-heptane (C<sub>7</sub>H<sub>16</sub>) makes a useful substitute for diesel [42]. Diesel and liquid propane (C<sub>3</sub>H<sub>8</sub>) injections were made using Lagrangian particles, and the distribution of the injection drops was determined by the size of the nozzle. Spray break-up was achieved using the Kelvin Helholtz-Rayleigh Taylor (KH-RT) design [111] with the KH model including a breakup time constant of 36, a KH model size constant of 0.61, a RT model size constant of 0.68, and a breakup length constant of 18 for the RT model. When pilot fuel droplets collided, the no-time counter collision model was used to simulate the collision and the O'Rourke turbulent dispersion simulation model was used to simulate the effects of turbulent flow on spray droplets. Using the SAGE chemistry solver, the combustion kinetics were calculated [43]. Prior to solving the transport equations, each time step determines the mass fractions of the new species and the reaction rates for every elementary reaction. It is considered a source when the species mass fractions change. The source term in the species transport equation couples the transport solver to the system. The simulations are accelerated by the independent parallelization of the chemistry and flow solvers.

**Table 3.5** Simulation initial and boundary conditions

<b>Boundary &amp; initial conditions</b>	<b>Value</b>
TKE of cylinder region	62.03 m <sup>2</sup> /s <sup>2</sup>
Pressure of intake	101 kPa
Piston Temperature	553 K
Cylinder wall initial temperature	353.15 K
Initial pressure of cylinder	101 kPa
Initial temperature of cylinder	298 K
Grid size	0.004 m

The full surface of the in-cylinder RCEM was modeled using CAD 3D Sledworks software. The full geometry of the surface model was required because the positions of the two injectors cannot be observed by slicing part of the model. The grid size was changed to 4 mm and the automatic mesh refinement (AMR) tool was used to update the main area valves to ensure simulation fidelity. AMR was used to produce a highly refined grid with a smaller base grid size without increasing simulation time in order to predict complex phenomena like flame propagation or high-velocity flow. The AMR algorithm embeds higher grid resolution where the flow-field is most inadequately resolved or where the sub-grid field is largest, i.e., where the gradient of a particular field variable is the highest.

### **3.4 Test procedure.**

The experiment was conducted on RCEM by modifying the cylinder head to be compatible for dual injector installation. Three heater bans were installed in the cylinder body and one heater ban was attached to the cylinder head. The in-cylinder temperature was maintained at 353.15 K, which implies that this is the warm-up end point from the aspect of engine stabilization [115], for at least for 30 minutes to ensure the homogeneity distribution of heat in the cylinder. The compression ratio can be controlled by adjusting the screw of the connecting rod and the comparison of the moving stroke and in-cylinder volume can be measured. The compression ratios used in this study were 17 and 19. The connecting rod's shaft is connected to the 22 kW electric motor which has a maximum speed of 1,200 RPM, which is reduced by a gear box to 240 RPM to maximize the sudden force of the RCEM mechanism. The piston was set at bottom dead center (BTDC) at the beginning of the experiment. The magnetic clutch delivers the force from the electric motor to the connecting rod for 360° rotation and the in-cylinder pressure was recorded.

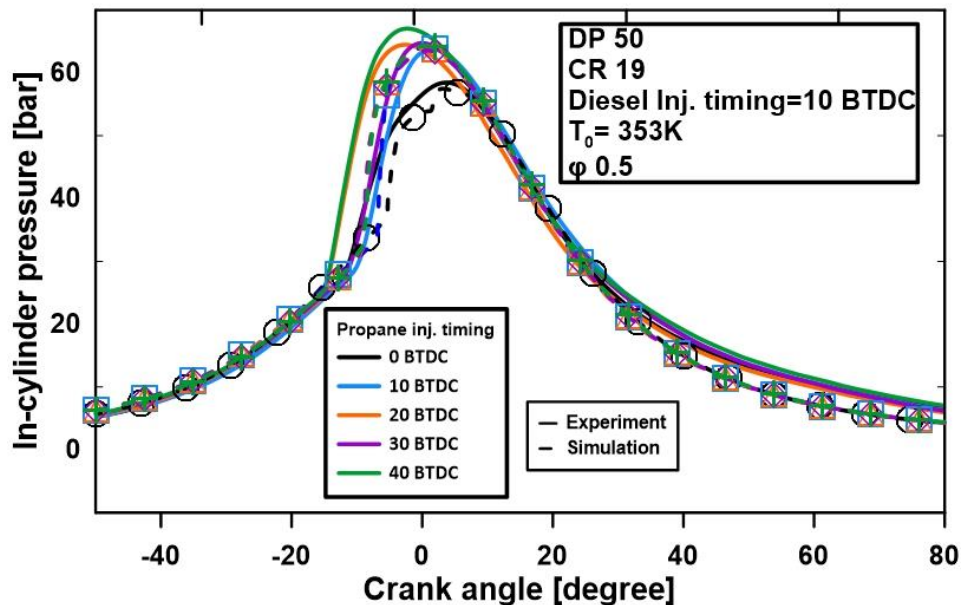
There are two stages of pressurization required before direct injection of LPG fuel can begin. The first is carried out using a fuel tank-mounted electric low-pressure pump and the second is carried out using a high-pressure plunger pump. The fuel pressure is increased to 8 bar in the first stage and 200 bar in the second stage. It is necessary to maintain LPG in its liquid phase in order for the fuel pump to work properly. In this regard, the current study determined that the fuel injection pressure should be 200 bar, taking the durability and performance of the pump into consideration. Meanwhile, the injection pressure for the diesel was maintained at 500 bar. The

diesel fuel is considered as the ignitor of the combustion and the injection timing was maintained at 10° BTDC. To find the best combustion characteristics produced by the LPG, the injection timing varied from early injection (40°BTDC) to late injection (0°BTDC). To determine the most efficient fuel composition, a wide range propane percentage from 10% to 100% was applied based on the low heating value comparison with diesel. The details of the current study are shown in Table 3.6.

**Table 3.6** Experimental conditions

Properties	Diesel	Propane
Injection pressure [bar]	500	200
Fuel injection timing [BTDC]	10°	0°-40°
Fuel percentage	0-90%	10-100%
Initial pressure	1 atm	
Compression ratio	17 and 19	
Initial temperature [K]	353.15	
Engine speed [RPM]	240	

### 3.5 Model validation



**Figure 3.5** Validation of CFD modeling based on in-cylinder pressure of RCEM

The physical representation is verified using different experimental data in terms of the pressure between the experimental data and simulation results. Table 3.4 provides a quick description of the models applied in this investigation. On a Windows computer with a 60 GHz Intel® Core i7™ 77003 processor and 32 GB of RAM, this simulation was conducted. At the input and outflow, 383 K and 1 bar of pressure, respectively, were set as the temperatures. The case set up was carried out on the RCEM with the spark model according to the parameters that were determined.

Fig. 3.5 displays the validation of the simulated and experimental findings for driving pressure and crank angle. To ensure that the readings for each test circumstance were accurate, three pressure measurements were taken. Propane's high-octane rating caused the in-cylinder pressure of the RCEM to rise to its ideal level, which was reached around the top dead center. The pressure dropped 0.183 MPa from the diesel engine. At a crank angle of 10.83 degrees, the highest pressure was recorded (-9.08 degrees).

### **3.6 Summary**

This chapter has detail explained about the research platforms of experiment and simulation. Based on this experimental system, the combustion characteristics and emission characteristics will be obtained using diesel and propane fuels. This output experimental data will be used to validate the engine simulation model.

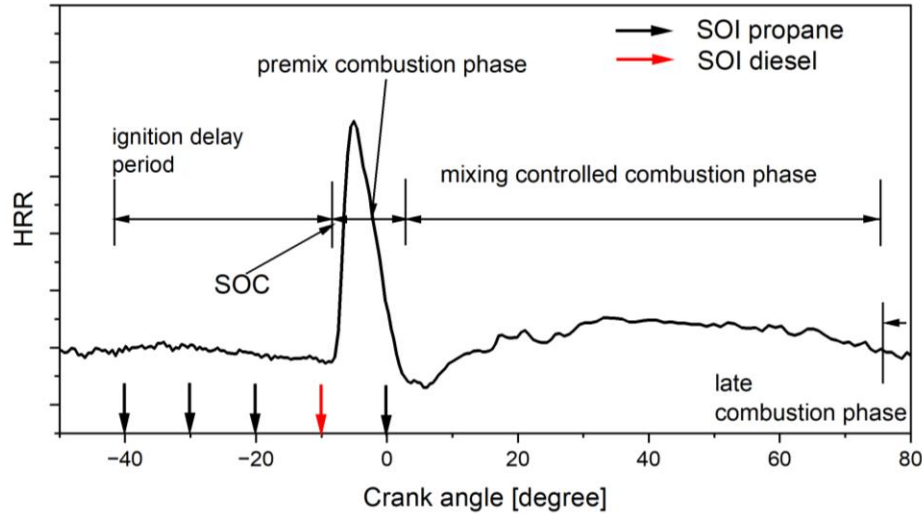
This chapter has explained the simulation modeling setup base on the Converge software with version 3.0. The simulation is validated base on the comparison between simulation results and experimental results in cylinder pressure. The investigation the effect of spark discharge duration on engine performance and emission characteristics could be carried out via simulated approach. A detail of optimization operating parameter of spark discharge duration on the performance and emission characteristics will be investigated in chapter 4, 5, and 6.

## **4. INVESTIGATION OF THE COMBUSTION CHARACTERISTICS OF A DUAL DIRECT INJECTION FUEL (DIESEL-PROPANE) STRATEGY ON A RAPID COMPRESSION EXPANSION MACHINE**

### **4.1 Combustion performance**

#### **4.1.1 Cycle Analysis**

By measuring the in-cylinder pressure, one can determine the charge's thermodynamic state. It is possible to find out more about the rate the process of combustion using the first law of thermodynamics and a few fundamental assumptions. This method calculates the beginning of ignition to occur at the maximum apparent heat release rate, which is the rate of heat release consistent with the observed pressure change, by ignoring heat transfer and assuming ideal gas behavior. The highest  $dP/dt$  value on the pressure trace serves as a gauge for this. It was found that this measurement is quite sensitive to changes in the combustion mode and noise in the pressure signal [116]. Figure 4.1 shows the identification of combustion based on the HRR trace. The ignition delay was identified as the range of delay from the first SOI until the combustion occurs. In this study, different SOIs of propane and a wide range of propane injection proportion modes were used on RCEM engines with compression ratios of 17.0 and 19.0, simulating compression ignition engine conditions. For reference, various test conditions were also used to simulate the corresponding cylinder pressures. The main effects observed in this set of experiments and simulations can be attributed to the effect of the optimal injection position of propane, the energy fraction of propane, and the variation of compression ratio mode because the engine speed, injection pressure, and equivalence ratio were held constant.



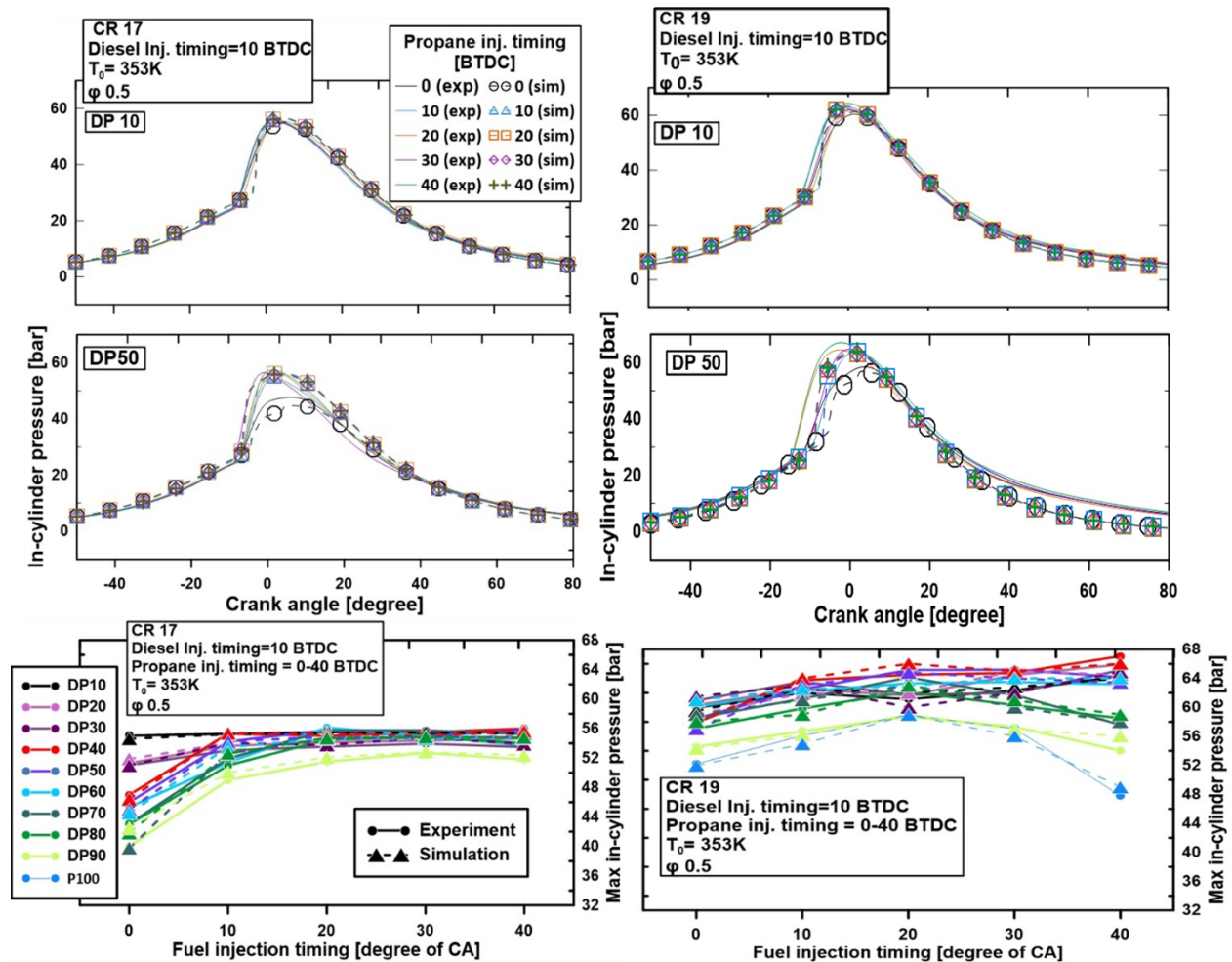
**Figure 4.1** Identification of the combustion phase.

Figure 4.2 compares the measured cylinder pressure traces and peak pressure of compression for compression ratios of a) 17 and b) 19 in addition to the calculated cylinder pressure for five propane injection cases and 10, 50, and 90% propane energy fractions. Moreover, the measured maximum in-cylinder pressure was compared with the simulated values. The charge's thermodynamic state can be determined from the pressure inside the cylinder. With the help of the first law of thermodynamics and a few fundamental presumptions, it is possible to learn more about the rate of combustion. In order to define the start of ignition as the time at the maximum apparent heat release rate, which is the rate of heat release consistent with the observed pressure change, this method disregards heat transfer and assumes ideal gas behavior. This is determined by evaluating the pressure trace's maximum slope ( $\max dP/dt$ ). This measurement was found to be very sensitive to changes in the combustion mode and noise in the pressure signal.

At CR 17, all P100 (propane 100%) parameters were misfire for every variation injection timing tested. Therefore, the propane auto-ignition test at CR 17 is not shown in this study. The increase of propane from DP10-50 resulted in improvement of peak pressure at early propane injection. However, the pressure dropped significantly as propane was injected closer to TDC. As the propane increases (more than 50%), the trend of the in-cylinder pressure kept decreasing and finally, misfire occurred at 100% propane for all injection timings. The in-cylinder pressure produces the highest point of in-cylinder pressure at DP 40, 40°BTDC propane injection timing

i.e., 58.26 bar. The lowest pressure produced was 39.19 bar at DP90, 0°BTDC propane injection timing.

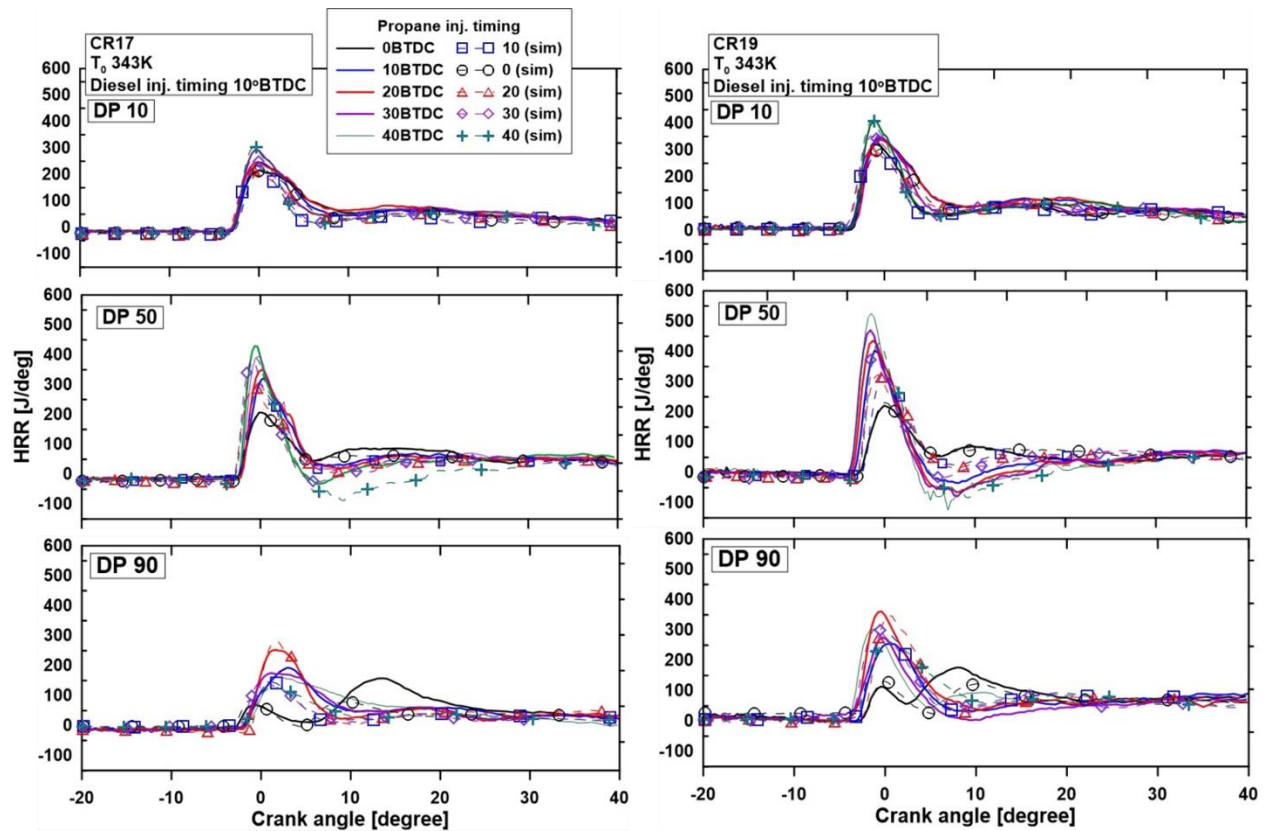
At CR 19, similar behavior to CR 17 was produced for all propane injection timing and propane energy fraction conditions. However, a significant in-cylinder pressure improvement was produced when the compression ratio of 19 was applied for all parameters tested. Moreover, more reactive combustion can be found at propane energy fractions less than 50% at early propane injection timings. At this condition, 40°BTDC propane injection timing produces the highest in-cylinder pressure compared among all of the propane injection timing variations. However, when the energy fraction of propane increased above 50% (DP50), a significant drop of the in-cylinder pressure was produced for early and late injection timings. At this condition, it produces the highest in-cylinder pressure at a 20°BTDC propane injection timing. The lowest in-cylinder pressure was produced at DP100, 40°BTDC propane injection timing, i.e., 47.81 bar.



**Figure 4.2** In-cylinder pressure for propane energy fractions of 10-100% for propane injection timings of 0o-40o BTDC and compression ratios of a) 17 and b) 19.

Proper combustion was expected using LPG fuel as it has a low evaporation temperature and higher LHV compared to diesel fuel. Hence, it has better atomization characteristics and produces a higher amount of heat released during combustion. However, in the direct injection strategy, propane was injected to the chamber in the liquid phase, which has a very low temperature (-43°C). Furthermore, the current common rail system applied fuel injection pressure is much lower compared to diesel for safety purposes. Consequently, lower atomization characteristics were produced for the propane injection case. This will lower the reactivity of the fuel in low compression ratio and high quantity of propane condition. As a result, it improves the possibility of wall impingement, which reduces the cylinder wall temperature. Decreasing the in-cylinder temperature reduced the peak cylinder pressure and increased ignition delay, which agrees with results in previous research by Verde [117]. Furthermore, it affects the ambient temperature of diesel injection condition. A low ambient temperature would alter the Sauter mean diameter (SMD) distribution, spray tip penetration, decelerate diesel fuel evaporation, and reduce diesel fuel activation [118].

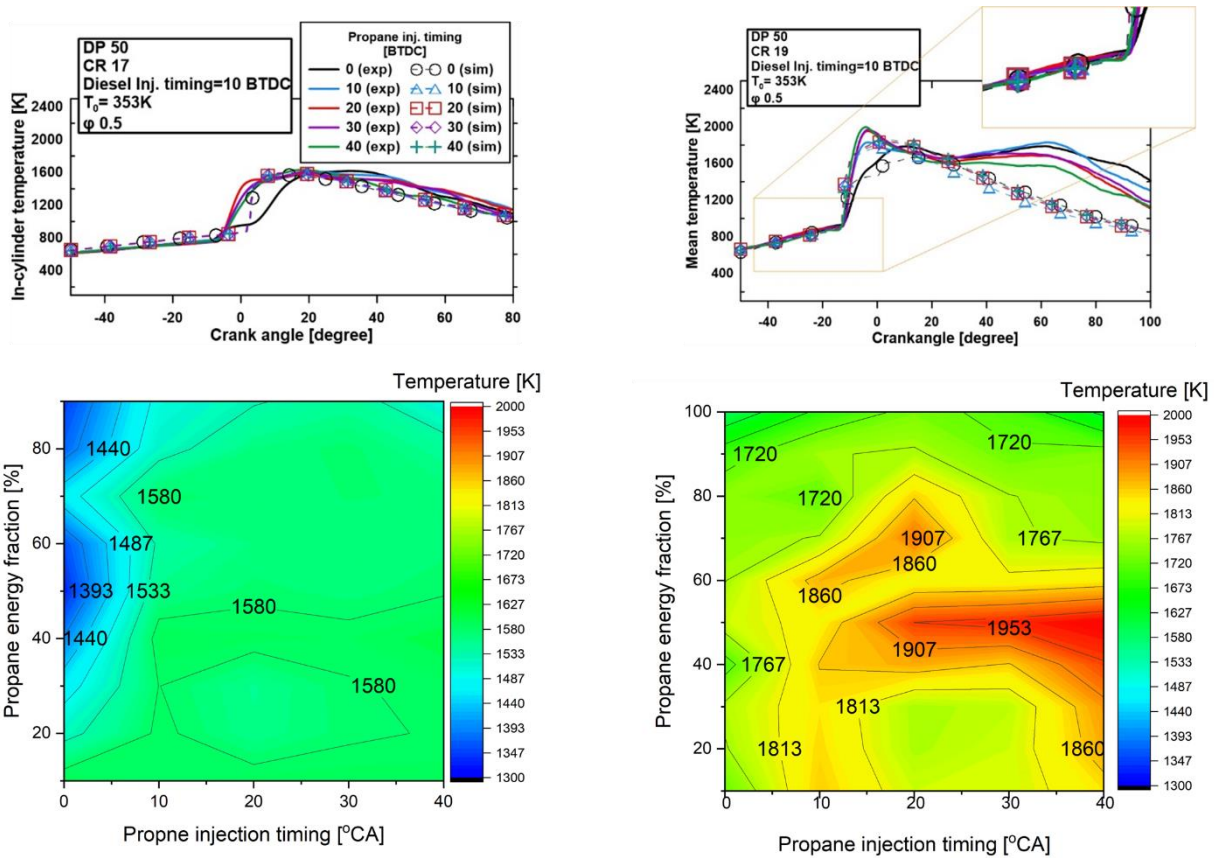




**Figure 4.3** HRR under propane energy fractions of 10-100% for propane injection timings of 0°-40°BTDC and compression ratios of a) 17 and b) 19.

HRR is an important combustion parameter obtained by applying the first law of thermodynamics to the in-cylinder gas pressure. The phases of combustion are classified using HRR. The Start of Combustion (SoC) and the End of Combustion (EoC) were determined from the HRR profiles. Figure 4.3 shows the comparison of HRR for various propane injection timings from 0°BTDC-40°BTDC, propane energy fractions, and compression ratios of 17 and 19. The heat release rate of compression ratio 17 is lower than that of compression ratio 19. The increase of propane energy fraction from 10% to 50% enhances the peak of HRR, while increasing it above 50% resulted in a reduction of the peak of HRR for both CR17 and CR19. It was noticed that low quantity of propane benefits the early injection strategy with an energy fraction of propane below 50%. Better atomization characteristics combined with longer ignition delay enhance the reactivity of the fuel, consequently producing better combustion quality. A higher quantity of propane above 50% reduces the reactivity of propane due to the high research octane number in the fuel. The second peak of the HRR decreased as the propane ratio rose, delaying the combustion phase [119].

In the case of propane energy fractions above 50%, the highest peak of HRR was produced at a 20°BTDC propane injection timing. The non-reactive effect of propane can be observed clearly at DP90 with a 0°BTDC propane injection timing. The propane was injected in the position after diesel auto ignition occurs. The development of HRR significantly decreased in the position that propane was injected. It can be noticed that at CR19, the HRR was activated earlier than for diesel. This indicates that propane provides the auto ignition reaction in the combustion process. This behavior can be observed at a propane injection timing of 20°BTDC or earlier. Moreover, an auto ignition test for 100% propane (DP100) was conducted even though a low peak pressure and peak HRR were produced.



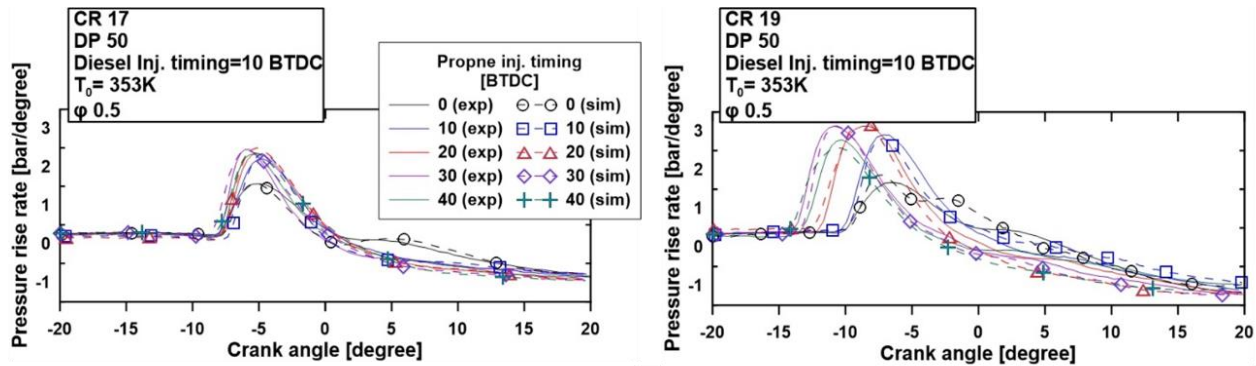
**Figure 4.4** In-cylinder temperature under propane energy fractions of 10-100% for propane injection timings of 0°-40°BTDC and compression ratios of a) 17 and b) 19.

Figure 4.4 shows the experimental and simulation data of the in-cylinder temperature under propane energy fractions of 10-100% for propane injection timings of 0°-40°BTDC and compression ratios of a) 17 and b) 19. The earlier propane is injected to the chamber, the lower the

ambient temperature produced, which will affect the temperature required for the auto ignition event. In the condition of CR17, in the in-cylinder temperature trace, the highest peak temperature was produced in the main combustion area. This indicates the slow combustion of propane, even when it occurs after the diesel auto ignition process. The significant development of temperature mostly occurs after the diesel auto ignition area. This can be observed by comparing the 0°BTDC propane injection timing with the other propane injection timing cases. At a 0°BTDC propane injection timing, significant development of temperature occurred earlier compared to the other propane injection timings. This indicates that the propane fuel does not provide auto ignition behavior in the CR17 condition and delayed the auto ignition characteristics of diesel. The propane was injected at temperatures of 673 K at 40°BTDC, 721 K at 30°BTDC, 754 K at 20°BTDC, 773 K at 10°BTDC, and 1310 K at 0°BTDC. Even though it was injected at temperatures exceeding the auto ignition temperature of propane (481 K), misfire was spotted in the case of a 100% energy fraction of propane. Better spray quality could improve the auto ignition characteristics of propane by increasing the injection pressure for future study.

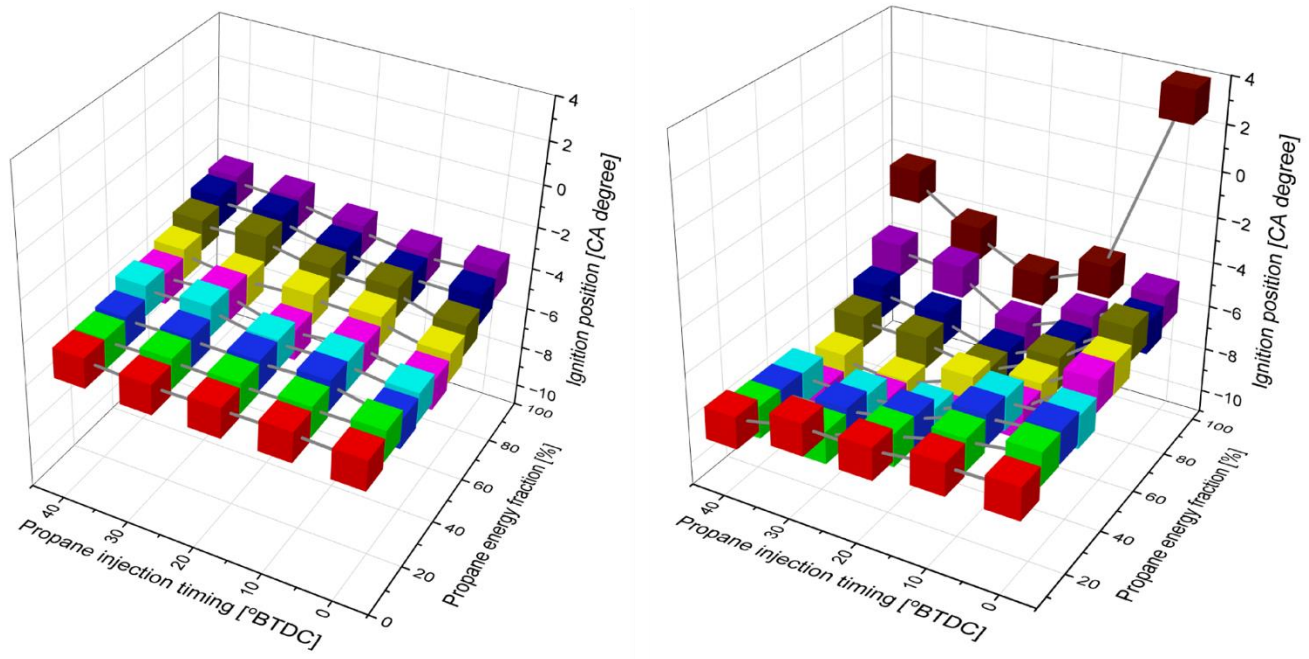
The development of temperature and max in-cylinder temperature for the propane energy fraction and propane injection timing variations at CR 19 are shown in Figure 4.4b. By observing the development of the in-cylinder temperature trace, it was noticed that a significant development of temperature occurred earlier than the diesel auto ignition area for propane injection timings of 40°-10°BTDC, which is much higher compared to CR17. This indicates the auto ignition behavior of propane. Moreover, it occurs earlier than the auto ignition of diesel. The addition of propane produces higher temperature development in the early stage of combustion (before 0°CA). The second temperature increase was noticed at 28°CA for all propane injection timing cases. It seems that propane fuel could not perform perfect combustion in the early stage of combustion. The low temperature of fuel reduces the ambient temperature. Moreover, the propane was injected in the liquid phase, which makes it harder for the heat transfer process. For that reason, LPG produce lower NO<sub>x</sub> emissions due to the lower temperature inside the engine [120], which agrees with a previous study using an LPG direct injection strategy [22]. An improvement of the max in-cylinder temperature was noticed for CR 19 for all SOIs of propane and propane energy fraction cases. As mentioned before, at CR 19, the highest peak temperature was produced in the early-stage reaction which occurs in the BTDC area due to the reactivity of propane. In the mixing-controlled combustion area, there is not a significant discrepancy of peak temperature. For that reason, there

is an insignificant maximum temperature gradient in the CR17 condition. Even so, there are similar behaviors of the maximum in-cylinder temperature trace for both compression ratios. The steady improvement of the maximum in-cylinder temperature was noticed under a 50% propane energy fraction by increasing the propane energy fraction and by injecting propane earlier than 20°BTDC. In the case of a 10°BTDC propane injection timing, it produces a slightly higher temperature compared to 0°BTDC and 20°BTDC propane injection timings. This is caused by unaffected ambient temperature degradation due to the early propane injection. Consequently, it improves the auto ignition characteristics of diesel. The maximum in-cylinder temperature becomes lower when the propane energy fraction is greater than 50%. In this condition, the earlier the propane injection timing, the lower the maximum in-cylinder temperature produced.



**Figure 4.5** PRR under a propane energy fraction of 50% for propane injection timings of 0°-40°BTDC and compression ratios of a) 17 and b) 19.

Figure 4.5 shows the pressure rise rate (PRR) of the engine for compression ratios of a) 17 and b) 19 with the variation of injection timing from 0°-40°BTDC and a percentage of propane of 50%. Propane has a faster rate of flame propagation than LPG-air mixtures, as demonstrated by the significantly higher values of  $P_{max}$  and  $(dP/dt)_{max}$  [121]. Because of this, high pressure rise rates are produced, which, if an adequate proportion is not given, can harm engine components [122]. The increase of propane fraction up to 60% produces a higher MPRR. However, an addition fraction of propane of more than 50% shows the tendency to reduce the MPRR for both CR 17 and 19. Lean propane operation conditions reduce combustion temperatures and lower NOx formation without the need for expensive after-treatment by slowing the high flame speed and pressure rise rate [122]. Even so, CR 17 shows a significant degradation of MPRR as the propane fraction increases above 50% and when the early injection timing was applied.



**Figure 4.6** SoC of dual direct injection fuel under different propane energy fractions, SOI of propane, and CRs of a) 17 and b) 19.

Ignition delay is one of the important parameters to identify the combustion characteristics produced in combustion. In the case of the direct injection strategy, the characteristics of the fuel and spray play larger roles that affect the ignition delay and combustion characteristics. A fuel that poses higher volatility has a higher possibility to produce better combustion quality as a longer ignition delay is applied. Due to its strong resistance to auto-ignition, which lengthens the ignition delay and allows for additional mixing before combustion, fuels like petrol have value in a CI engine. In this study, propane was expected to have a similar characteristic as it has a higher RON and much lower boiling point compared to gasoline. Figure 4.6 shows the SoC of the RCEM with the variation of propane energy fraction, SOI of propane, and compression ratio. The ignition delay was calculated by the interval of SOI of the diesel until the ignition occurs. In the case of 100% propane, the ignition delay was calculated from the SOI of propane. At CR 17, there were no significant fluctuations in the ignition delay as the energy fraction of propane increases and the SOI of propane changes. The auto ignition produced by diesel was a misfire for the propane 100% test at all SOI values of propane. A lower energy fraction of diesel slightly increases the ignition delay. The auto ignition of diesel without the interference of propane can be observed at a 0°BTDC



SOI of propane. At the same auto ignition temperature, a lower fraction of diesel produces a weaker PRR and HRR which makes the ignition location fluctuate. However, the difference is very small and can be negligible. The longest ignition delay was produced at DP90% and 40°BTDC, which has an auto SoC at 3°CA BTDC.

The auto ignition reactivity was identified at CR19. It was able to produce combustion at 100% propane, which is an indication of the reactivity of propane in the combustion process. Faster ignition is produced with an increase of the propane energy fraction. Moreover, the longer ignition delay as the early SOI of propane was applied enhanced the reactivity of fuel and improved the reduction of the ignition delay. The earliest SoC was produced at DP50 and 40°BTDC which has an auto SoC at 9.8°CA BTDC. However, the ignition delay starts to happen more slowly as the propane content exceeds 50%. The increase of fuel quantity with the constant fuel injection pressure increases the possibility of larger fuel droplet production. The low temperature characteristics of liquid propane reduce the reactivity of fuel on combustion and decrease auto ignition characteristics. At this condition, the delay of ignition increased significantly as the early SOI of propane was applied.

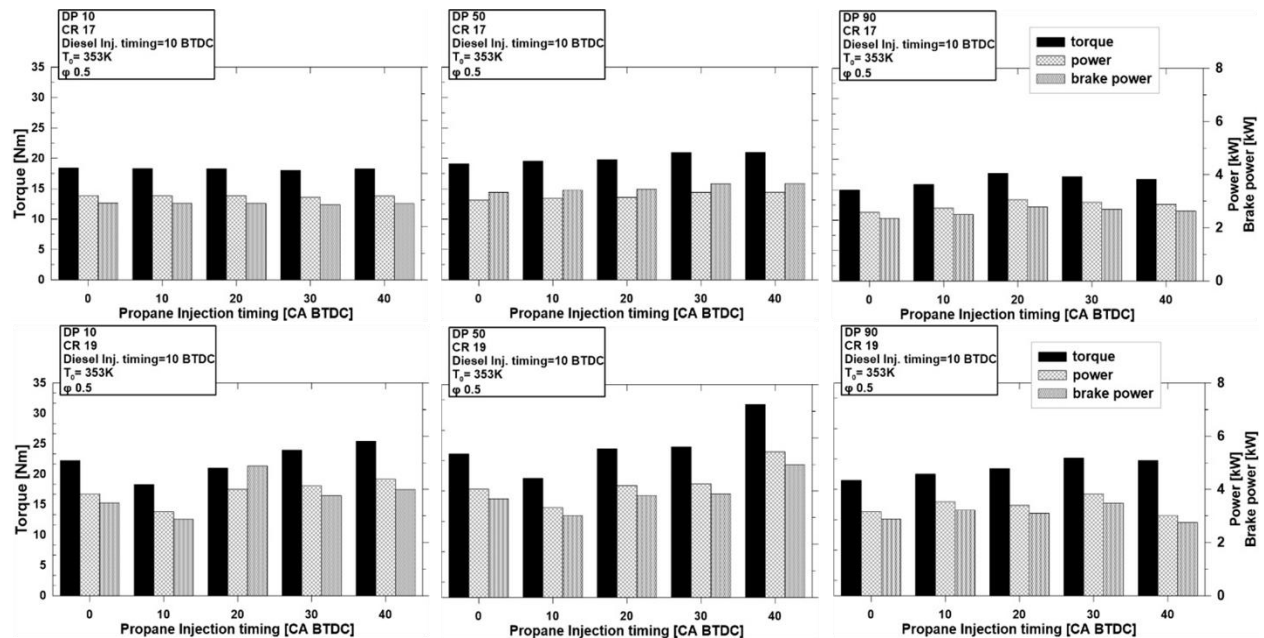
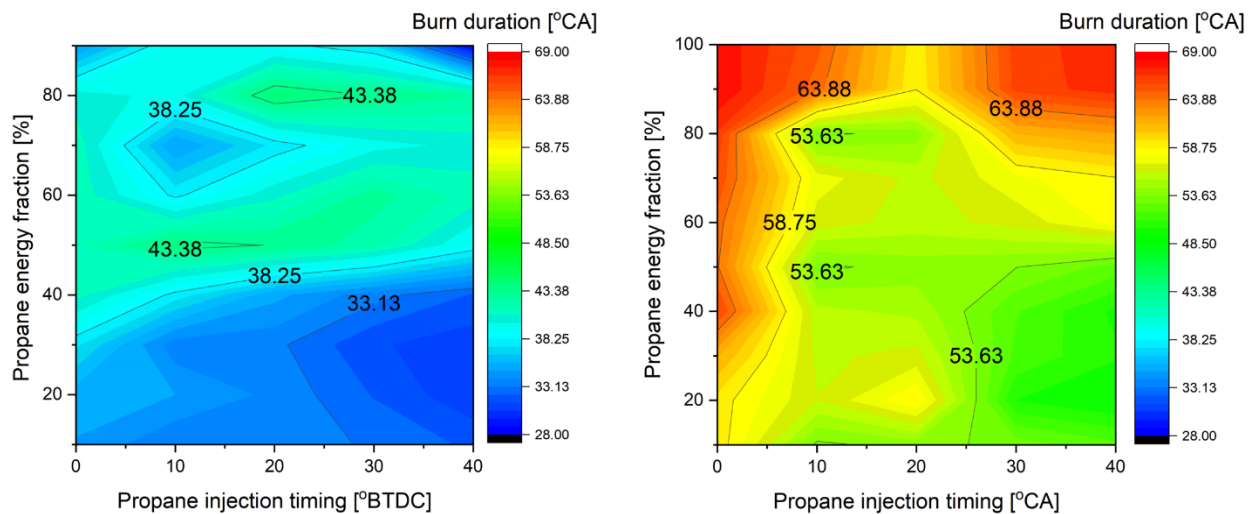


Figure 4.7 Torque, brake power, and indicated power.

Furthermore, the analysis of torque, indicated power, and power of the experiments in RCEM for the dual direct injection application is shown in Figure 4.7. A higher power output was attained at the higher compression ratio. This attribute also can be applied by increasing the propane fraction up to 50%. A higher power also can be achieved by injecting propane earlier for both CR17 and CR19. A slight improvement of power was obtained at late propane injection timings for lean fractions of propane and become stronger when a higher CR was applied. For rich fractions of propane, consistent degradation of power for both CR17 and CR19 was observed. This behavior can also occur when the early propane injection timing is applied.

#### 4.1.2 Combustion duration

Data on heat release can be used to predict when the combustion will take place. The duration of combustion, which also affects emissions and thermal efficiency, is referred to as the burning time. At the top of the compression stroke (TDC), in an ideal engine, all of the energy from combustion would be instantly released. Hence, a high HRR and temperature develop at the premix combustion phase as the main energy consumption. However, since all fuels have a limited rate of combustion, some fraction of fuel remains unburned in this stage. As a result, a mixed controlled combustion phase developed because a given amount of fuel burned in the premix combustion phase produced less power than the ideal cycle would have, which decreases the thermal efficiency. Therefore, by comparing the burning position to the crank angle, the combustion time was calculated.

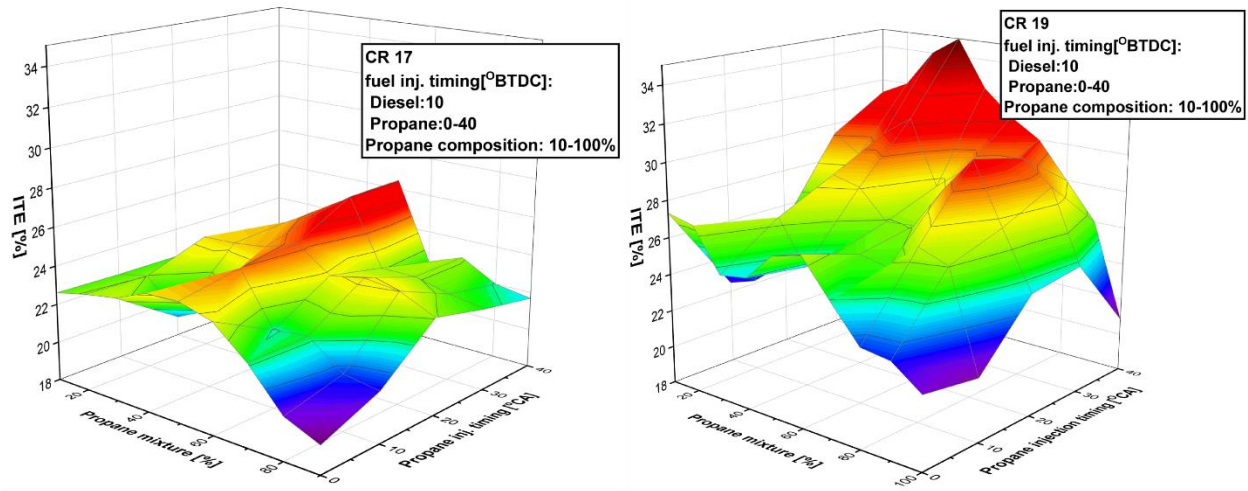


**Figure 4.8** Combustion duration.

The combustion duration with a dual direct injection application strategy is shown in Figure 4.8. The combustion duration was calculated as the interval between the start of combustion (CA10) when approximately 10% of the total thermal value of the fuel is supplied and the end of combustion (CA90) is when 90% of the total heat value of the fuel is supplied. The increase of the propane energy fraction has the tendency to produce a longer combustion duration. The non-reactive characteristics of propane direct injection reduce the reaction in the premix combustion phase and produce a lower peak pressure. Consequently, the combustion duration is lengthened due to the higher temperature and HRR at the mixed controlled combustion phase due to the late combustion reaction, which decreases the efficiency of combustion. Improving the reactivity of propane by increasing the compression ratio from 17 to 19 produces a significantly longer combustion duration. This phenomenon occurs due to the significant improvement reaction in the premix combustion phase and earlier auto ignition, which makes the calculation of the mass burn fraction occur earlier. However, at this condition, the higher temperature and HRR also identified at the mixed controlled combustion phase indicate rich unburn fuel at late combustion phases. Consequently, a significant combustion duration was produced. Under a 50% propane energy fraction, a shorter combustion duration was produced when the early SOI of propane was applied. A better air-fuel mixture due to a longer ignition delay improves the reactivity of propane and enhances the combustion reaction in the premix combustion phase. However, a longer combustion duration was produced at the early SOI of propane when the energy fraction of propane was more than 50%. At CR 17, a reduction of the combustion duration was produced at a 90% propane energy fraction. In this condition, the reaction mostly occurs from the lean diesel fraction.



## Efficiency



**Figure 4.9** Indicated thermal efficiency.

Figure 4.9 shows the indicated thermal efficiency of the engine at compression ratios of 1) 17 and b) 19, with the variation of injection timing from 0°-40°BTDC and percentage of propane from 10-100%. The transition of compression ratio from 17 to 19 improved the ITE significantly. The ITE shows similar behavior for both compression ratios. The ITE with less than 50% propane showed improvement when the propane was injected earlier. Applying a lower quantity of propane at a constant fuel injection pressure reduces the possibility of larger fuel spray droplets and ambient temperature reduction. In this condition, earlier injection timing, which has a longer ignition delay, produces a better air fuel mixture and enhances the quality of combustion. In lean mixtures of propane, the lowest ITE when the propane and diesel were injected at the same time (10° BTDC). An improvement of the ITE occurred when propane was injected after the diesel injection timing (0°BTDC).

With more than 50% propane, early injection timing of propane produced a lower ITE. This requires a higher ambient temperature and pressure as the proportion of propane increased due to the high-octane characteristics of propane. In non-reactive conditions, the liquid phase of propane will reduce the in-cylinder temperature and cause disturbance to the diesel auto ignition process. With early propane injection timings, the higher quantity of propane enhances the possibility of in-cylinder wall wetting, causing a cylinder wall temperature reduction and producing larger fuel

droplets around the cylinder wall. Improvement of the ITE at propane injection timings of 20°-30°BTDC was observed. Significant degradation of ITE occurred when propane was injected closer to TDC. The lowest ITE was produced when 100% propane was applied. The best achievement of ITE for CR 17 and 19 occurs at 40% propane and a 40° propane injection timing.

#### 4.2 In-cylinder Temperature distribution

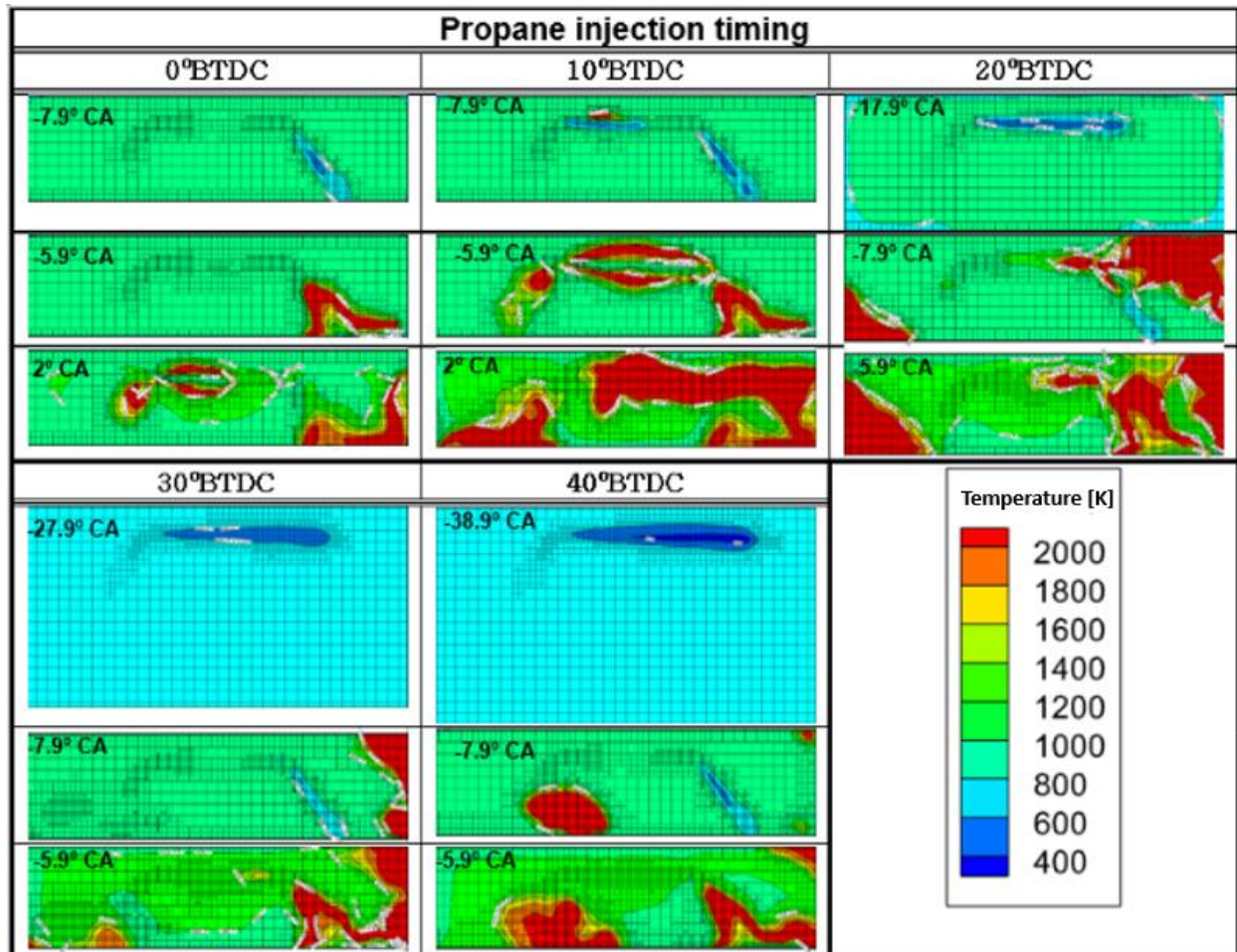


Figure 4.10 Temperature distribution.

The in-cylinder temperature at PD50, CR 19, and propane injection timings of 0°-40°BTDC are illustrated in Figure 4.10. The results show the effect of the early propane injection timing to the diesel auto ignition characteristics and the development of temperature when propane was injected in the combustion area. At a 0°BTDC propane injection timing, the auto ignition characteristics of the diesel were observed without intervention of propane. The ignition delay can

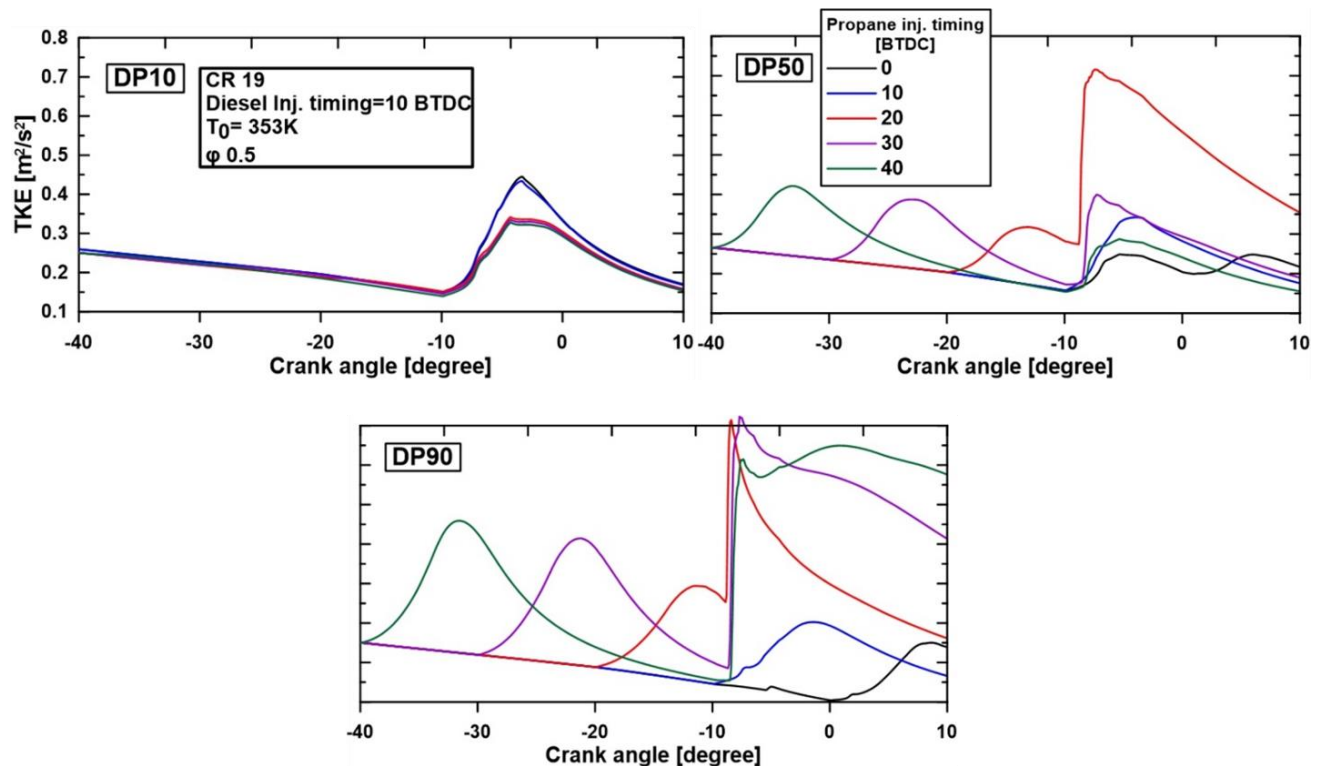
be identified the moment after diesel was injected without any significant temperature increase around the spray area. The auto ignition of propane that occurs after TDC inhibits the temperature propagation that is produced from diesel auto ignition. The results at 10°BTDC confirm that propane ignites faster compared to diesel. However, this occurs due to the higher compression ratio being applied and it became less reactive as the fraction of propane increased. For early propane injection timings (30° and 40°BTDC), the development of temperature starts at the wall cylinder and around the surface of the piston. This indicates the accumulation of fuel in a particular area while the delay of ignition in the process known as wall wetting. The fuel droplets that adhere to the wall will start a fire along with the cylinder wall in a vertical direction, concentrating heat and pressure on the outside of the cylinder, leaving the center of the cylinder at a lower temperature. The higher concentration of fuel impingement causes a decrease of the cylinder wall temperature. Consequently, auto-ignition resistance is promoted, resulting in a higher unburnt fuel concentration and CO emissions [123]. At propane injection timings of 20°, 30°, and 40°BTDC, diesel was injected at the propane auto ignition area. This increases the temperature of diesel spray and reduces the ignition delay of diesel. This temperature development became weaker as the early propane injection timings were applied. It was identified that the 40°BTDC propane injection timing produces the lowest diesel spray temperature compared to 20° and 30°BTDC propane injection timings.

## **4.3 Flow analysis**

### **4.3.1 Turbulent kinetic energy**

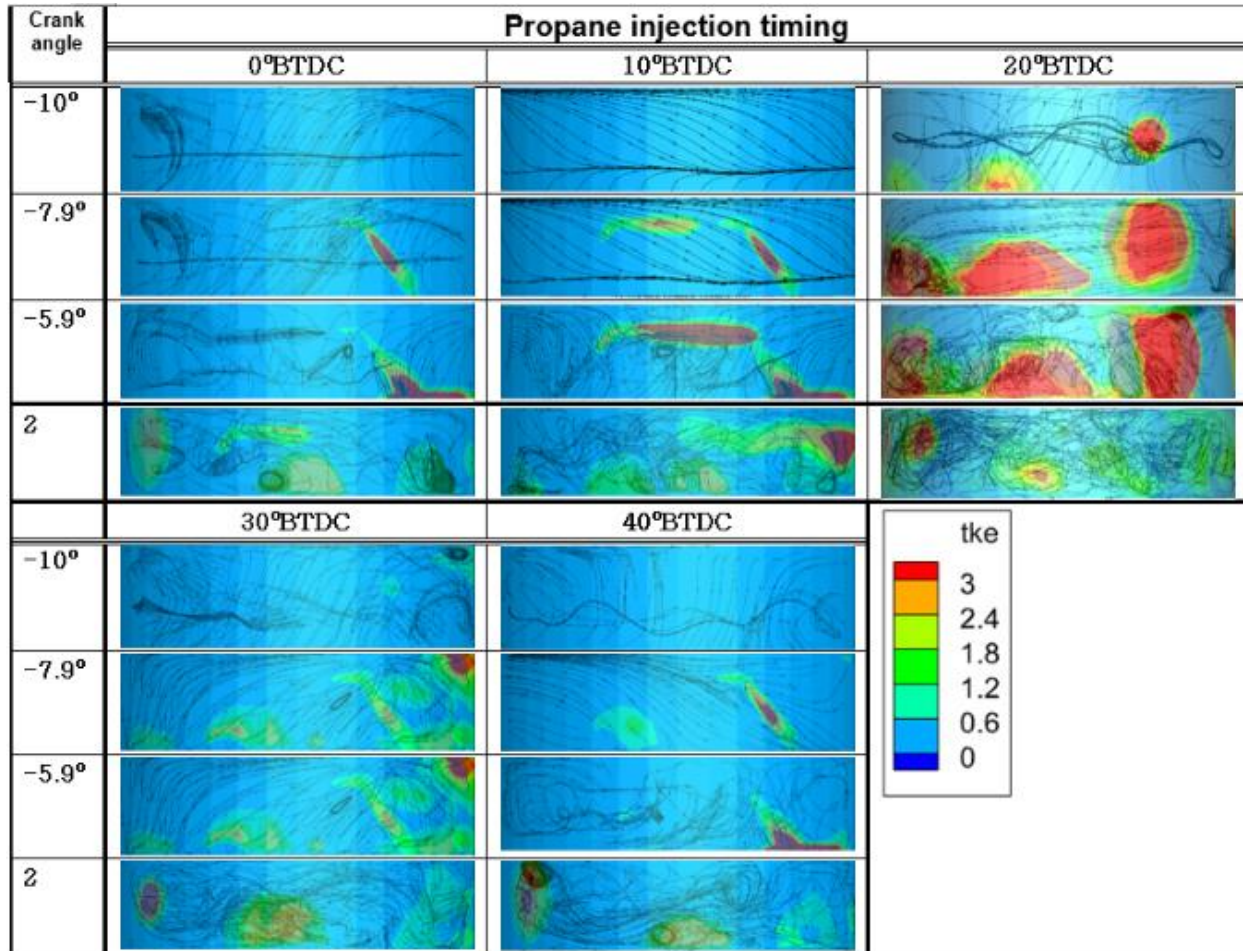
Most of the turbulence that occurs inside the combustion cylinder is caused by large-scale gas motion that splits into smaller vortices. However, spray-induced turbulence, another potential source of turbulence, is frequently disregarded. This turbulence is created when a fuel spray with a high injection pressure imposes regionally high velocities and significant velocity gradients, which can be utilized to improve fuel-air mixing [124]. In the internal combustion engine, the TKE is mostly affected by the intake flow characteristics. The development of TKE starts from the intake step and is expected to improve fuel spray atomization. For that reason, it is difficult to identify the effect of fuel spray itself on the TKE. In this study, the experiment was started at bottom dead center, which is without any initial TKE development. The effect of fuel spray on

TKE can be analyzed without the intake flow interference. Figure 4.11 illustrates the variation of turbulent kinetic energy in relation to different propane energy fractions and propane injection timings. According to the graph, the lean mixture of propane does not produce a significant effect on the early development of TKE. However, it lowers the peak TKE in the auto ignition area if an earlier propane injection timing is applied. The turbulent flow is destroyed by the fuel injected into the injector nozzle. A higher TKE results from the breakdown of the tumbling vortex, which increases turbulence flow. The ambient TKE on the fuel injection timing is one of the parameters that influences the peak of TKE. In the dual fuel injection, there are two peaks of TKE produced by the first and second injections. By increasing the quantity of propane, the early development of TKE by propane injection becomes greater. It reaches the peak of early TKE development 7°-8°CA after fuel injection and becomes lower as the crank angle continues its compression stroke. At 40°BTDC, it produces the highest peak of early TKE as the propane was injected at the highest ambient TKE compared to the other propane injection timing. The highest peak of the second TKE was produced at a 20°BTDC propane injection timing as the diesel was injected at the highest point of first stage TKE compared to the 30° and 40°BTDC propane injection timings.





**Figure 4.11** Streamline flow visualization from the TKE flow pattern of dual direct injection fuel (diesel-propane) at CR 19, a propane energy fraction of 50%, and propane injection timings from 0°-40°BTDC.

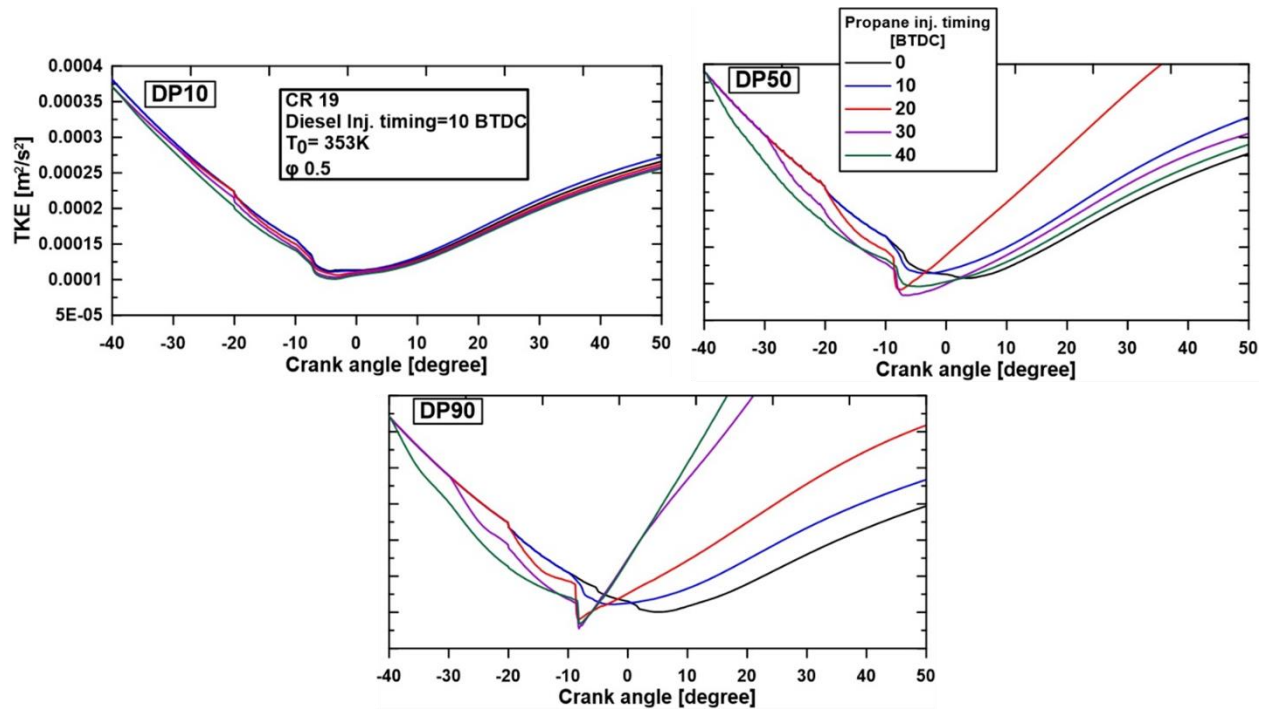


**Figure 4.12** Streamline flow visualization from the TKE flow pattern of dual direct injection fuel (diesel-propane) at CR 19, a propane energy fraction of 50%, and propane injection timings from 0°-40°BTDC.

Figure 4.12 shows the TKE starts at 10°BTDC, which corresponds to the diesel injection timing. It identifies the effect of propane fuel injection on the surrounding air flow and its effect before diesel injection, the moment of diesel injection, ignition, and late propane injection event. The unaffected air flow from propane injection is also shown in the propane injection timings of 10° and 0°BTDC. It can be used as the comparison between the standard TKE and TKE affected by propane injection. The TKE at a 40°BTDC propane injection timing at 10°CA shows similar

behavior as the TKE which unaffected by the propane injection. It shows the degradation of TKE after it reaches the peak point and calms down at the moment it reaches diesel injection timing. At the 20°BTDC propane injection timing, the highest TKE was observed for all events. Diesel was injected when the TKE reached the highest point. The higher TKE contributes to the better air fuel mixture and improves the auto ignition characteristics of the fuels. This causes enhancement of the TKE growth at the main combustion event.

### 4.3.2 Turbulent kinetic viscosity



**Figure 4.13** Turbulent kinetic viscosity.

Figure 4.13 depicts the characteristics of the turbulent kinetic viscosity showing the effects of the propane injection timing variation and propane energy fraction. The turbulent kinematic viscosity and turbulent eddy viscosity both refer to the parameter of momentum flux when a small vortex is present in the flow. The non-linear interaction between the large and small scales of motion causes the eddy formation, which spreads the fluid's kinetic energy over a variety of eddy sizes. Large eddies absorb energy from the mean flow, then dissipate it at the Kolmogorov microscales by transferring it to smaller scales [125]. A steady flow of energy from the mean motion must be fed to the turbulent fluctuations at the largest scales to maintain turbulence. At the

higher kinetic energy, the fluid flow dissipates the eddy formation and produces a lower TKV. At the smallest eddy scales, the energy is dissipated into heat by viscous effects. In the DP90 for 30° and 40°BTDC SOI of propane, there was no indication of dissipation of TKV in the mixed controlled combustion phase area. As a result, there is very little indication of combustion or the formation of a flame in this area. Figure 4.13 shows the reduction of TKV on the compression stroke, followed by the increment to a peak as the expansion stroke occurs. The TKV poses high sensitivity on the change of propane injection timing and the quantity of the propane that is injected into the chamber. Propane has a greater effect on this phenomenon due to its better atomization characteristics compared to diesel. The droplet diameter decreases as atomization characteristics increase because there is a greater likelihood of atomization and more intense turbulence. However, after a certain amount of inlet pressure, the droplet diameter gradually increases as a result of particle collisions [126]. For this reason, there was a significant decrease on the TKV in the propane injection timing area. The development of TKV on the expansion stroke was mostly affected by the amount of peak TKE. The higher TKE was produced, the more energy available for turbulent fluctuations formation.

#### 4.4 Conclusion

This study used simulations and experiments to determine how the energy fraction of propane affected the dual direct injection RCEM's in-cylinder characteristics. CONVERGE computational fluid dynamics were used to study temperature distribution, velocity distribution flow, and turbulent kinetic energy. From this study, the following conclusions can be drawn.

1. A non-reactive combustion characteristic of propane was observed at CR17 as the ignition was only promoted by diesel. Consequently, a reduction of the ambient temperature occurred as propane was injected and the reaction of diesel was prolonged as the fraction of the propane increased and the early propane injection timing was applied. The longest ignition delay was obtained at 7°CA at DP90 for 40°BTDC SOI of propane. The improvement of the reactivity of propane was obtained at CR 19 as the auto ignition of propane was identified before the ignition of diesel and finally, auto ignition was produced at 100% propane.

2. The reactive combustion state of propane (at CR19) increases the mean temperature in the premix combustion phase ( $7^{\circ}$ - $0^{\circ}$ BTDC) significantly. This phenomenon occurs due to the flame produced by propane developing much faster compared to diesel. Consequently, the MPRR and peak pressure increased during combustion. However, it produces a higher HRR in the mixing-controlled combustion phase as the fraction of the propane increases. This results in a longer burn duration and reduces the combustion efficiency.
3. The highest ITE was observed for the lean propane mixtures at early SOI of propane. Early injection poses a higher ignition delay. Hence, it improves the air-fuel mixture and the quality of combustion. The highest ITE was produced at PR40 and SOI of propane at  $40^{\circ}$ BTDC for both CR 17 and 19 with values of 26.4% and 35.2%, respectively. However, with more than 50% propane, a low ITE was produced at early SOI of propane. It has a higher possibility to produce larger droplets in the injection spray. This consequently reduces the reactivity of the fuel due to the low temperature characteristics of liquid propane.
4. Enhancement of the turbulence kinetic energy was obtained as the propane energy fraction was increased. The higher TKE contributes to the better air fuel mixture and improves the auto ignition characteristics of the fuels. The early SOI of propane has the highest advantage on the TKE development in the rich fraction of propane which ends up being consumed to become turbulence kinetic velocity. However, in the DP90,  $30^{\circ}$  and  $40^{\circ}$ BTDC SOI of propane, there was no indication of dissipation of TKV in the mixed controlled combustion phase area. This indicates that there is very little indication of combustion or formation of a flame in this area.

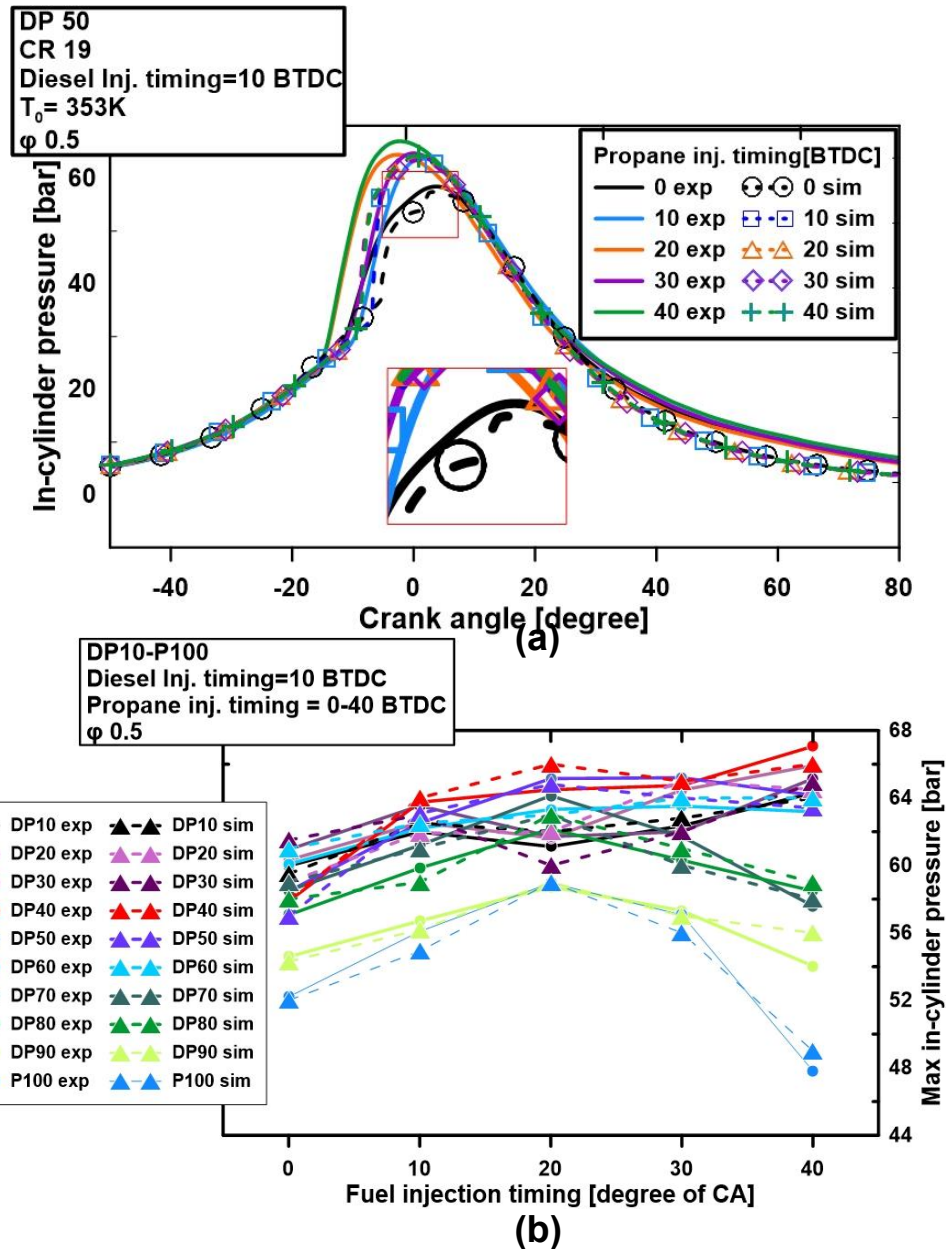


# **5. AN INVESTIGATION OF THE EFFECT OF PROPANE ENERGY FRACTION AND THE START OF INJECTION ON THE COMBUSTION AND EMISSIONS CHARACTERISTICS OF LOW CARBON HIGH-PRESSURE LPG DIRECT INJECTION ENGINE**

In this chapter, the effects of energy fraction and SOI of propane applied on dual fuel injection strategies on low carbon combustion and emissions are investigated with a rapid expansion and compression machine research engine. An experimental system and simulation model were established to investigate in-cylinder combustion performance and emission characteristics. Cylinder pressure, temperature, and heat release rate are three of the factors affecting in-cylinder performance and were used to validate the data from the CFD modeling.

## **5.1 Validation of the CFD modeling on combustion characteristics**

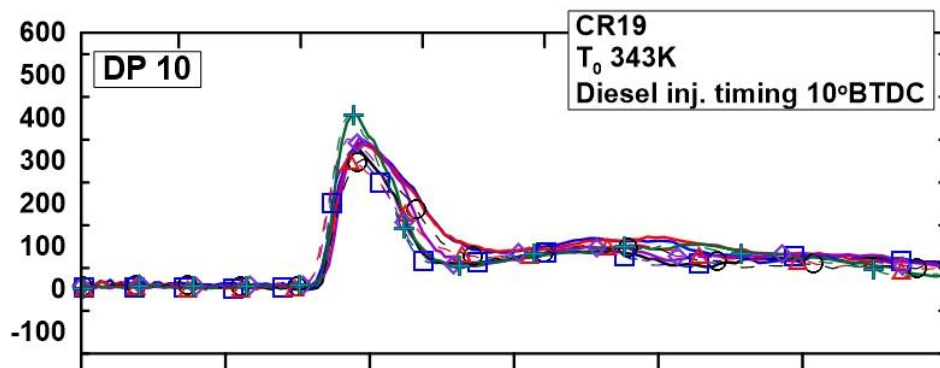
The simulated pressure, heat release rate (HRR), and temperature of all the cases are validated against the experimental data. It can be seen that no significant differences were observed with the simulation-experimental validation data. The simulated and experimental pressure have a good consistency in all these cases and the maximum deviation is less than 5%. The simulation data will be used to analyze the detailed emission propagation on dual-fuel LPG-DI engines.

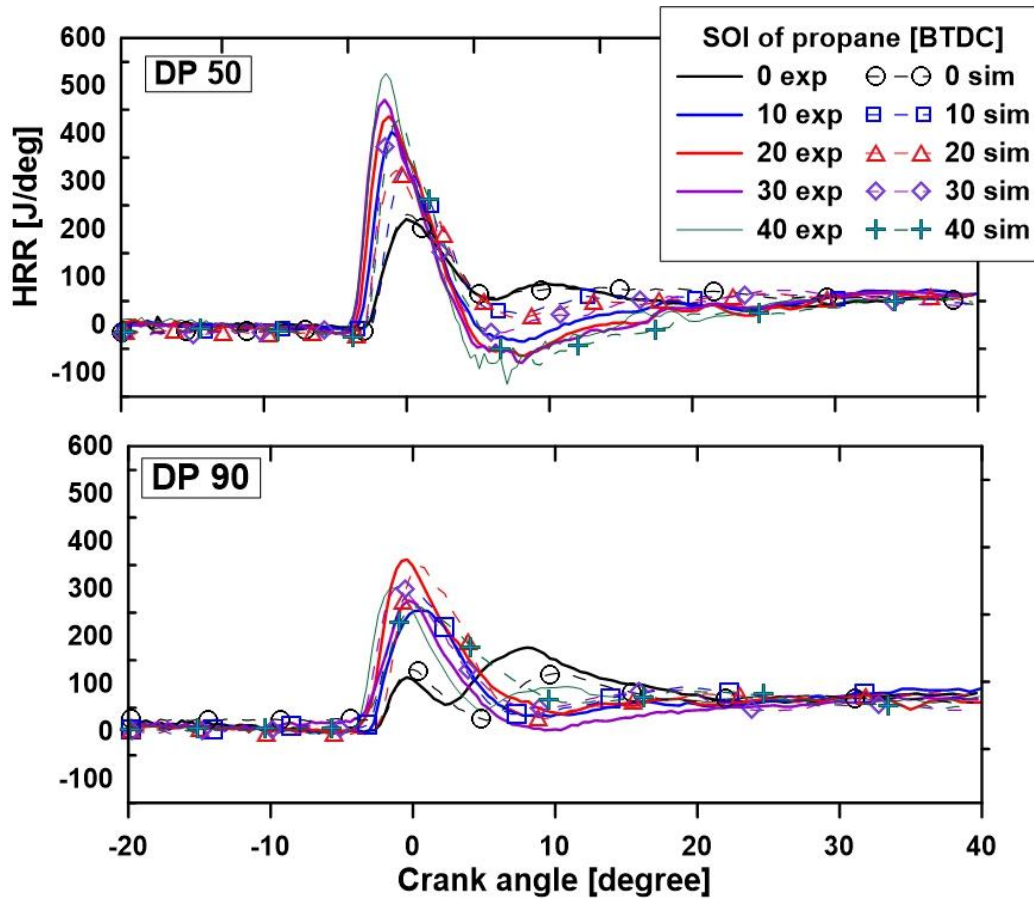


**Figure 5.1** In-cylinder pressure (a) and max in-cylinder pressure (b) of dual direct injection fuel (diesel-propane) under 10%-100% energy fraction and 0°-40°BTDC SOI of propane.

Figure 5.1 shows the experimental end simulation data of in-cylinder pressure and max pressure of dual direct injection fuel (diesel-propane) under variation of SOI and energy fraction of propane. The more reactive combustion can be found at propane energy fractions less than 50% at early propane injection timings. At this condition, 40°BTDC propane injection timing produces the highest in-cylinder pressure compared to all of the propane injection timing variations.

However, when the energy fraction of propane increased above 50% (DP50), a significant drop of the in-cylinder pressure was produced for early and late injection timings. At this condition, it produces the highest in-cylinder pressure at a 20°BTDC propane injection timing. The lowest in-cylinder pressure was produced at DP100, 40°BTDC propane injection timing, i.e., 47.81 bar. Proper combustion was expected using LPG fuel as it has a low evaporation temperature and higher LHV compared to diesel fuel. Hence, it has better atomization characteristics and produces a higher amount of heat released during combustion. However, in the direct injection strategy, propane was injected to the chamber in the liquid phase, which has a very low temperature (-43°C). Furthermore, the current common rail system applied fuel injection pressure is much lower compared to diesel for safety purposes. Consequently, lower atomization characteristics were produced for the propane injection case. This will lower the reactivity of the fuel in a low compression ratio and high quantity of propane condition. As a result, it improves the possibility of wall impingement, which reduces the cylinder wall temperature. Decreasing the in-cylinder temperature reduced the peak cylinder pressure and increased ignition delay, which agrees with the results in previous research by Verde [117]. Furthermore, it affects the ambient temperature of diesel injection conditions. A low ambient temperature would alter the Sauter mean diameter (SMD) distribution, and spray tip penetration, decelerate diesel fuel evaporation, and reduce diesel fuel activation [118].

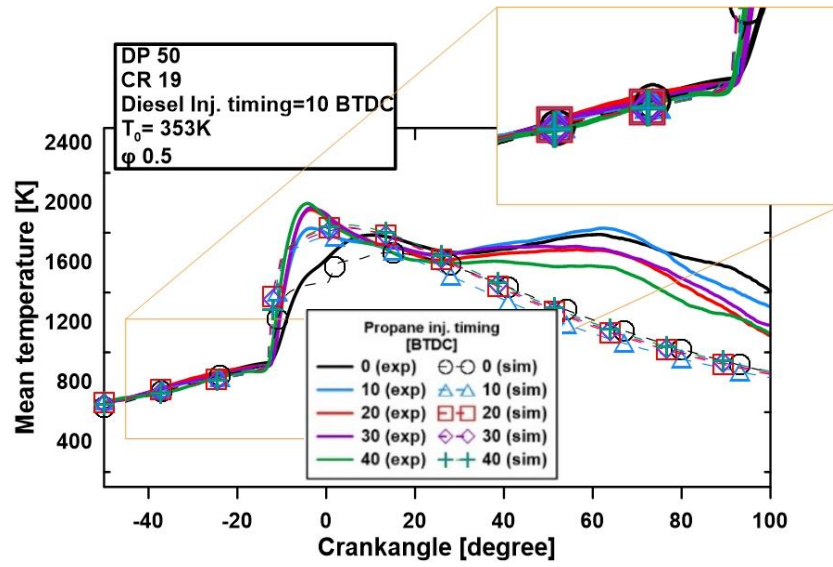




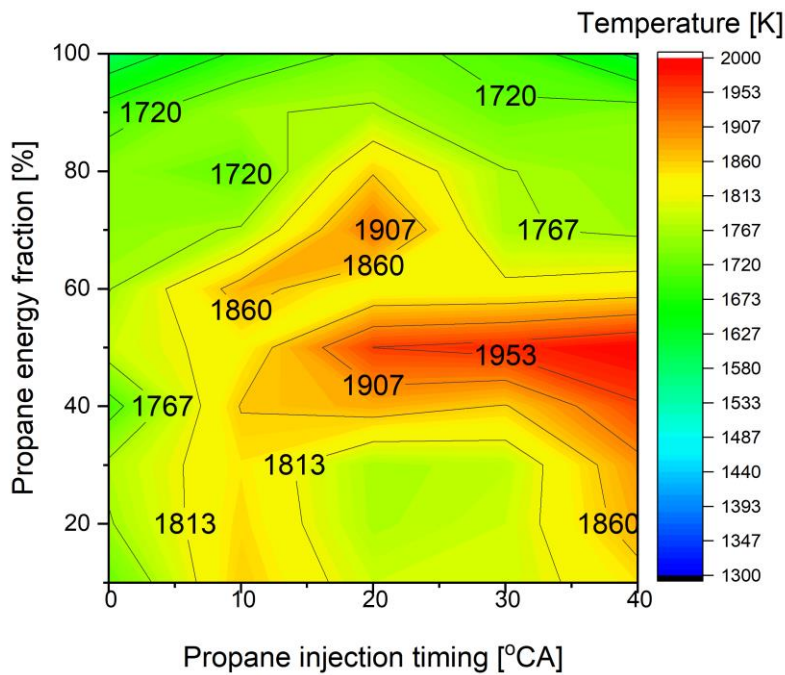
**Figure 5.2** HRR of dual direct injection fuel (diesel-propane) under 10%-100% energy fraction and 0°-40°BTDC SOI of propane.

Heat release rate (HRR) is an important combustion parameter obtained by applying the first law of thermodynamics to the in-cylinder gas pressure. The phases of combustion are classified using HRR. The Start of Combustion (SoC) and the End of Combustion (EoC) were determined from the HRR profiles. Figure 5.2 shows the experimental end simulation data HRR of dual direct injection fuel (diesel-propane) under variation of SOI and energy fraction of propane. The increase of propane energy fraction from 10% to 50% enhances the peak of HRR, while increasing it above 50% resulted in a reduction of the peak of HRR. It was noticed that low quantity of propane benefits the early injection strategy with energy fraction of propane below 50%. Better atomization characteristics combined with longer ignition delay enhance the reactivity of the fuel, consequently producing better combustion quality. A higher quantity of propane above 50% reduces the reactivity of propane due to the high research octane number in the fuel. The second peak of the HRR decreased as the propane ratio rose, delaying the combustion phase [119]. In the case of

propane energy fractions above 50%, the highest peak of HRR was produced at a 20°BTDC propane injection timing. The non-reactive effect of propane can be observed clearly at DP90 with a 0°BTDC propane injection timing. The propane was injected in the position after diesel auto-ignition occurs. The development of HRR significantly decreased in the position that which propane was injected. It can be noticed that at CR19, the HRR was activated earlier than for diesel. This indicates that propane provides the auto-ignition reaction in the combustion process. This behavior can be observed at a propane injection timing of 20°BTDC or earlier. Moreover, an auto-ignition test for 100% propane (DP100) was conducted even though a low peak pressure and peak HRR were produced.



(a)



(b)

**Figure 5.3** Mean temperature (a) and max in-cylinder temperature (b) of dual direct injection fuel (diesel-propane) under 10%-100% energy fraction and 0°-40°BTDC SOI of propane.

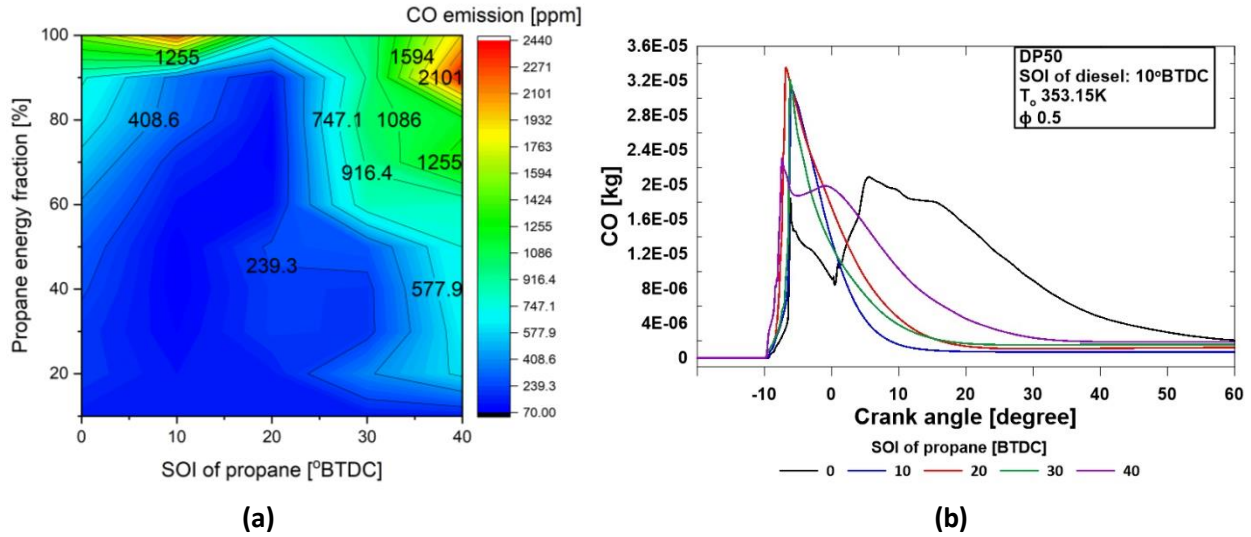
The development of mean temperature and max in-cylinder temperature for the propane energy fraction and propane injection timing variations are shown in Figure 5.3. The addition of propane produces higher temperature development in the early stage of combustion (before 0°CA). It can

be identified by observing Figure 5.3a, the significant temperature increase at 10°CA to 0°CA BTDC. The second stage temperature increase was noticed at 28°CA ATDC for all propane injection timing cases. It seems that propane fuel could not perform perfect combustion in the early stage of combustion. The low temperature of propane reduces the ambient temperature. Moreover, the propane was injected in the liquid phase, which makes it harder for the heat transfer process. For that reason, LPG produces lower NO<sub>x</sub> emissions due to the lower temperature inside the engine [120], which agrees with a previous study using an LPG direct injection strategy [22]. An improvement of the max in-cylinder temperature was noticed for all SOIs of propane and propane energy fraction cases. The highest peak temperature was produced in the early-stage reaction which occurs in the BTDC area due to the reactivity of propane. The steady improvement of the maximum in-cylinder temperature was noticed under a 50% propane energy fraction by increasing the propane energy fraction and by injecting propane earlier than 20°BTDC. In the case of a 10°BTDC propane injection timing, it produces a slightly higher temperature compared to 0°BTDC and 20°BTDC propane injection timings. This is caused by unaffected ambient temperature degradation due to the early propane injection. Consequently, it improves the auto-ignition characteristics of diesel. The maximum in-cylinder temperature becomes lower when the propane energy fraction is greater than 50%. In this condition, the earlier the propane injection timing, the lower the maximum in-cylinder temperature produced.

## **5.2 Effect of energy fraction and SOI of propane on the emissions of a CI engine**

### **5.2.1 Carbon monoxide emissions (CO)**



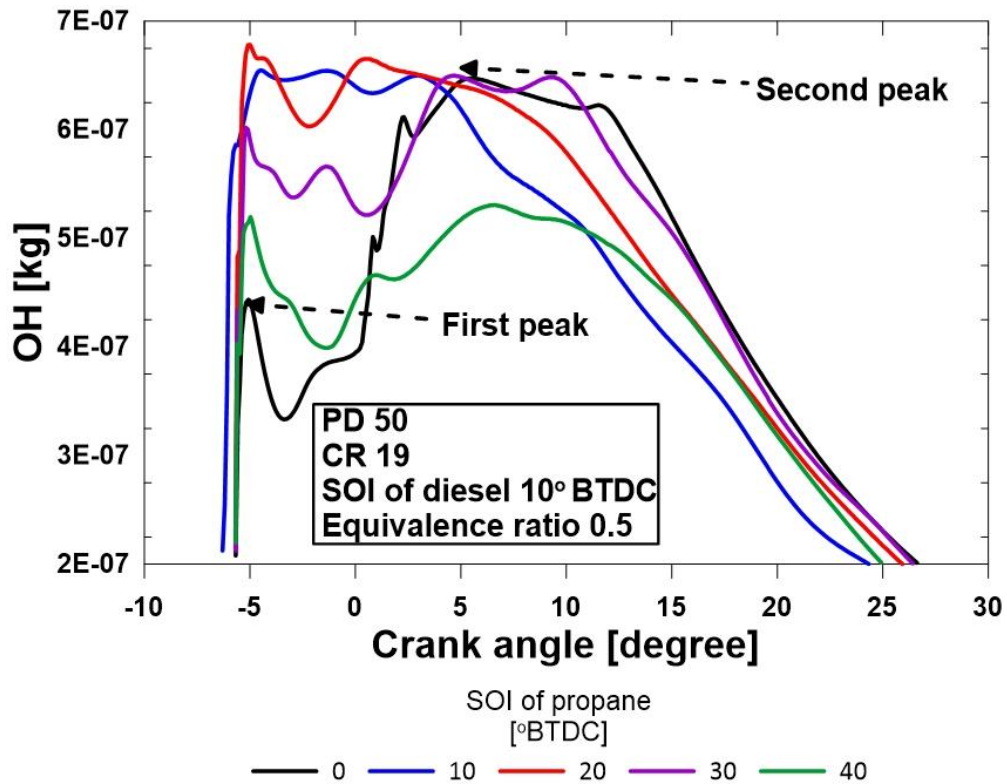


**Figure 5.4** Total CO emission (a) and CO emission (b) of dual direct injection fuel (diesel-propane) under 10%-100% energy fraction and 0°-40°BTDC SOI of propane.

Figure 5.4 shows the total CO emissions with the variation of energy fraction and SOI of propane (a) and the development of CO at SOI 0°BTDC to 40°BTDC (b) in the in-cylinder dual-fuel (diesel-propane) engine. The total CO emissions show a significant increase at 90% or more of propane energy fraction application in dual direct injection CI mechanism. At low propane energy fractions, the higher total CO emission was produced at earlier injection timing. The ideal SOI of propane that results in low CO emissions was exponentially delayed as the percentage of propane increased. Under 60% of propane energy fraction, the total CO emission increases when the late SOI of propane (10°-0°BTDC) is applied. This effect became stronger as the percentage of propane increased. The development of CO emissions during combustion can be observed in Figure 5.4b. It is clear that the formation of CO increases significantly at the crank angle -10° to -4°. It appears that the combustion phase and CO formation are correlated, with CO primarily forming in the CA 0 to CA 10 regions and decreasing dramatically after this point. It shows that the ability to burn carbon content in the fuel after ignition determines the total amount of CO released. Similar behavior of CO development was shown at SOI of propane 0° and 10° BTDC. There were two maximum CO peaks seen under these circumstances and produced a higher total CO emission compared to the other parameters. Low CO emissions are mostly produced by fuels with the ability to provide complete combustion. Propane exhibits a strong indication of auto-ignition resistance because of its high octane number content. Improper SOI of propane delays the



auto-ignition significantly, whether due to the wall wetting under early SOI or late combustion under late SOI. Fuel droplets that attach to the wall will generate fire in the vertical direction along the cylinder wall, causing the distribution of heat and pressure to focus on the outer wall of the cylinder [123]. Leaving the center of the cylinder at the lower temperature. For that reason, the greater the percentage of fuel attached to the cylinder wall, the more difficult it is for fuel to burn perfectly due to un-even temperature distribution and fuel deposits [127]. Consequently, higher total CO emission was produced. This is because the carbon of the fuel did not combust completely under fuel-rich conditions [127], and the main product of heterogeneous oxidation on the surface of unburned char is CO ( $2C + O_2 \rightarrow 2CO$ ) [128].

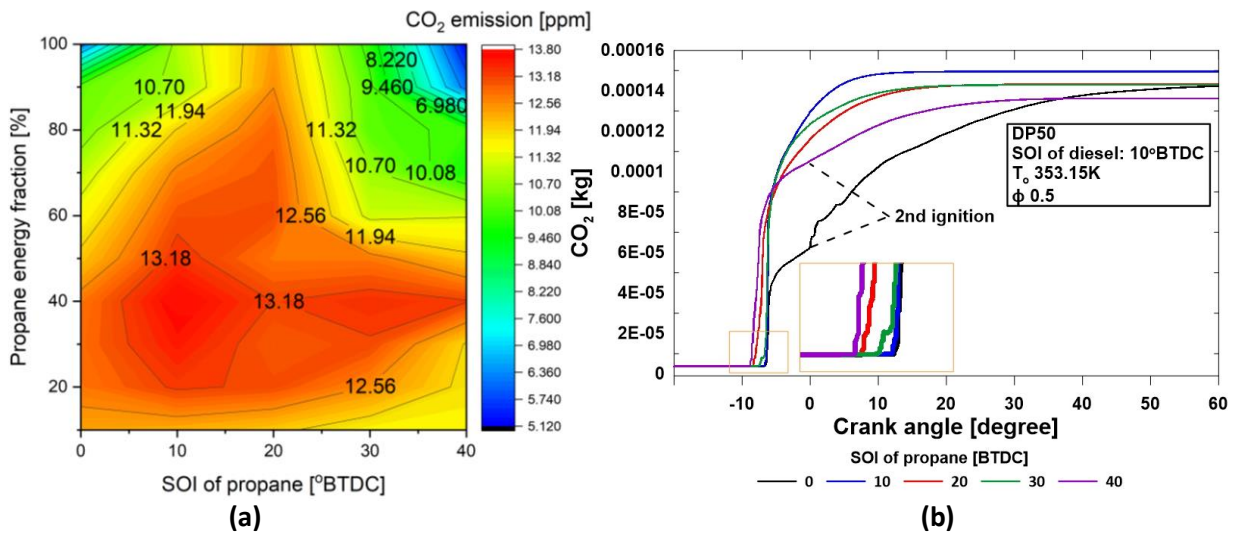


**Figure 5.5** OH formation at PD 50, SOI of propane 0° to 40° BTDC under dual direct injection fuel strategy.

Figure 5.5 shows the OH formation trace of PD 50 at SOI of propane 0° to 40° BTDC during the combustion process. The significance of hydroxyl radical (OH) in combustion kinetics and surface modification manufacturing processes makes it a valuable diagnostic tool. It's a common intermediate in combustion that can show the completeness of combustion and map the flame

structure. When the oxygen has reached its peak during ignition and is propagating quickly, this is considered the ideal condition of combustion. The OH propagation indicates the length of combustion that occurs in the process. Propane application on an LPG-DI engine at CR 19 shows the longer propagation of OH. This is because liquid propane has a high auto-ignition resistance and, when applied to a dual fuel (diesel and propane) LPG-DI engine, exhibits two peaks of OH formation. Indicates a two-stage ignition in the combustion process. The two peak propagations of the OH and CO emissions can be clearly distinguished at 0° and 40° BTDC SOI of propane. This demonstrates the linear correlation between CO and OH formation.

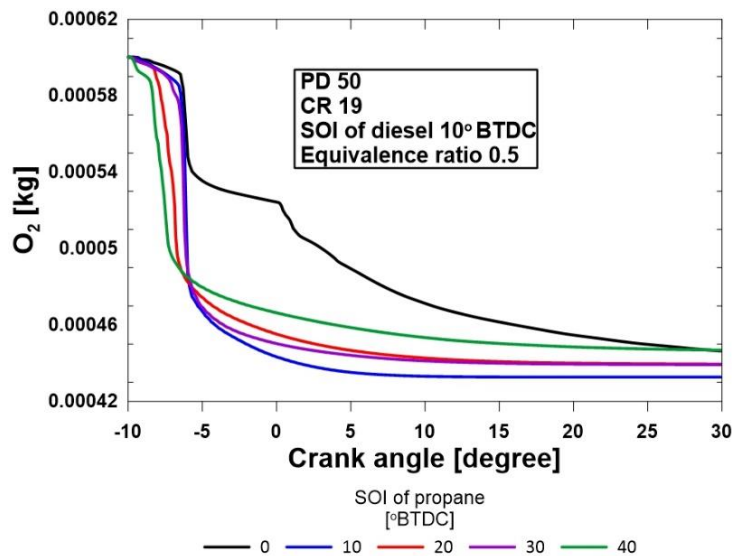
### 5.2.2 Carbon dioxide emissions (CO<sub>2</sub>)



**Figure 5.6** Total CO<sub>2</sub> emission (a) and CO<sub>2</sub> emission (b) of dual direct injection fuel (diesel-propane) under 10%-100% energy fraction and 0°-40°BTDC SOI of propane.

Figure 5.6 shows the total CO<sub>2</sub> emissions with the variation of energy fraction and SOI of propane (a) and the development of CO<sub>2</sub> at SOI 0°BTDC to 40°BTDC (b) in the in-cylinder dual-fuel (diesel-propane) engine. The total CO<sub>2</sub> emission shows a contrary number to the total CO emission. Low propane content led to higher CO<sub>2</sub> emissions; this is in line with the findings of Jeong et al [129]. They found that CO<sub>2</sub> emissions, a fuel mixture with 25% propane content exhibited higher emissions than 5% of propane. While propane with content greater than 50% showed a notable decrease in CO<sub>2</sub>. It shows that applying more than 50% of propane on a direct injection strategy at CR 19 will reduce the quality of the combustion. The CO<sub>2</sub> emission showed

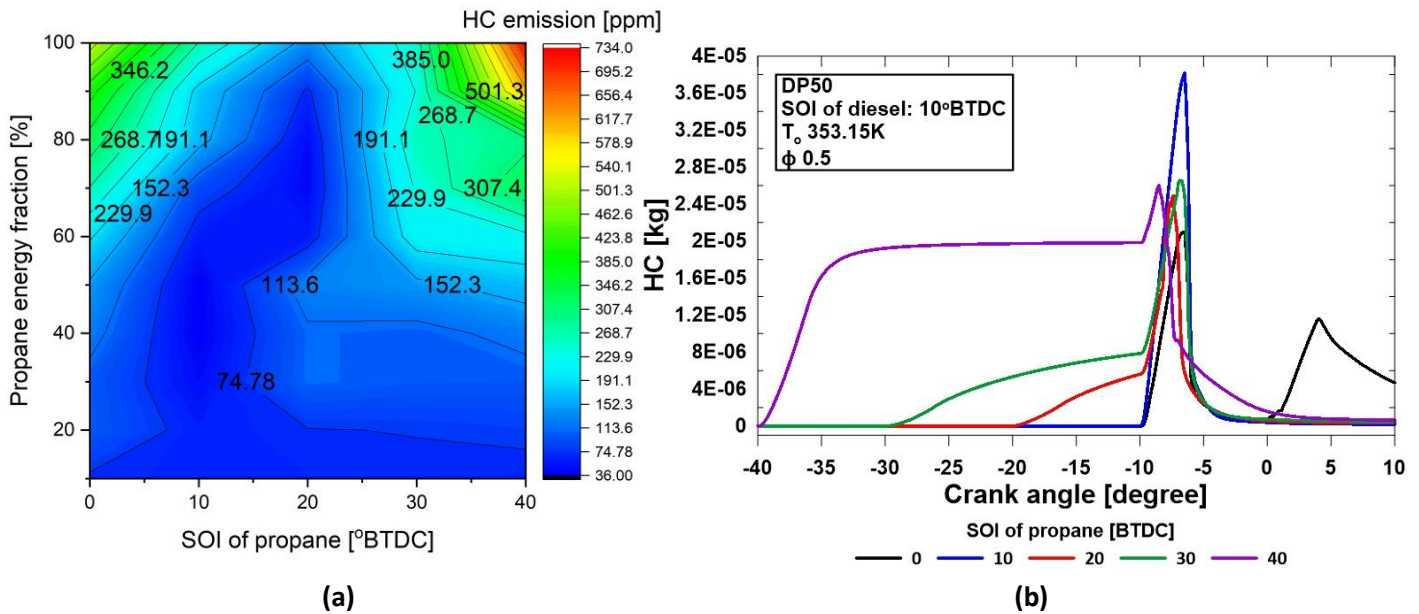
an increase when the early SOI of propane (40°BTDC) was applied on propane under 50%. A lower quantity of propane with constant injection pressure produces better fuel atomization. At this condition, an early SOI of propane enhances the air-fuel mixture and improves the auto-ignition characteristics of fuels (diesel and propane). However, as the propane increased by more than 50%, the early (40°BTDC) and late (0°BTDC) SOI of propane showed a significant reduction in total CO<sub>2</sub> emission. The formation of CO<sub>2</sub> emissions during the combustion process is shown in Figure 5.6b. As shown in the highlighted Figure 5.6b, the formation of CO<sub>2</sub> emission starts from the ignition process. As combustion progresses, it shows a steady increase until it reaches the maximum point. It indicates that the formation of CO<sub>2</sub> was determined by the quality of the ignition in the fuel-rich region. The complete reaction of fuel (diesel and propane) and oxygen will produce a higher concentration of CO<sub>2</sub>. Lower CO and greater CO<sub>2</sub> reflect more effective fuel use and improved combustion quality. Due to the lower C/H ratio of propane compared to diesel [85], less CO<sub>2</sub> is expected for complete combustion. Lean air-fuel ratios can result in instability and insufficient combustion. The use of propane in direct injection and compression ignition at CR 19 demonstrates how the fuel's low auto-ignition characteristics result in increased emissions of CO and HC. Indicate that a higher compression ratio could be used in the propane direct injection compression ignition strategy to improve the propane's auto-ignition properties. The second ignition stage can be identified at SOI of propane 0° and 40°BTDC. At this condition, a lower CO<sub>2</sub> emission was produced compared to the other parameters.



**Figure 5.7** O<sub>2</sub> consumption at PD 50, SOI of propane 0° to 40° BTDC under dual direct injection fuel strategy.

Figure 5.7 shows the O<sub>2</sub> formation trace of PD 50 at SOI of propane 0° to 40° BTDC during the combustion process. PD 10 shows the significant oxygen consumption during the combustion process and the lowest total oxygen emissions. The earliest oxygen consumption can be observed at PD 40. However, compared to PD 10, it only consumes 63% of O<sub>2</sub> until it reaches the TDC. Even the lowest O<sub>2</sub> consumption before the crank angle reaches TDC was found at 0°BTDC SOI of propane. The lowest total O<sub>2</sub> consumption was found at 40°BTDC SOI of propane. At 0°BTDC SOI of propane, the consumption of oxygen still continues until it reaches 86°CA. Meanwhile, at 40°BTDC SOI of propane, the oxygen consumption stopped at 36°CA. The combustion processes that propane goes through are comparable to those of other alkanes. One of the main basic types of reactions is a combustion reaction. When oxygen gas and a hydrocarbon or other similar fuel are burned, combustion takes place, producing a variety of energies. There are two types of combustion reactions: complete and incomplete. In an excess of oxygen gas, a complete combustion occurs, yielding carbon dioxide and water vapor as byproducts. Propane burns in the presence of excess oxygen to produce carbon dioxide and water ( $C_3H_8 + 5 O_2 \rightarrow 3 CO_2 + 4 H_2O + \text{heat}$ ). When there is insufficient oxygen present, incomplete combustion occurs, with carbon monoxide and water vapor being the main byproducts, furthermore, fuels based on hydrocarbons may contain nitrogen or oxygen, which may result in the production of nitrogen gas. This reaction not only yields chemical products but also energy in the form of light and heat. Propane burns incompletely when there is not enough oxygen present to cause complete combustion, producing carbon dioxide, water, and carbon ( $C_3H_8 + 3.5 O_2 \rightarrow CO_2 + CO + C + 4 H_2O + \text{heat}$ ). The oxygen concentration within the chamber remains constant in the present investigation, and the air mixture within the chamber is not influenced by any external factors. Thus, the low reaction of propane-oxygen in the current situation is caused by an imperfect reaction during combustion rather than a lack of oxygen concentration.

### 5.2.3 Hydrocarbon emissions (HC)



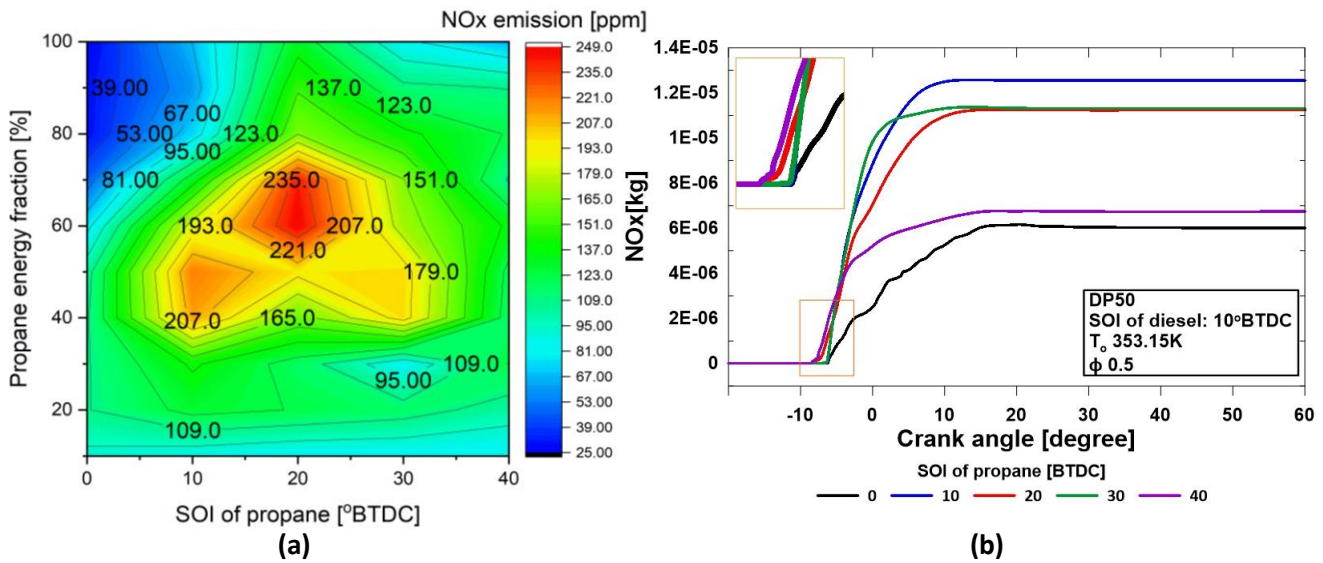
**Figure 5.8** Total HC emission (a) and HC emission (b) of dual direct injection fuel (diesel-propane) under 10%-100% energy fraction and 0°-40°BTDC SOI of propane.

Figure 5.8 shows the total HC emissions with the variation of energy fraction and SOI of propane (a) and the development of HC at SOI 0°BTDC to 40°BTDC (b) in the in-cylinder dual-fuel (diesel-propane) engine. Hydrocarbon emissions are the consequence of incomplete combustion of the hydrocarbon fuel [130]. The application of propane was expected to reduce the HC emission due to its lower carbon atom compared to diesel. However, improper SOI of propane direct injection causing poor mixing quality, flame quenching, and rich premixed mixture at this condition led to incomplete combustion [131]. In general, the application of higher propane energy fraction on direct injection on CI engine results in a higher total HC emission. When the propane energy fraction exceeds 50%, a significant total hydrogen emission is observed. Even with an increase in propane's energy fraction, the steady HC concentration is only visible at 20°BTDC SOI of propane. Figure 5.6b shows the formation of the HC during the injection and combustion process. The formation of HC starts from the injection of the first injection followed by the second injection and decreases as combustion occurs. The quantity of the total HC depends on the capability to burn the total fuel in the first stage of combustion. In comparison to 40°, 30°, and 10°BTDC SOI of propane, the lowest peak HC propagation is observed at 20 BTDC SOI. In



addition, Figure 5.8b illustrates that when compared to the other parameters, it burns the HC more quickly and completely. The second stage propagation of HC was observed at the expansion step at 0°BTDC SOI of propane, indicating imperfect combustion at the first stage of combustion. As the increase of the propane energy fraction, a higher second stage of HC propagation was also spotted at the early SOI of propane.

### 5.2.4 Nitrogen oxides emissions (NO<sub>x</sub>)

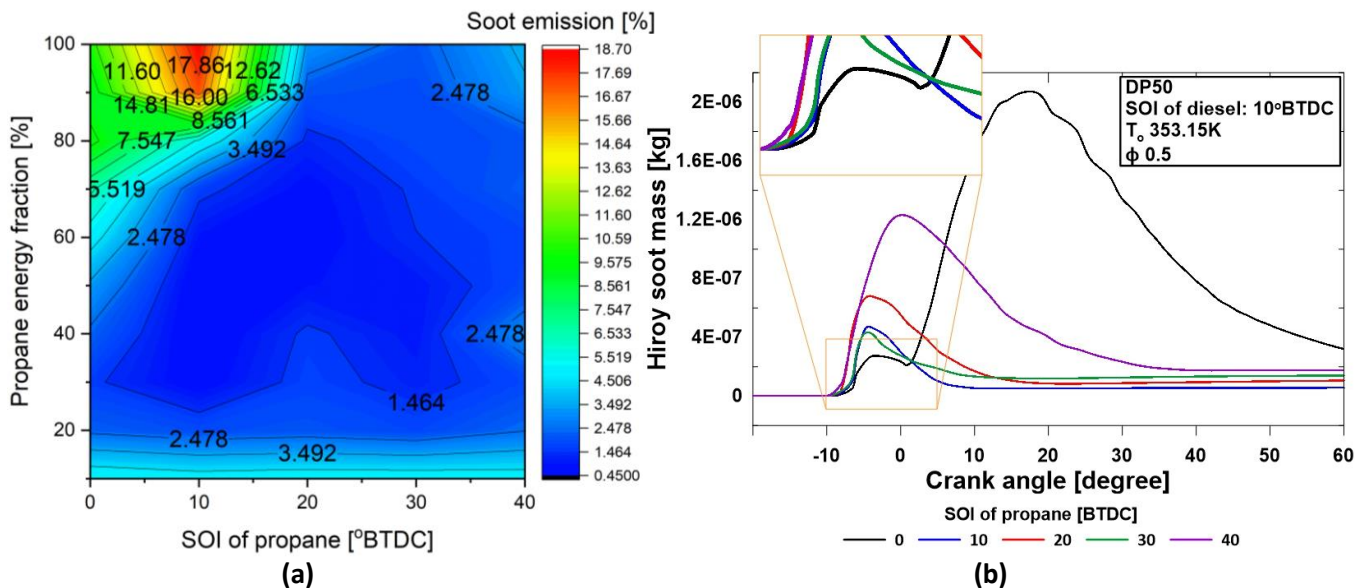


**Figure 5.9** Total NO<sub>x</sub> emission (a) and NO<sub>x</sub> emission (b) of dual direct injection fuel (diesel-propane) under 10%-100% energy fraction and 0°-40°BTDC SOI of propane.

Figure 5.9 shows the total NO<sub>x</sub> emissions with the variation of energy fraction and SOI of propane (a) and the development of NO<sub>x</sub> at SOI 0°BTDC to 40°BTDC (b) in the in-cylinder dual-fuel (diesel-propane) engine. It is clear that the high total NO<sub>x</sub> concentration was produced at propane concentration 40% to 80% at SOI of propane 10 to 30 BTDC. Thermal NO<sub>x</sub> is formed when nitrogen and oxygen in the combustion air combine with one another at high temperatures in a flame. Thermal NO<sub>x</sub> makes up the majority of NO<sub>x</sub> formed during the combustion of gases and light oils. The rate of NO<sub>x</sub> formation generally increases significantly above 1800K flame temperature. Though diesel fuel and propane do not contain nitrogen, NO<sub>x</sub> is formed by taking the nitrogen from the air because 78% of nitrogen is present in the air [132]. Figure 5.2b confirms that the high concentration of NO<sub>x</sub> present was generated in the region with the highest maximum temperature. However, even at SOI of propane 40°BTDC produces the highest maximum in-

cylinder temperature, it generates a lower  $\text{NO}_x$  concentration compared to  $20^\circ$  to  $30^\circ$ BTDC SOI of propane. As shown in Figure 5.2a, the temperature propagation at  $40^\circ$ BTDC SOI of propane at the second stage of combustion is the lowest compared to the other parameters. Despite the fact that propane was injected before diesel, even with the help of diesel's auto ignition, propane's auto-ignition occurred very late. It indicated that part of the propane has been reaching the cylinder wall and producing lower temperature and pressure during combustion. Figure 5.9b shows the formation of  $\text{NO}_x$  of dual direct injection fuel at DP50 during the combustion process. The  $\text{NO}_x$  is generated in two stages caused by the ignition of the diesel and propane. The formation of  $\text{NO}_x$  by propane shows a slower generation compared to diesel. At  $30^\circ$  BTDC SOI of propane, shows a little distinction of  $\text{NO}_x$  formation speed, indicating an auto-ignition occurred almost at the same time. At the expansion stage, the  $\text{NO}_x$  shows a constant number despite the lower temperature as the cylinder volume increases. Rapid cooling (below 1800 K), due to the expansion stroke, does not allow the products to attain chemical equilibrium and some intermediate products (including NO) “freeze” and leave NO concentrations far in excess of levels corresponding to equilibrium at exhaust conditions [133].

### 5.2.5 Soot emissions



**Figure 5.10** Total soot emission (a) and soot emission (b) of dual direct injection fuel (diesel-propane) under 10%-100% energy fraction and  $0^\circ$ - $40^\circ$ BTDC SOI of propane.

Figure 5.10 shows the total soot emissions with the variation of energy fraction and SOI of propane (a) and the development of soot at SOI 0°BTDC to 40°BTDC (b) in the in-cylinder dual-fuel (diesel-propane) engine. The total soot reduction can be observed when the percentage of propane is increased. A significant increase of propane was produced at the percentage of propane more than 60% at the late SOI of propane (20°- 0°BTDC). The SOI of propane at 30°BTDC mostly produces the lowest soot compared to the other SOI. The formation process of soot is generally divided into two stages: (1)The formation stage of soot, which includes the formation of radicals in gaseous reaction and soot nucleation. (2)The growth stage of soot, which mainly involves the surface growth, agglomeration, and oxidation of soot [134]. The formation of soot during combustion can be observed in Figure 5.10b. It is very clear that the SOI of propane 0° and 40° BTDC shows significant soot formation. It happened due to the nonreactive stage of propane when too early or late SOI was applied to the propane DI strategy. The soot reactivity in dependence on the nanostructure was shown after deducting the effect of oxygen concentration and temperature. The increase in resistance toward oxidation was associated with the increase of the structural order for the in-cylinder soot [135].

### 5.3 Conclusion.

Experimental and computational studies to investigate the emission of the dual direct injection fuel (diesel-propane) engine on the CI mechanism were conducted. The impact of a low-carbon combustion fuel proportion shows the feasibility and promise of a novel direct injection propane and SOI application variation. The following conclusions can be drawn from the results of the present study.

1. Incomplete combustion was shown by applying propane on the direct injection compression ignition engine at CR 19. The auto-ignition resistance of propane causes the second-stage ignition at the expansion state causing the reduction of power and enhancing the emissions. It indicates that the current parameter is not suitable to maximize the combustion characteristics of propane.
2. The fluctuation of CO/CO<sub>2</sub> shows the indication of better combustion performance when propane up to 50% was applied. The lower CO<sub>2</sub> emission on the other propane energy fraction indicates the incapability to burn the fuel efficiently during the combustion process.



The lower CO<sub>2</sub> is shown at PD50, 40°BTDC SOI of propane despite the highest temperature produced due to the better air-fuel mixture. It shows that by improving the combustion quality, the physicochemical propane fuel properties of low-carbon can be attained.

3. The application of higher propane energy fraction on direct injection on CI engine results in a higher total HC emission. The quality of the auto-ignition characteristic of fuel determines the formation of HC. Injecting propane closer to its auto-ignition point lowers the ambient temperature reduction and burns the HC much faster.
4. An increase in the propane energy fraction indicates a rise in NO<sub>x</sub> when the LPG-Di was applied at CR 19. The auto-ignition resistance of propane makes a longer NO<sub>x</sub> formation compared to diesel. The NO<sub>x</sub> formation was identified even at the expansion stroke as the effect of the second stage auto-ignition of propane. Consequently, higher NO<sub>x</sub> concentration was identified when the higher propane energy fraction was applied. By delaying the SOI of propane to 30°BTDC the total NO<sub>x</sub> can be reduced significantly.
5. A higher propane energy fraction shows the indication of soot reduction. However, propane shows high auto-ignition resistance when 0° and 40°BTDC were applied. Consequently, significant soot emission was produced.

There are numerous challenges when setting up a direct injection on a compression ignition engine running on propane fuel. Liquid propane injections generate a large amount of emissions and significantly reduce engine performance due to their high auto-ignition resistance. Further research is required to optimize the propane auto-ignition characteristics, including SOI, initial temperature, ambient pressure, and so on. The proposed strategy could improve engine performance by reducing exhaust emissions and increasing engine lean combustion efficiency in future high-efficiency engines.

## **6. Combustion characteristic prediction of dual direct injection fuel (diesel-propane) on RCEM based on an artificial neural network approach.**

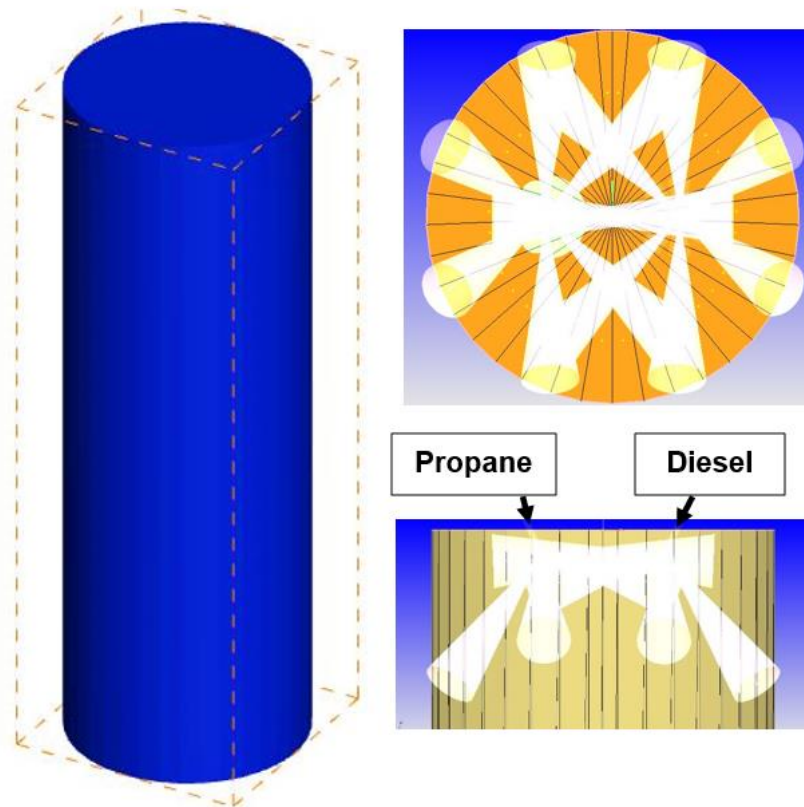
It is challenging to optimize of the objectives at once issues including conflicting dual objectives in compression ignition engines that are in a trade-off relationship (for example, using alternative fuel with low carbon content deflate HC and smoke pollutants but increases NOx emissions). The purpose of chapter 6 is to conduct both experimental and numerical investigations to learn more about the dual direct injection effect on performance and emission characteristics of low carbon propane combustion with high pressure direct injection is optimized and investigated. For a compression ignition propane engine, essential operational parameters were optimised using a genetic algorithm (GA) technique. The GA was used to identify the ideal circumstances that result in start of combustion (SoC), and efficiency, as well as reduced emissions of CO, and NOx. Additionally, engine in-cylinder pressure and thermo-physical characteristics for varied Start of Injection (SoI) of propane and energy fraction (%P) were examined and contrasted. Finally, it was compared how the engines running on diesel and propane performed and what emissions they produced. The convergence of ANN and genetic algorithms is a novel aspect of this study as a promising approach for optimum operating parameter optimization of spark duration on low-carbon combustion of high pressure direct-injection propane.

### **6.1 CFD modeling and Artificial neural network construction**

#### **6.1.1 CFD modeling**

CONVERGE CFD software was used in this study to simulate internal combustion engine processes. Advanced numerical methods and physical models of the spray, turbulence, and combustion processes, as well as their nonlinear interactions, are included in CONVERGE. To better understand the behavior of combustion in dual fuel engines, dual fuel combustion was modelled. Surfaces for the geometry were produced both before and after simulation using a full mesh construction method. Using the methods of fixed embedding, adaptive mesh refinement subdivision (AMR), and basic grid size, we modified the grid size and the total number of grid cells.

CONVERGE CFD 3.0 was used for the computational analyses. Closed cycle simulations were carried out using the combustion chamber's full sector geometry. A turbulence model must be used to obtain accurate CFD simulation results because turbulence has a significant impact on the rate at which momentum, energy, and species mix. The Renormalization Group (RNG)  $k-\epsilon$  turbulence model [109] performs better than the standard  $k$ -turbulence model for describing anisotropic and non-equilibrium effects. To use the discretized Navier-Stokes equation on the Cartesian grid, a finite volume indirect discretization method was selected. To save time, the computer simulates all three processes: combustion, compression, and expansion. Utilizing information gleaned from experimental observations, the initial fuel, ambient temperature, and air conditions were specified. The initial fields of temperature, flow velocity and pressure were generated until the motoring pressure from the experiments was met. Figure 6.5.1 shows the schematic diagram of RCEM in-cylinder chamber on CFD modeling.



**Figure 6.1** Schematic Diagram of RCEM for CFD investigation

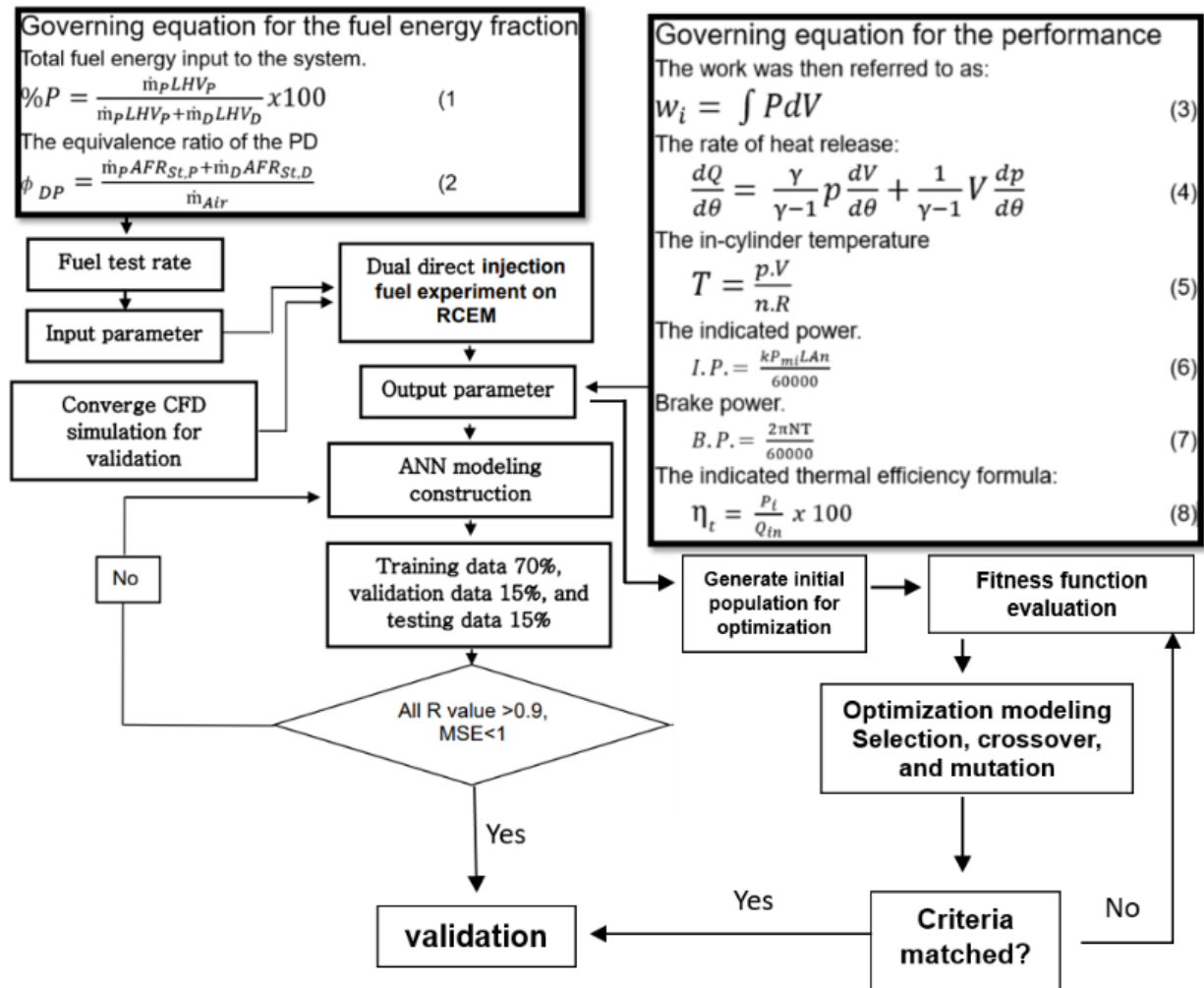
**Table 6.1** CFD parameter input

<b>Phenomenon</b>	<b>Model</b>
Turbulence flow	RNG k- $\epsilon$ [109]
Drop drag	Dynamic drop drag [110]
Break-up	KH-RT [111]
Drop collision	NTC [112]
Drop evaporation	Frossling [113]
Drop turbulent dispersion	TKE preserving [110]
Chemistry solver	SAGE [114]

### **6.1.2 ANN construction**

An ANN-based model for the factors affecting combustion has been developed. The experimental study's degree of error was determined using the ANN model. For the combustion

parameters, the findings of an ANN were compared with those of an experimental investigation that used FEBRIS analysis.



**Figure 6.2** Flow chart of the study.

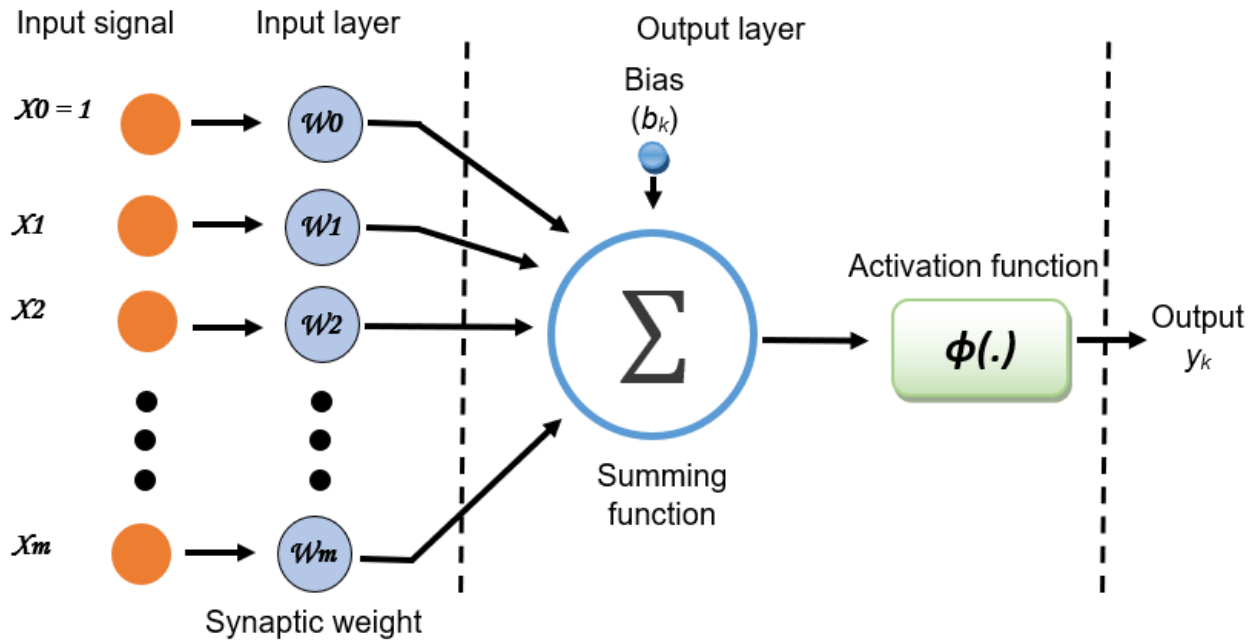
A computing system called an artificial neural network (ANN) was constructed to stimulate and process data in a manner similar to how the human brain does it. It employs artificial intelligence (AI) to find solutions to issues that are intractable or challenging for people [136]. Neurons are closely interconnected in a number of layers in an ANN system with the number of layers depending on the difficulty of the problems. Each neuron has a weight and bias that are assigned to it. Multi-layer perception (MLP), also known as multilayer neural networks, is the most well-known example of this type of neural network. The layers between the input and output layers are referred to as hidden layers, and they have a significant impact on how well the

developed ANN predicts outcomes. An artificial neural network (ANN) system is a device that receives input, processes the data, and outputs the results. The input is comprised of an array of data. When an input is sent to a neural network and a matching desired or target response is set to the output, an error occurs when there is a discrepancy between the desired response and the actual system output. The system uses the error as input and modifies all of its parameters in accordance with a learning rule (back propagation). Until the intended outcome is achieved satisfactorily, this process is repeated (in iterations or epochs). By utilising the gradient descent method, the back propagation algorithm refines the model and increases the degree of agreement between the predicted and actual values. A straightforward model of the process element that was inspired by biological neurons is shown in Figure 6.3. In this model, i., the output of the process element is given in Eq. (9)

$$y(t + 1) = a(\sum_{j=1}^m w_{ij}x_j(t) - \theta_i) \quad (9)$$

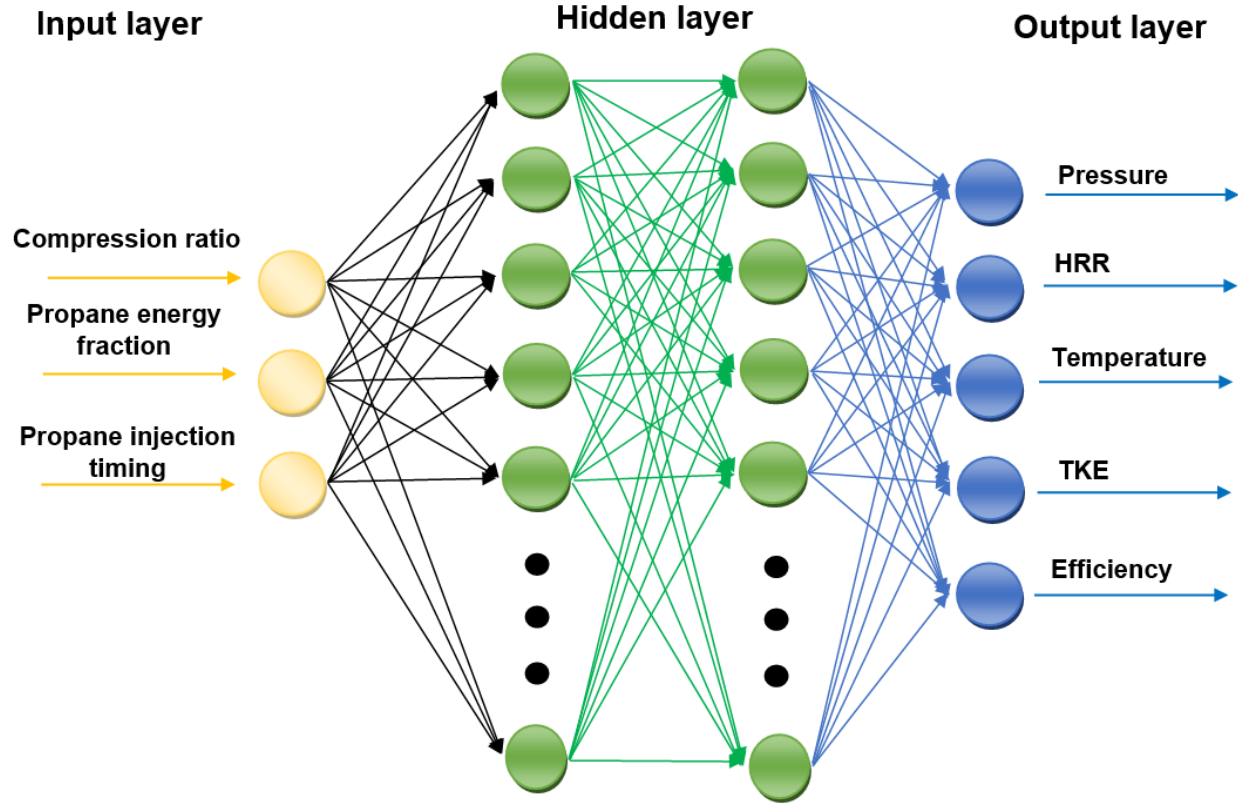
where  $\theta_i$  is the processing element's threshold value and  $a(\cdot)$  is the activation function. Input and output make up the two components of the processing element information processing. By combining the input data  $x_j$  received from the outside over the  $w_{ij}$  weights to which they are connected, a processing element produces a net value. The net value of the processing element is calculated using Eq. (10)

$$net = (\sum_{j=1}^m w_{ij}x_j - \theta_i) \quad (10)$$



**Figure 6.3** Representation of a model neuron.

In the current study, MATLAB/artificial neural network module was used to train the feed forward multilayer ANN model. The input layer, output layer, and hidden layer are the three layers that make up an ANN, which can have any number of layers [24], as shown in Figure 6.4. All the input parameters are contained in the input layer. The hidden layer computes the data from the input layer, and the output layer computes the output vector that follows. The estimation process using the ANN technique entails three sequential steps: modelling, learning (or training) phase, and testing phase [37]. The engine's chosen input and output factors were used to build an ANN model during the modelling stage. The network was set up to produce a target prediction based on input data during the training phase. Test results were compared with the estimated data regarding the test procedure. Once the test error reached the desired level, the network's training phase was terminated [24].



**Figure 6.4** Artificial neural network structure for RCCEM.

The models' estimation success was assessed using regression coefficients and mean square error (MSE), which were developed using the ANN model's targets and outputs. The evaluation was conducted using the following equations:

$$R^2 = 1 - \left( \frac{\sum_{i=1}^n (t_i - o_i)^2}{\sum_{i=1}^n (o_i)^2} \right) \quad (11)$$

$$MSE = \frac{1}{n} \sum_{i=1}^n (y_i - t_i) \quad (12)$$

Where "t" is the actual output, "o" is the estimated output value, and "n" is the number of dots in the data set. An ANN model with a low error rate was developed using experimental data as a basis. In this study, propane injection timing, propane energy ratio and engine compression ratio were selected as input parameters for input layer and mean pressure and smoke were chosen as output parameters for the output layer.

In this study, a neural network was employed for estimating the combustion characteristics of RCCEM powered by diesel and propane by a dual direct injection strategy. Energy fraction ratio of



propane, propane fuel injection timing and the compression ratio were selected as input factors, while mean pressure, in-cylinder temperature, power, TKE, and indicated thermal efficiency were selected as output factors. The neural network methodology in this study also applied the same data set, which included 20 test trials. In particular, 70% of the data trials were utilized for neural network training, 15% for verification, and 15% for testing. The ANN was created using the following methods: feed-forward backpropagation network type, mean square error (MSE) performance function, Logsig transfer function, Levenberg-Marquardt (Trainlm) training function, and gradient descent with momentum weight and bias learning function (LEARNGDM). This was done using the feed-forward backpropagation network type, which is typically used to describe challenging system modelling and identification issues. MSE determined the network's failure function using the Levenberg-Marquardt (Trainlm) training function, which is typically used for precise estimates [137]. The majority of researchers discovered that the logistic sigmoid activation function (logsig) produces superior results to other functions [138]. Table 6.2 provides specifics regarding the neural network and the development of the ANN model [139].

**Table 6.2** Particulars of the neural network [139].

Network	3 inputs, 5 outputs and one hidden layer
Data	Training: 75% randomly selected data from experimental data Test: 25% randomly selected data from experimental data
Network Type	Feed-forward back propagation
Training function	Trainlm
Adaptation learning function	Learngdm
Transfer function	Logsig
Performance function	Mean square error

Stopping criteria      Break the training of network when the confirmation error begins increasing

---

## 6.2 Data generation for artificial neural network optimized

It is challenging to optimize of the objectives at once issues including conflicting dual objectives in compression ignition engines that are in a trade-off relationship (for example, using alternative fuel with low carbon content deflates HC and smoke pollutants but increases NOx emissions). The purpose of this study is to conduct both experimental and numerical investigations to learn more about the SoI and energy fraction of propane effect on performance and emission characteristics of low carbon propane combustion with high pressure direct injection is optimised and investigated. For a compression ignition propane engine, essential operational parameters were optimised using a genetic algorithm (GA) technique. The GA was used to identify the ideal circumstances that result in greater heat release rate, efficiency, and braking power as well as reduced emissions of SoC (start of combustion), %P (percentage of propane), CO, and NOx. Additionally, engine in-cylinder pressure and thermo-physical characteristics for varied spark durations were examined and contrasted. Finally, it was compared how the engines running on diesel and propane performed and what emissions they produced. The convergence of ANN and genetic algorithms is a novel aspect of this study as a promising approach for optimum operating parameter optimization of dual direct injection strategy on low-carbon combustion of high-pressure direct-injection propane.

### 6.2.1 Regression modelling

The mathematical formulae for the engine performance and emission parameters are provided for the input function of the GA toolbox. Regression analysis was used to create the models using experimental data for the selected SoI, and energy fraction of propane (%P) propane on RCEM with dual direct injection application. The 756 data sets were collected by engine testing at different values of SoI and %P as predictors or independent variables. The selected in-cylinder combustion and performance characteristics considered as responses 95 (dependent variables) were ITE and SoC, respectively. CO and NOx were the selected emission components considered as responses. The in-cylinder combustion, performance and emission parameters can be stated mathematically as a regression equation, as seen in Eq. 13

$$f(x) = b_0 + \sum_{i=0}^n (b_i x_i + b_{ii} x_i^2) + \sum_{i < j}^n (b_{ij} x_i x_j + b_{ii} x_i^2) + \epsilon \quad (13)$$

where  $b_0$  is the intercept's constant, ' $b_i$ ' and ' $b_{ii}$ ' are their respective coefficients, and ' $b_{ij}$ ' is the result of the linear interaction between ' $x_i$ ' and ' $x_j$ '. As a result, the response includes terms for linear, squared, and cross products. The regression analysis is carried out using Minitab software. A separate set of polynomial equations or models is developed for each response. Before the final coefficients and R2 are calculated for the responses, the inconsistent terms are eliminated using the backward elimination procedure. Table 6.3 displays the predictor symbols for the regression model. Table 6 lists the independent factors in the regression model for the performance measures and the emitters.

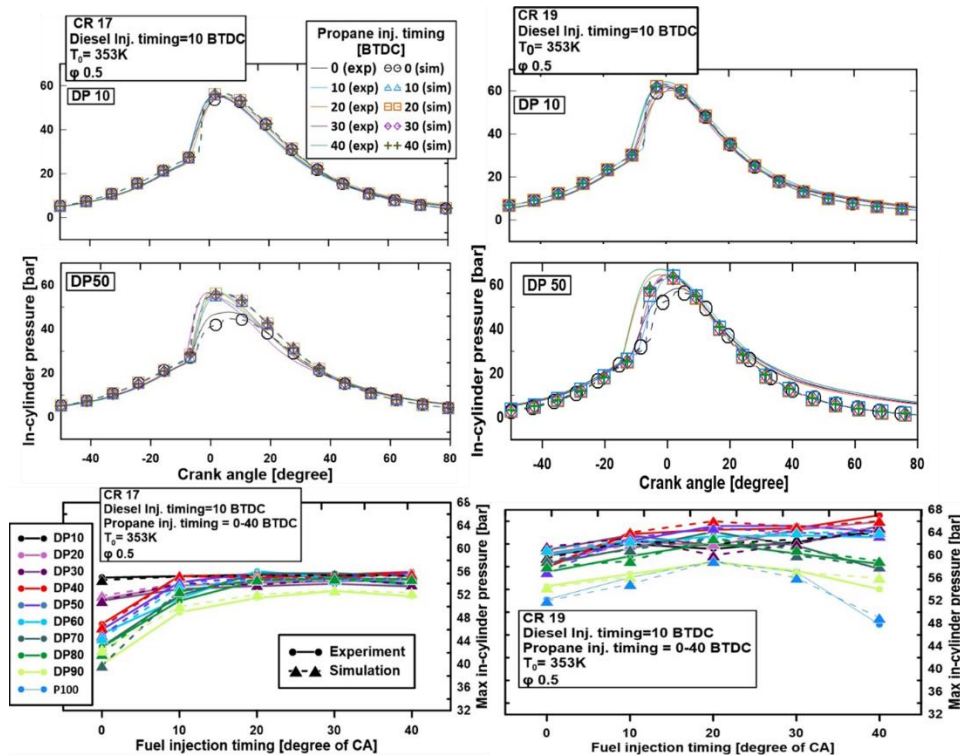
**Table 6.3** Symbol used in modelling for the variables in the regression formulas

Parameters	Symbol	Range
Propane energy fraction [%]	x1	0-100
SOI of propane [°BTDC]	x2	0, 10, 20, 30, 40

**Table 6.4.** Regression model

Response	Regression model
ITE	$27.81 - 0.1240 x_1 - 0.682x_2 + 0.00276x_1^2 + 0.02920x_2^2 + 0.01279 x_1 x_2 - 0.000022x_1^3 - 0.000226 x_2^3 - 0.000040x_1^2 x_2 - 0.000250 x_1 x_2^2$
SoC	$3.375 + 0.0157 x_1 - 0.0287 x_2 - 0.000030x_1^2 + 0.00164x_2^2 + 0.000314 x_1 x_2 - 0.000002x_1^3 - 0.000006 x_2^3 + 0.000002x_1^2 x_2 - 0.000022 x_1 x_2^2$
CO	$-7.80 + 0.1269 x_1 + 0.0392 x_2 - 0.00310x_1^2 + 0.00079x_2^2 - 0.00618 x_1 x_2 + 0.000026x_1^3 - 0.000067x_2^3 + 0.000006x_1^2 x_2 + 0.000130 x_1 x_2^2$
NO <sub>x</sub>	$58.96 + 0.091 x_1 - 0.641 x_2 - 0.00018x_1^2 + 0.0334 x_2^2 - 0.01251 x_1 x_2 + 0.000003x_1^3 - 0.000571x_2^3 + 0.000063x_1^2 x_2 + 0.000217 x_1 x_2^2$

A training set and a validation set were created by randomly dividing the dataset. 70% of the data set is made up of the training set, and the remaining 30% is made up of the validation set, for a total of 756 data sets. The first was used to create a regression model that matched the replies, and the second was used to evaluate how well the models were working. Model performance metrics are regarded as the mean squared error (MSE) and the correlation coefficient (R2 ).

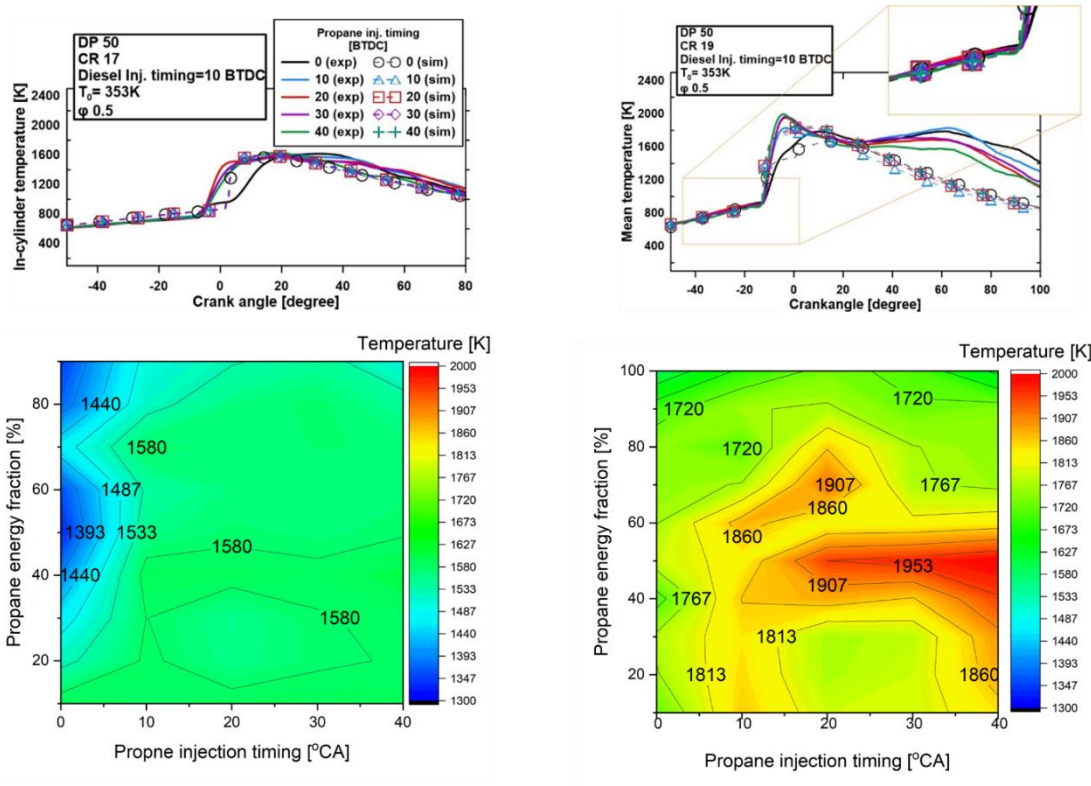


**Figure 6.5** In-cylinder pressure under propane energy fraction 10-100%, Propane injection timing 0o-40o BTDC and compression ratio of: a) 17 and b) 19.

### 6.3 Input data parameter

Figure 6.5 compares the measured cylinder pressure traces and peak pressures of compression: a) 17 and b) 19 and calculated cylinder pressure for five propane injection cases and propane injection quantity cases for 10, 50 and 90% propane energy fractions. Moreover, the measured maximum in-cylinder pressures were compared with their simulated values. The charge's thermodynamic state can be determined from the pressure inside the cylinder using the first law of thermodynamics and a few fundamental presumptions.

We expected to get proper combustion using LPG fuel as it has a low evaporation temperature and higher LHV compared to diesel fuel. Hence, it has better atomization characteristics and produces a higher amount of heat released during combustion. However, in the direct injection strategy, propane was injected to the chamber in liquid phase, which has very low temperature (-43°C). Furthermore, the current common rail system requires much lower fuel injection pressures compared to diesel for safety purposes. Consequently, lower atomization characteristics were produced for propane injection case. It will lower the reactivity of the fuel based on low compression ratio and high quantity of propane. As a result, it will improve the possibility of wall impingement, which reduces cylinder wall temperature. Decreasing the in-cylinder temperature reduced peak cylinder pressure and increasing ignition delay, which agree with those in previous research by Verde [117]. Furthermore, it affects the ambient temperature of diesel injection condition. Low ambient temperature would alter the Sauter mean diameter (SMD) distribution, spray tip penetration, decelerate diesel fuel evaporation, and reduce diesel fuel activation [118].



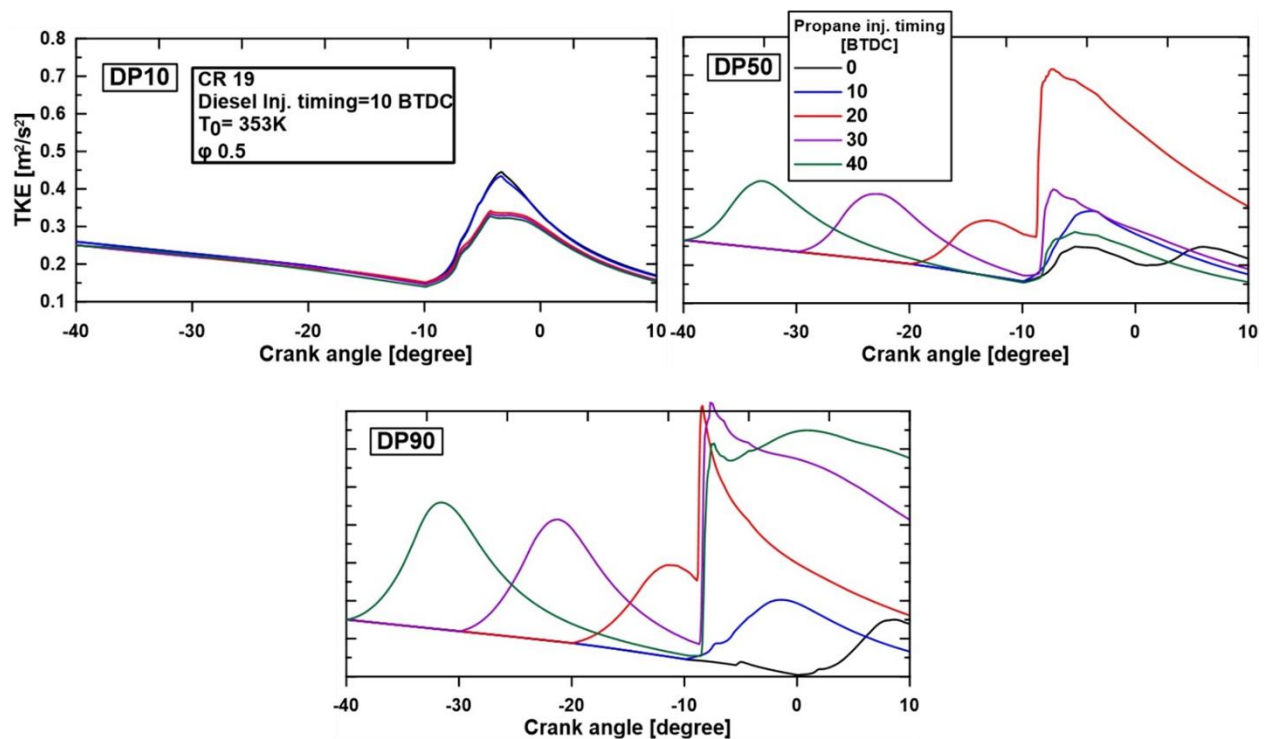
**Figure 6.6** In-cylinder temperature under propane energy fraction 10-100%, propane injection timing 0o-40o BTDC and compression ratio of: a) 17 and b) 19.

Figure 6.6 shows experiment and simulation data in-cylinder temperature under propane energy fraction 10-100%, Propane injection timing  $0^{\circ}$ - $40^{\circ}$  BTDC and compression ratios of: a) 17 and b) 19. Earlier propane injection into the chamber results in lower ambient temperature produced and it will affect the temperature required for the auto ignition event. At the condition of CR17, in the in-cylinder temperature trace, the highest peak temperature was produced in the main combustion area. This indicates the slow combustion of propane, even when it occurs after diesel auto ignition process. The significant development of temperature mostly occurs after the diesel auto ignition area. This can be observed by comparing the  $0^{\circ}$ BTDC propane injection timing with the other propane injection timing case. At  $0^{\circ}$ BTDC propane injection timing, a significant development of temperature occurred earlier compared to the other propane injection timing parameter. This indicates the propane fuel does not provide auto ignition behavior for the CR17 condition, which delayed the auto ignition characteristics of diesel. The propane was injected at ambient temperature 673 K at  $40^{\circ}$ BTDC, 721 K at  $30^{\circ}$ BTDC, 754 K at  $20^{\circ}$ BTDC, 773 K at  $10^{\circ}$ BTDC and 1310 K at  $0^{\circ}$ BTDC. Even though propane injection exceed the auto ignition temperature of propane (481 K), a misfire was spotted for 100% energy fraction of propane. Better spray quality could improve auto ignition characteristics of propane by increasing the injection pressure for future studies.

The development of temperature and max in-cylinder temperature of propane energy fraction and propane injection timing variation at CR 19 are shown in Figure 6.7b. Observing the development of in-cylinder temperature trace, we noticed that a significant development of temperature occurred earlier than diesel auto ignition area for propane injection timing  $40^{\circ}$ - $10^{\circ}$ BTDC, which was much higher compared to CR17. This indicates the auto ignition behavior of propane. Moreover, it occurs earlier than the auto ignition of the diesel. The addition of propane produces higher temperature development in the early stage of combustion (before  $0^{\circ}$ CA). The second temperature increase was noticed at  $28^{\circ}$ CA for all propane injection timing cases. This seems that propane fuel did not undergo perfect combustion in the early stage of combustion. The low temperature of fuel reduces the ambient temperature. Moreover, propane injection in the liquid phase makes the heat transfer process harder. For that reason, LPG produces lower  $\text{NO}_x$  emission due to the lower temperature inside the engine [120], which agrees with previous studies using an LPG direct injection strategy [22]. An improvement of max in-cylinder temperature was noticed in CR 19 for all SOI of propane and percentage propane energy fraction case. As mentioned before,



the highest peak temperature was produced at CR 19 in the early-stage reaction, which occurs in the BTDC area due to the reactivity of propane. In the mixing-controlled combustion area, there was not a significant difference in peak temperature. For that reason, there is an insignificant maximum temperature gradient in CR17 condition. Even so, there are similar behaviors of maximum in-cylinder temperature trace for both compression ratios. The steady improvement of maximum in-cylinder temperature was noticed under 50% propane energy fraction by increasing the propane energy fraction and by injecting propane earlier than 20°BTDC. 10°BTDC propane injection timing produces slightly higher temperature compared to 0°BTDC and 20°BTDC propane injection timing. This is unaffected by ambient temperature degradation due to the early propane injection which improves the auto ignition characteristics of diesel. The maximum in-cylinder temperature becomes lower as the propane energy fraction is greater than 50%. In this condition, earlier propane injection timing and lower maximum in-cylinder temperatures were produced.

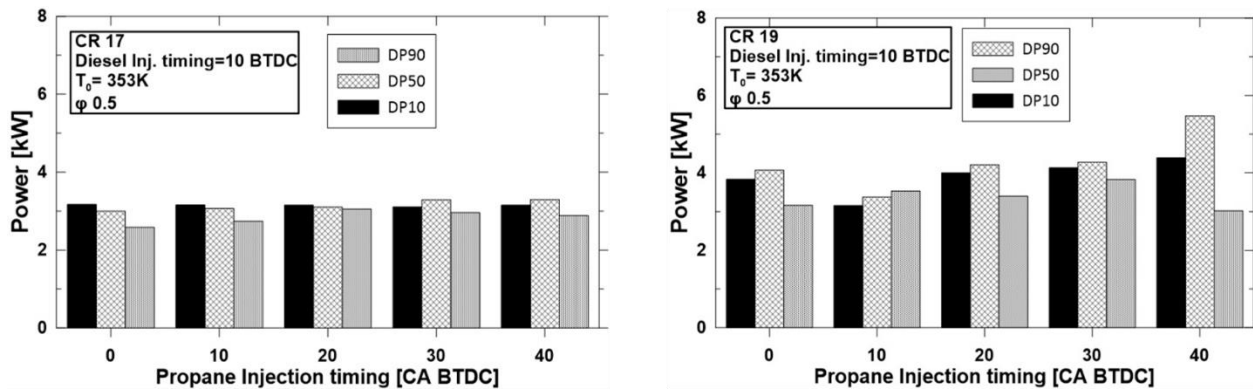


**Figure 6.7** TKE flow pattern of dual direct injection fuel (diesel-propane) at CR 19, propane energy fraction 50% and propane injection timing 0°-40°BTDC.

Figure 6.7 shows the TKE starts at 10°BTDC, i.e., at the diesel injection timing. Figure 6.7 identifies the effect of propane fuel injection on the surrounding air flow and its effect before diesel injection, the moment of diesel injection, ignition, and a late propane injection event. The

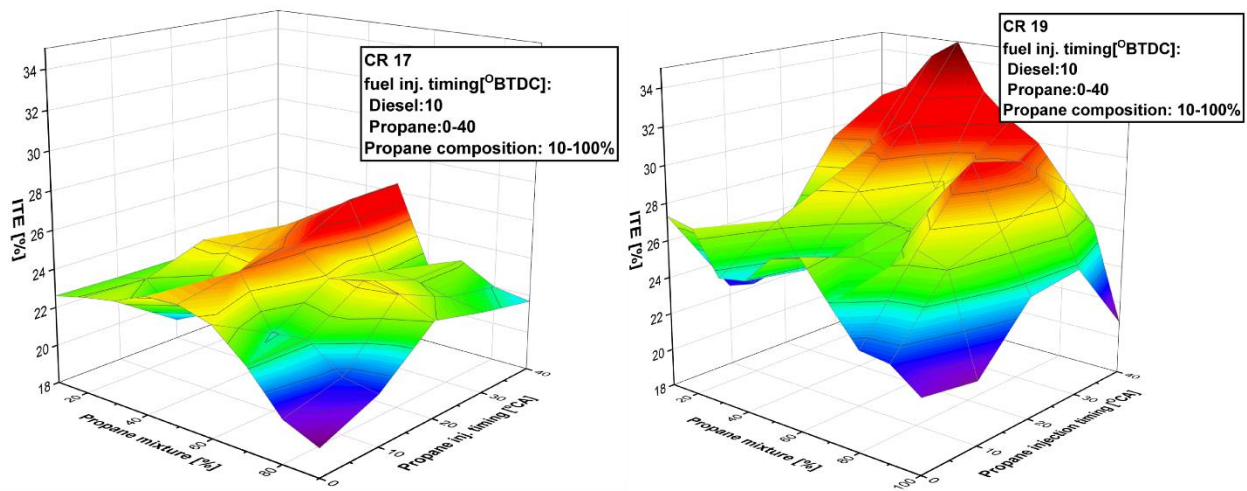


unaffected air flow from propane injection is also shown in the propane injection timing  $10^\circ$  and  $0^\circ$  BTDC. It can be used to compare standard TKE and TKE affected by propane injection. The TKE at  $40^\circ$  BTDC propane injection timing at  $10^\circ$  CA showed similar behavior compared to the TKE, which was unaffected by the propane injection. Degradation of TKE was observed after it reached the peak point, and it calmed down at the moment it reached the diesel injection timing. The  $20^\circ$  BTDC propane injection timing showed the highest TKE for all events. Diesel was injected when the TKE reached the highest point. A higher TKE contributes to a better air fuel mixture and improved the auto ignition characteristics of the fuels. This enhances the TKE at the main combustion event.



**Figure 6.8** Power of RCEM for variations in CR, propane energy fraction, and SOI of propane.

Furthermore, we analyzed the power from the experiments using RCEM with dual direct injection applications shown in Figure 6.8. A higher power output was obtained at a higher compression ratio. This also can be achieved by increasing the propane fraction up to 50% and by injecting propane earlier for both CR17 and CR19. A slight improvement in power was spotted at late propane injection timing in the lean fraction of propane, and it became stronger when a higher CR was applied. For rich fractions of propane, consistent degradation of power was observed for both CR17 and CR19. This behavior was also observed when early propane injection timing was applied.



**Figure 6.9** Thermal efficiency of RCEM under variation of CR, propane energy fraction and SOI of propane.

Figure 6.9 shows the indicated thermal efficiency of the engine: a) compression ratio 17, b) compression ratio 19 with the variation of injection timing from 0°-40° BTDC and percentage of propane from 10-100%. The transition of compression ratio from 17 to 19 improved the ITE significantly. The ITE shows similar behavior for both compression ratios. The ITE for quantities of propane under 50% showed improvement when the propane was injected earlier. Applying a lower quantity of propane at a constant fuel injection pressure reduced the possibility of larger fuel spray droplets and an ambient temperature reduction. In this condition, earlier injection timing, which has longer ignition delay, produces a better air fuel mixture and enhances the quality of combustion. In a lean mixture of propane, the lowest ITE was observed when the propane and diesel were injected at the same time (10° BTDC). An improvement in ITE was observed when propane was injected after diesel injection timing (0° BTDC).

For conditions with more than 50% propane, the early injection timing of propane produced a lower ITE. It requires higher ambient temperature and pressure as the proportion of propane increased due to the high-octane characteristics of propane. In non-reactive conditions, the liquid phase of the propane reduced the in-cylinder temperature and disturbed the diesel auto ignition process. In early propane injection timing, the higher quantity of propane enhanced the possibility of in-cylinder wall wetting, causing a reduction in cylinder wall temperature, producing larger fuel droplets around the cylinder wall. This shows an improvement of ITE at propane injection timings of 20°-30° BTDC. Significant degradation of ITE when propane was injected closer to TDC. The

lowest ITE was produced when 100% propane was applied. The best ITE for CR 17 and 19 occurred at 40% propane and 40 propane injection timing.

## 6.4 Optimization of in-cylinder combustion, performance and emission using genetic algorithm

Inferred mean effective pressure, suggested thermal efficiency, heat release rate, and turbulent kinetic energy all grow or decrease simultaneously at various levels of selected engine operating parameters, according to experimental and simulation findings. The column range of Table 6.3 displays the upper and lower boundaries for the remaining restrictions. After comparing the results of various targets while taking into account in-cylinder performances and emission operating settings, the optimization procedure is used to choose the optimum outcomes. The utilized GA algorithm by the MATLAB optimization toolbox has the properties presented in Table 6.5.

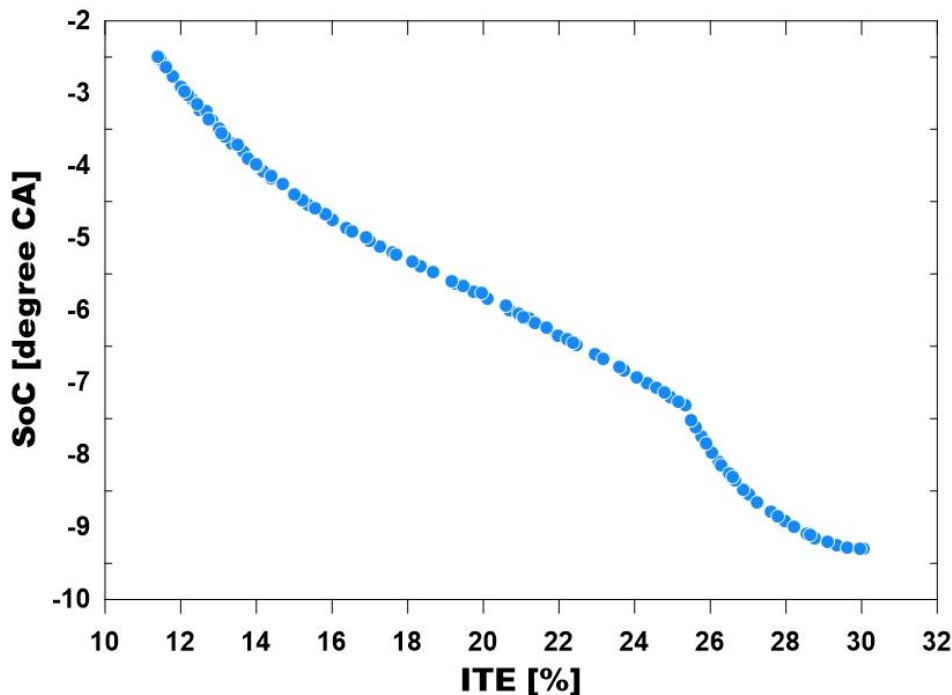
**Table 6.5** Properties of GA algorithm in Matlab

<b>Genetic algorithm parameters</b>	
<b>Number of input variable</b>	2
<b>Lower limit range [%propane, SoI]</b>	[0 0]
<b>Upper limit range [%propane, SoI]</b>	[100 40]
<b>Crossover operator</b>	Two cross predictor and terms in the model
<b>Maximum number of generation</b>	200
<b>Pareto font population fraction</b>	0.35
<b>Regression validation</b>	50 -fold cross-validation

### 6.4.1 Optimization of engine power based on the ITE and SoC

The in-cylinder combustion parameters, specifically the turbulent kinetic energy and heat release rate, are taken into account while determining the optimization goals. Both of them are anticipated to have greater values in order to improve the engine's in-cylinder combustion process. For optimization in the GA toolbox, the polynomials models in Table 6.3 that were derived by regression analysis as fitness functions are stored as.m files. The best values are noted after a few iterations of runs that eliminate the impacts of initiation. The Pareto front is shown in Fig. 6.10, with the objectives of increasing ITE and SoC. The objective function space's Pareto front plot

displays several sets of points for varying objective values. The software uses these criteria to find the ideal values of predictors for performance responses in order to balance two objectives. When all established result points have a broad distribution, the scores of the best predictors can be obtained via the stated objective space, but the majority of the final optimal Pareto front solutions are localized in the leading region with both higher ITE and SoC, indicating that the genetic algorithm prefers the optimized solutions in this region. For objectives 1 and 2, the locations between -5-0 and 20-25 were discovered to provide the best level of predictors. Finally, it is discovered that the best values for %P of 51.729% and SoI of propane at 20.609°BTDC respectively.

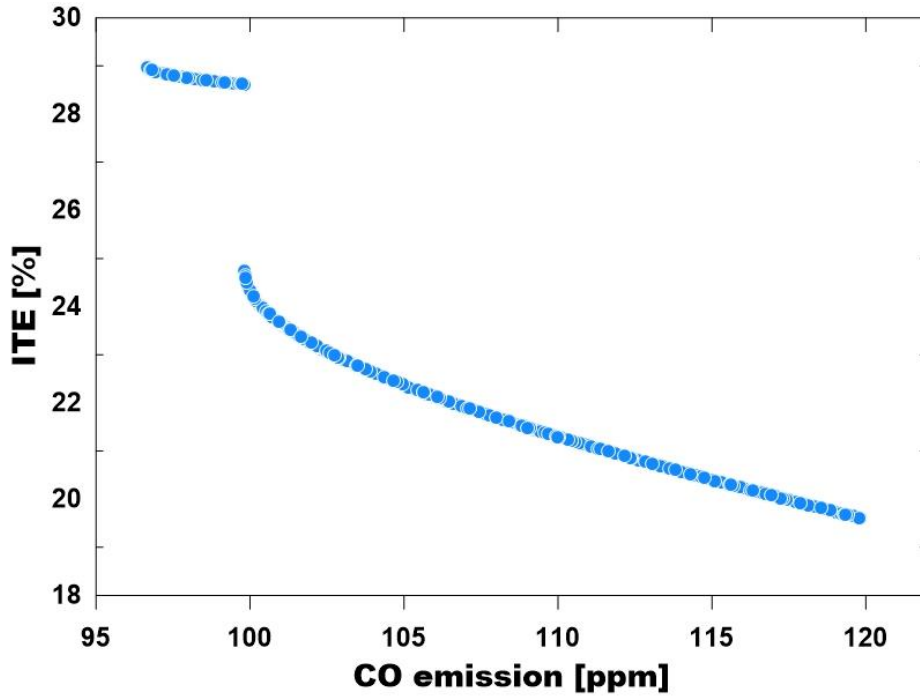


**Figure 6.10** Pareto front for optimization considering SoC and ITE

#### 6.4.2 Optimization of engine power based on the ITE and CO

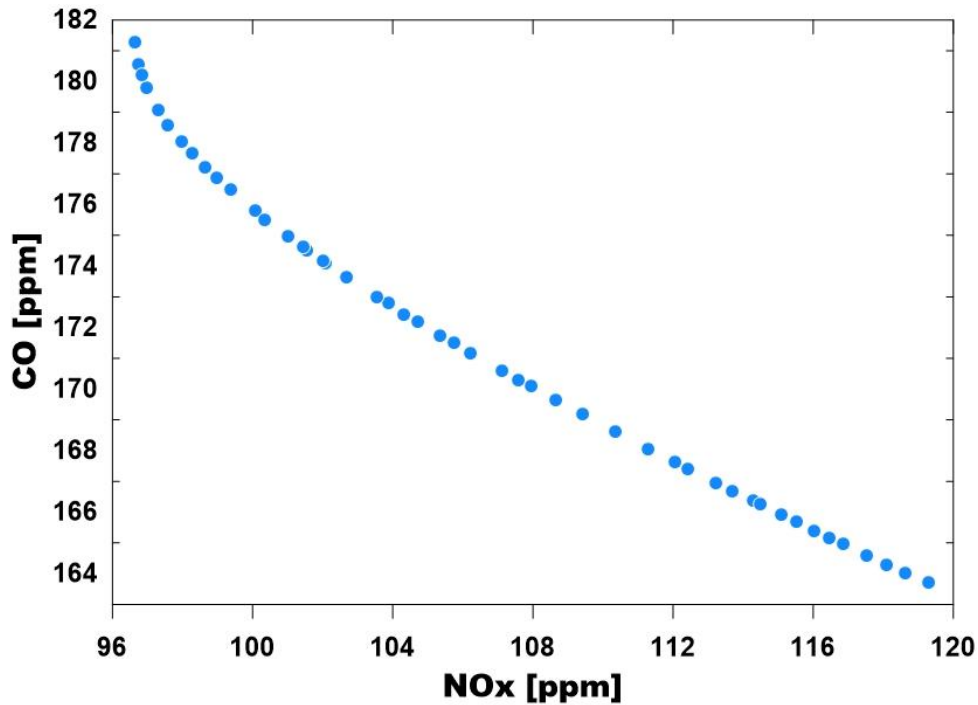
The process for performing the optimization is the same as it was in the past. One of the two goals in this situation is to perform better or to the fullest. Therefore, increasing ITE and reducing the CO characteristics is one of the goals. In MatLab, all of the polynomials listed in Table 6.4 are employed as a fitness function. The Pareto front is depicted in Fig. 6.11, with objective 1 being to maximize ITE and CO. The Pareto front's goal space displays a collection of points that correspond to the best options. For objectives 1 and 2, the points of optimum

values were located between 0 and 0.5 and 30 and 35, respectively. It is discovered that the ideal values for the input parameters %P of 54.73 and SoI of propane at 13.273°BTDC respectively.



**Figure 6.11** Pareto front for optimization considering ITE and CO

#### 6.4.3 Optimization of engine power based on the CO and NO<sub>x</sub>



**Figure 6.12** Pareto front for optimization considering CO and NO<sub>x</sub>

The engine operating parameters are optimized by taking into account all of the elements of exhaust pollution, including CO, CO<sub>2</sub>, HC, NO<sub>x</sub>, and smoke. Uncompleted fuel combustion or the dissociation of CO<sub>2</sub> produce carbon monoxide. The equivalency ratio is the main factor that affects CO emissions from internal combustion engines. Significant amounts of CO will be present when the equivalency ratio is stoichiometric or highly fuel-lean due to CO<sub>2</sub> dissociation. As a result of the insufficient oxygen to complete the reaction to CO<sub>2</sub>, CO is easily generated in fuel-rich engines. Thus, reducing CO is one of the optimization's goals. The second is to reduce NO<sub>x</sub>. The Pareto front optimal solution in Fig. 6.12 compares the CO and NO<sub>x</sub> emissions from all estimated scenarios and has two aim functions of minimizing CO and NO<sub>x</sub>. Additionally, there is a link of some sort between CO and NO<sub>x</sub> emissions. To achieve a balance between the two goals, the Pareto front's points are applied. For the operating parameters %P of 10.008 and SoI of propane at 0.011°BTDC, respectively.

#### 6.4.4 Optimization of ITE based on the burn duration and SOC

Utilizing the MATLAB software, the optimization is done by setting input parameters. It was possible to acquire the response of parameter combinations (ITE, SoC, CO, and NO<sub>x</sub>) for the entire set of compression ignition operating circumstances by optimizing each of the input parameters in

order to meet the optimization aim and any pertinent constraints. For %P and Sol of propane, the optimized parameters have been chosen as shown in Table 9. In order to ensure that the engine operates effectively across a suitable range of operating conditions, a number of restrictions are specified while choosing the best solution. These constraints aim to minimize abnormality situations and partial fuel combustion brought on by inappropriate parameter values. After carrying out the multiple optimization runs by allocating different input parameters for in-cylinder combustion, performance, and emission

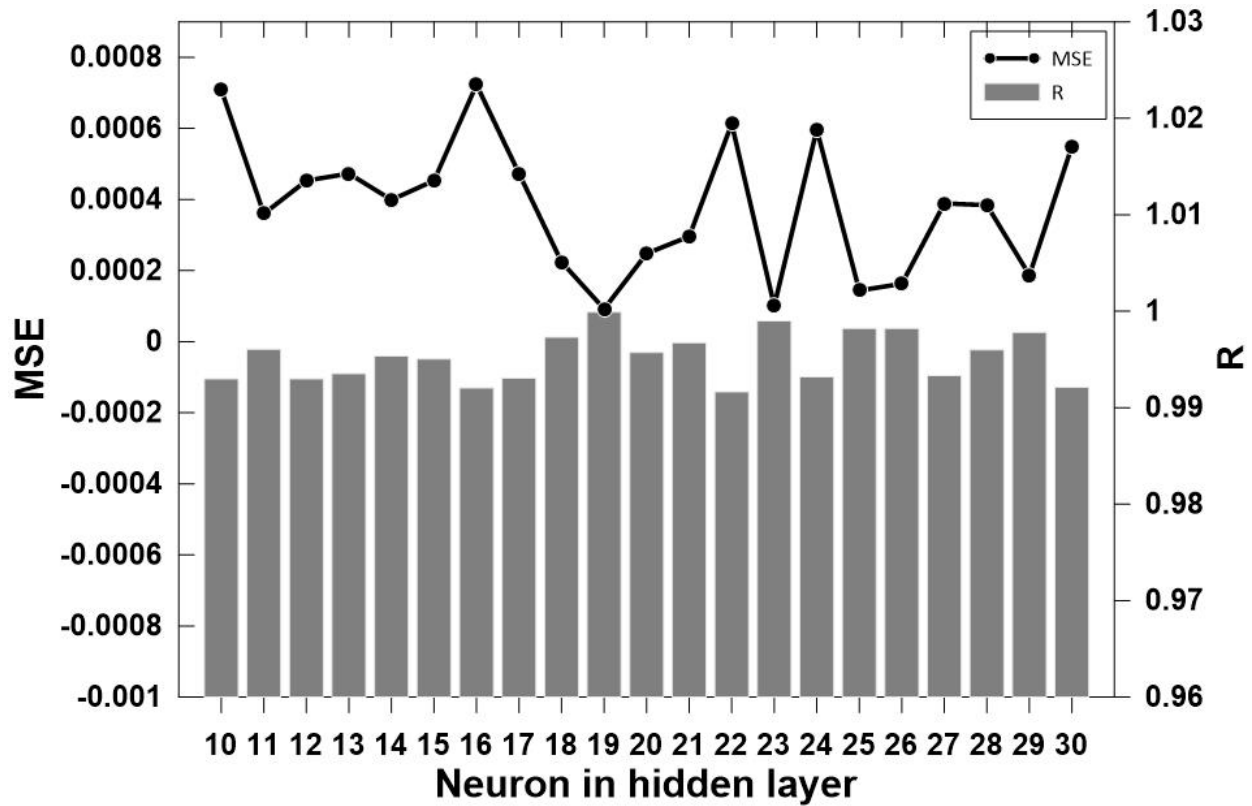
**Table 6.6** Optimum combination of selected operating parameters

<b>Respond of pareto font</b>	<b>%P</b>	<b>Sol</b>	<b>y(1)</b>	<b>y(2)</b>
<b>Objective of ITE y(1) and SoC y(2)</b>	51.729	20.609	30.036 %	-9.306°C
<b>Objective of ITE y(1) and CO y(2)</b>	54.73	13.273	28.983 %	96.646 ppm
<b>Objective of CO y(1) and NO<sub>x</sub> y(2)</b>	10.008	0.011	54.117 ppm	119 ppm

## 6.5 Evaluation of ANN results

The number of neurons in the hidden layer was changed to track changes in MSE without using a random ANN configuration (Figure 6.13). The MSE at 19 neurons in the hidden layer was lowest at 0.0000922 among neuron numbers of 10 to 30. As a result, the best model was an ANN with a 3-19-5 topological configuration that used the trainlm training algorithm and the feed-forward with back propagation learning algorithm with a logsig transfer function. The learning rate is concerned with the intensity of reducing the error after iterations, which has an impact on the portion of the individual adjustment to the previous weight. A rapid learning process is achieved when the learning rate is set to a high number. The network may not learn well when there is a significant amount of input set instability. Setting the learning rate to a high value is actually improper and detrimental to learning [139].





**Figure 6.13** Validation MSE and R values for different neuron numbers in the hidden layer.

The selected ANN model was trained to assess the accuracy of the cylinder pressure, rate of heat release, cumulative heat release, velocity of heat transfer, mass fraction burned and average gas temperature combustion parameters. For training, testing, and validation purposes, the engine's experimental data for CCM and the DFC mode of 1-hexanol with diesel/biodiesel are divided into three sets of 70%, 15%, and 15%, respectively [95]. Figure 6.11 makes it abundantly clear that the chosen ANN model was used to carry out reliable estimations for the previously mentioned combustion parameters. The highest R2 of 0.99981 for TKE and the lowest R2 of 0.96846 for power were obtained for training and testing conditions in the chosen ANN architecture, as shown in Figure 6.14. The extremely close data points surrounding the unity line in Figure 6.14 show that the ANN was successful and robust. In the current study, we suggest a model based on the excellent ANN prediction of the obtained combustion values. The ANN model's predicted values were 0.00038 of MSE. The ANN model produced reliable predictions through 204 iterations.

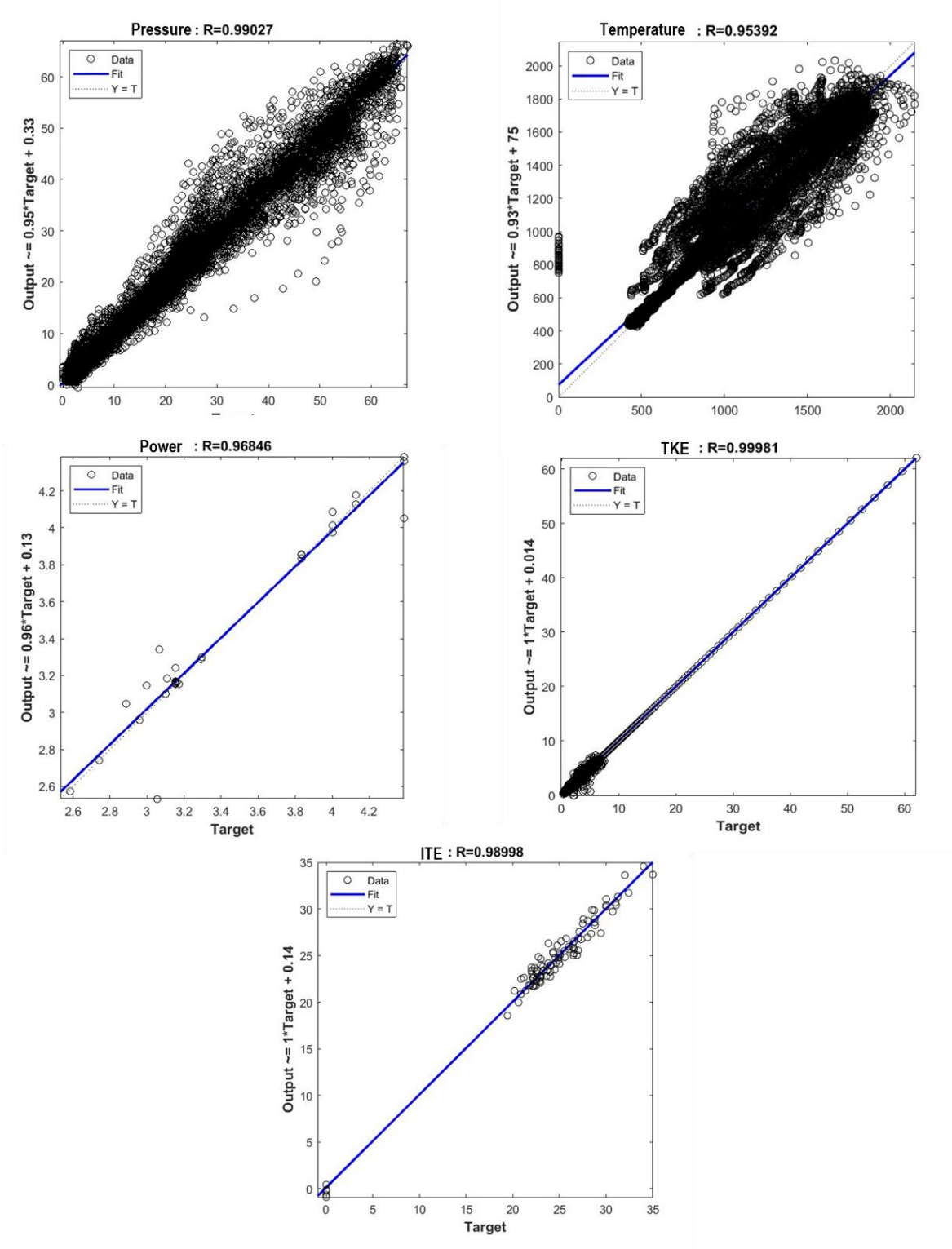


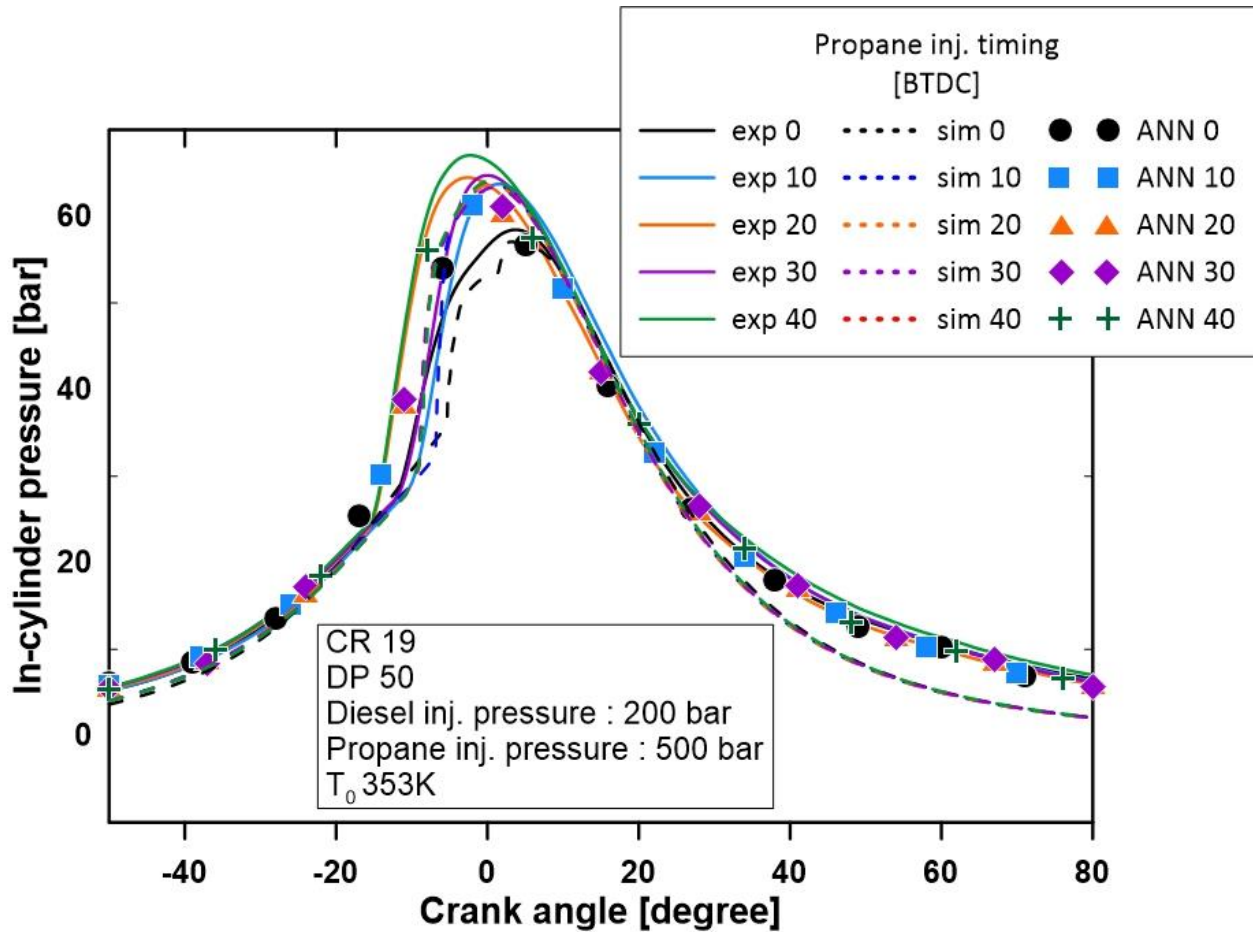
Figure 6.14 Plot of regression value of ANN performance for testing data prediction in 5 representative parameters.

## 6.6 Comparing experimental result and discussion in ANN modeling

Information from the experimental work is presented in this section, along with average gas temperature, mass fraction burned, rate of heat release, cumulative heat release, velocity of heat transfer, and cylinder pressure. The results for each parameter are displayed in two figures. The other compares experimental results with ANN values, while the first only contains experimental results. The experimental and ANN results are quite similar when all the figures were analyzed, and robust estimates were made to make predictions.

### 6.5.1 In-cylinder pressure

In-cylinder pressures of RCEMs employing dual direct injection fuel (diesel and propane) strategies at various propane SOIs are contrasted in Figure 6.15. The CFD modeling output of in-cylinder pressure reveals the under-prediction in the expansion area. This demonstrates that CFD modelling cannot provide an exact prediction of the uncertainty of the unburned fuel during ignition. The expansion phase's pressure and temperature were increased, and the combustion phase was prolonged. When compared to CFD modelling, the ANN modelling produced predictions that were more accurate. The prediction based on training and validating the data can increase the accuracy of the predicted data in addition to being produced faster and with fewer computer requirements. From 100 input data and 360000 total output sample data, the MSE was 0.942935.

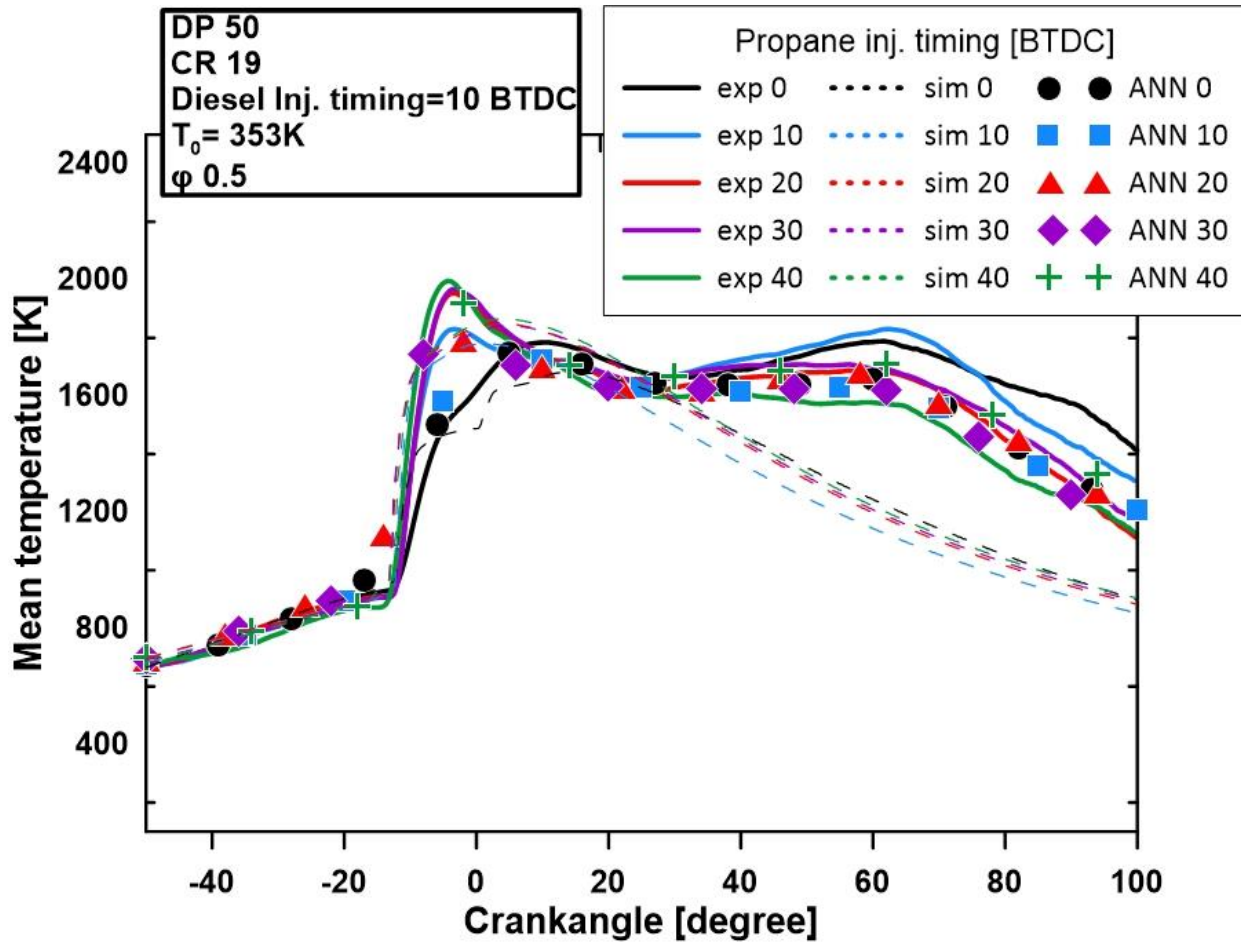


**Figure 6.15** Plot of in-cylinder temperature of experiment, simulation and ANN prediction.

### 6.5.2 In-cylinder temperature

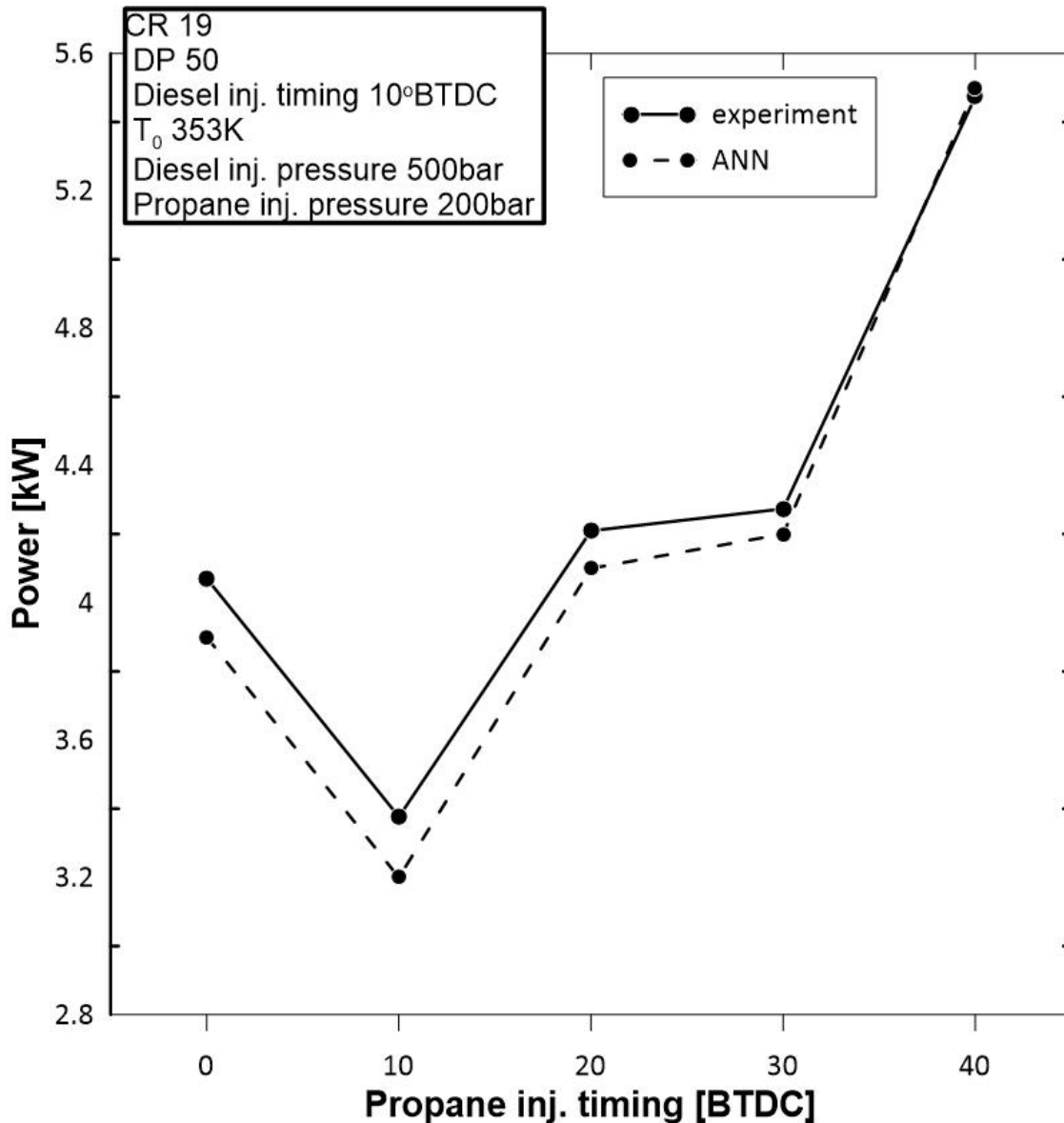
Figure 6.16 depicts the mean temperature of RCEMs running on dual direct injection fuel (diesel and propane) strategies at various propane SOIs. The under-prediction of data in the expansion state is more clearly observed in the mean temperature graph. When the fuel reaches the critical ignition point, the CFD modelling creates a chain reaction of combustion. The ignition process raises ambient temperature, which satisfies the requirement for fuel to reach temperatures higher than those required for auto ignition. In the experimental process, some propane spray came out as an iced phase due to the significant temperature drop when the propane was maintained as the liquid phase. This causes different ignition temperatures in the iced spray region, which requires a higher ignition temperature. This phenomenon is ignored by CFD modelling, which results in underprediction in the expansion area. Hence, the developed ANN models have great

potential to predict the real-time output values of the engine experiments. MSE was 0.837461 from 100 input data with 360000 total sample data.



**Figure 6.16** Plot of in-cylinder temperature of RCEM's experiment, simulation and ANN prediction data.

Figure 6.17 shows the predicted values of power inside the RCEM at CR19, DP50 and SOI of propane 0-40°BTDC on an ANN model, based on 100 data input and 100 total sample data. The overall forecast trend is positive, and the ANN model is quite precise in forecasting output power with MSE 0.024579.

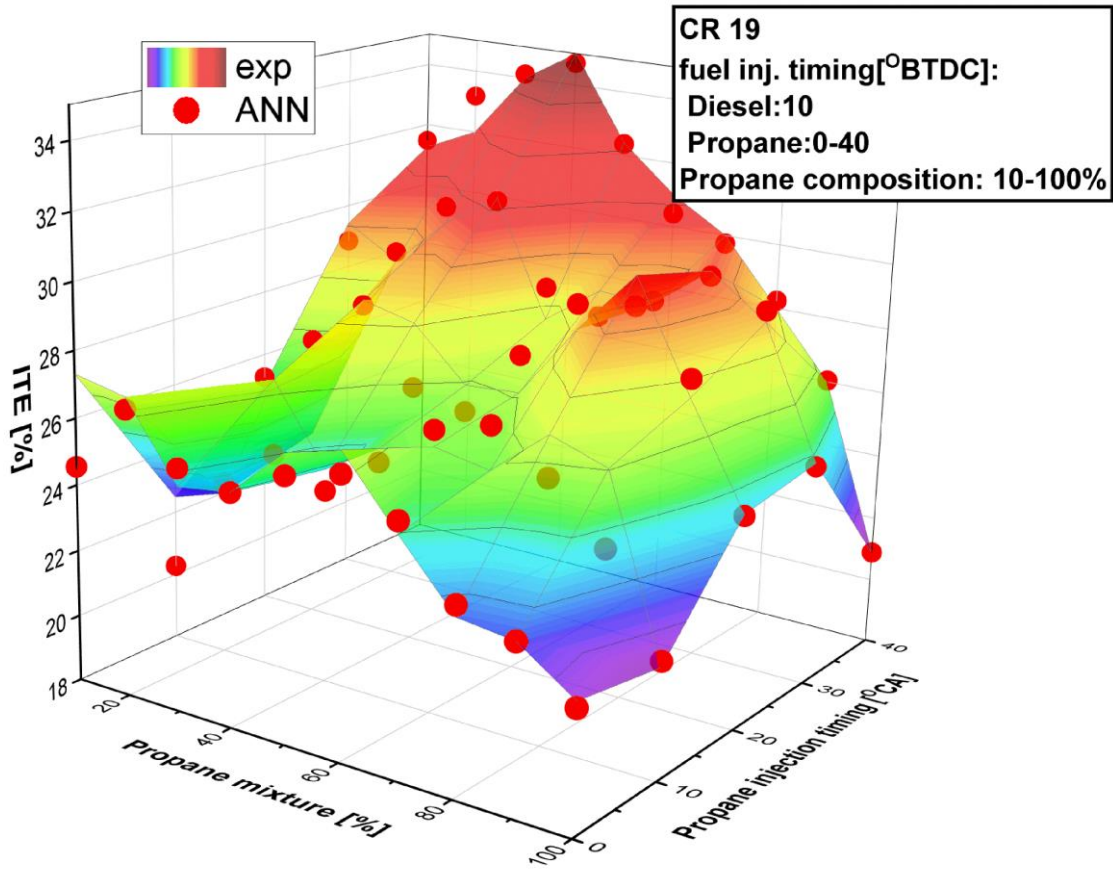


**Figure 6.17** Plot of power of RCEM experiments, simulation and ANN prediction data.

Figure 6.18 shows the thermal efficiency of the RCEM at CR19, DP10-100 at SOI of propane 0°-40° BTDC. For 19 neurons in the hidden layer, the MSE was equal to 0.022405 for 100 data inputs and 100 total sample data. Power predictions showed similar accuracy. The R and MSE for experimental data reached the optimum accuracy when the set of output sample data were at the minimum number. The pressure and the temperature have 100 set sample data in which each sample consists of 3600 data as the trace of temperature and pressure data were recorded from -180° BTDC CA to 180° ATDC. The trace data causes uncertainty when the cycle of compression, combustion and expansion occurs such as friction, graph distortion due to the electric disturbance



and the signal fluctuation of the sensor based on the electric current conversion. The data fluctuation from the pressure sensor is  $\pm 0.000002$  bar during idle data acquisition. Even if the value of the discrepancy is small, the accumulation of the different fluctuations causes low accuracy prediction in terms of MSE and R values.



**Figure 6.18** Plot of ITE of RCEM for experiment, simulation and ANN prediction data.

Figure 6.19 shows a comparison of the simulation and ANN prediction of TKE operated on RCEM on dual direct injection fuel strategy at CR19, PD50 and a SOI of propane at 0°-40° BTDC. The prediction of ANN shows a high accuracy compared to the TKE graph produced by the simulation, i.e., it showed an MSE of 0.003715 from 287900 sample data. Predictions on simulation data produced the highest accuracy compared to pressure and mean temperature prediction, which showed similarity in the number of output sample data. It even exceeds the prediction of power and ITE, which has the lowest output sample data. The minimum data set can



improve the accuracy of the prediction since it can minimize the prediction from the uncertainty of experimental data. However, the data produced by the simulation produced the minimum uncertainty in the fluctuation pressure data due to the voltage conversion from the pressure sensor. The pressure data acquired from simulation has zero fluctuation when operated in idle conditions. This indicated that the accuracy of the prediction will improve as the number of output sample data increases. A comparison of the values of the MSE and R of TKE indicate its higher accuracy for ITE and power.

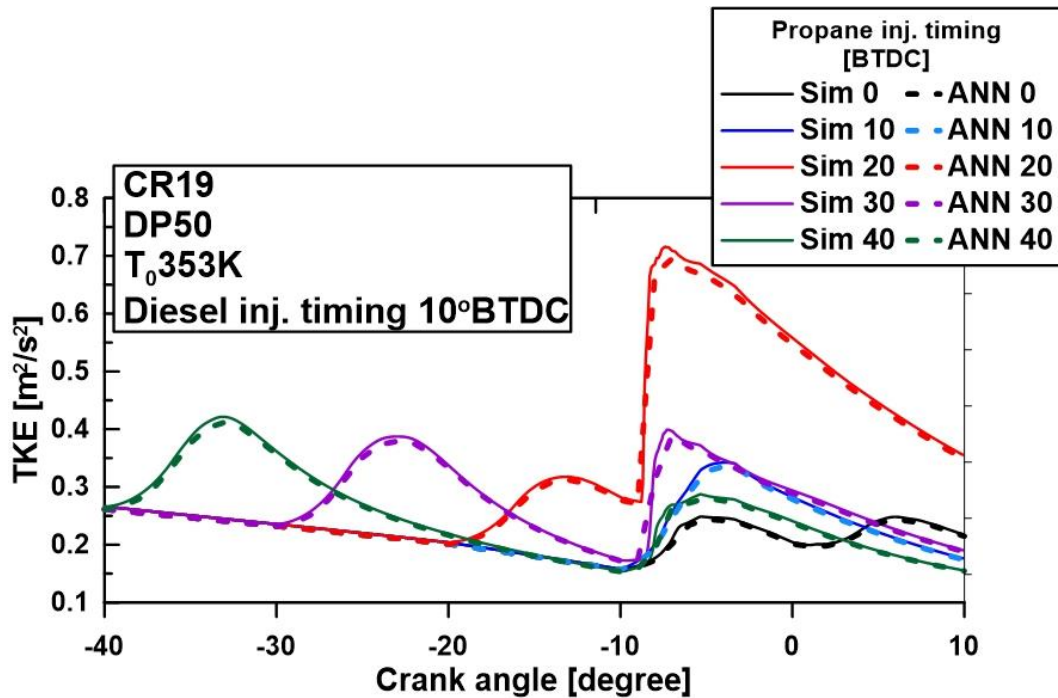


Figure 6.19 Plot of TKE of RCEM’s experiment, simulations, and ANN prediction data.

## 6.6 Conclusion.

Propane 10%–100% by energy fraction under a dual direct injection fuel strategy was examined using experimentally measured data of an engine combustion process for various engine operating conditions. The propane SOI ranged from 0 to 40 BTDC propane energy fraction 0–100%. To forecast the combustion process parameters, an engine combustion model was created using Converge software's ANN and CFD. Experimental and predicted results were compared to determine the prediction accuracy. The best ANN structure was established prior to training and validating the ANN with data from engine trials. We reached the following conclusions:

1. A polynomial equation models was established based on the regression analysis of the input variables and output variables. Based on the experimental data samples, it is feasible to construct the nonlinear relationship between operating parameters and response performance indicators.
2. The optimum combination of the operating parameters is decided by carrying out multi-objective optimization using a genetic algorithm tool. It is carried out by conventional method by considering individual performance and emissions. The optimum values of propane energy fraction and SoI of propane were found to be 54.26% and at 24°BTDC respectively.
3. Five parameters—pressure, temperature, power, TKE, and ITE—that were extracted from the engine performance map could be predicted by ANN with R values of 0.99027, 0.95392, 0.96846, 0.99981, and 0.98998 and MSE values of 0.942935, 0.837461, 0.024579, 0.022405, and 0.003715, respectively, which shows accurate forecasting of output data.
4. ANN generalization capability is relatively high even when operating in previously unexplored areas of engine performance if trained with sufficiently large databases. The dependability of the developed ANN methodology was demonstrated even when tested under real-world, dynamic performance conditions.

## 7. CONCLUSION AND CONTRIBUTION

This study focuses on the combination of experimental and simulation methods to investigate the effect of compression ratio, energy fraction, and Start of injection (SOI) of propane applied on dual direct injection engine on the compression ignition engine performance and emission characteristics on propane fuel combustion and optimize the data by using artificial neural network genetic algorithm to obtain the optimized parameters. Hereby, the conclusion of the current study;

Chapter 1

The benefit of the direct injection strategy and the usage of low-carbon fuel have been described in purpose to achieve higher efficiency and low emission on the combustion. Furthermore, the motivation behind the study is presented in relation to its background. Finally, a detailed description of the dual direct injection fuel strategy's goal of using low-carbon fuel to achieve improved combustion efficiency and reduced carbon emissions on compression ignition engines is provided.

Chapter 2

The application of LPG fuel to conventional engines with the concepts of efficiency and emission relations is reviewed in the literature review. As an alternative fuel in terms of material production and physical properties, LPG offers a bright future of application. Still, a number of studies demonstrate the challenges in optimizing LPG combustion to optimize fuel characteristics of low-carbon and high-energy fuel. Consequently, the present study proposes a combustion strategy to get around that challenge.

Chapter 3

The data experimental data acquisition was conducted on rapid compression expansion machine by modified its cylinder head in order to support the dual direct injection fuel strategy. The customized high pressure fuel pump was built to supply high pressure propane fuel to the combustion chamber. The fraction of propane from 10% to 100% compared to diesel with the constant low heating value input with the change of fraction. The SoI of propane was varied from 40oBTDC to identify the long ignition delay characteristics, and 0oBTDC to identify the ignition of diesel without propane intervention. The CFD modelling was used to analyze the turbulence phenomena caused by fuel injection and emission characteristics. Finally, the ANN genetic

algorithm modelling was used to optimize the parameter to achieve the optimum combustion and emission characteristics

#### Chapter 4

The combustion characteristics of the application of propane on a dual direct injection fuel strategy have been analyzed based on experimental and CFD modeling data. The improvement of the reactivity of propane was obtained at CR 19 as the auto-ignition of propane was identified before the ignition of diesel and finally, auto-ignition was produced at 100% propane. The highest ITE was observed for the lean propane mixtures at early SOI of propane. Early injection poses a higher ignition delay. Hence, it improves the air-fuel mixture and the quality of combustion. The highest ITE was produced at DP 40 and SOI of propane at 40°BTDC for both CR 17 and 19 with values of 26.4% and 35.2%. The highest peak of the TKE was produced at a 20°BTDC SoI of propane. The auto-ignition which occurs in the high TKE region will increase the TKE at the combustion region. Consequently, enhances the flame propagation and maintains the high ITE. Propane fraction can be increased to 80% with a steady increase in ITE of up to 5.71% by applying SoI of propane at 20° BTDC

#### Chapter 5

The emissions characteristics are detailed and analyzed by comparing the data with the combustion characteristics to fully understand the fluctuation of emission compared to the phenomenon during the combustion. The Incomplete combustion was shown by applying propane on the direct injection compression ignition engine at CR 19. SOI of propane at 20°BTDC has proven to produce the highest efficiency when applied on a higher fraction of propane. Applying propane up to 80%, reduces the HC 20.46 ppm. 20°BTDC SoI of propane shows the efficiency increase when applied to 80% of propane, and, it shows the CO<sub>2</sub> reduction 1.49%. At the ideal combustion, increasing propane up to 80% reduces the CO emission up to 41.331ppm with the lowest CO at 94.78. The ideal combustion of propane is proven able to reduce CO/CO<sub>2</sub> emission due to its lower carbon content.

#### Chapter 6

Finally, the optimization parameters of dual direct injection fuel strategy by applying an artificial neural network, and genetic algorithm method are analyzed in order to achieve the optimum combustion and emission characteristics. The simulation data shows the prediction of the expansion process when compared to the experimental data. Meanwhile, the ANN prediction

shows a better level of accuracy for the whole cycle trace. The data acquired from the sensor showed fluctuations in the data due to the electric conversion which increases the errors of the prediction. According to the prediction of the TKE, the ANN prediction of the in-cylinder trace phenomenon using the simulation output data samples had the highest accuracy. Based on the genetic algorithm results, the SoI of propane at 20.6°BTDC and 51.7% of propane is the ideal parameter to achieve optimum ANN generalization capability is relatively high even when operating in previously unexplored areas of engine performance if trained with sufficiently large databases.

The present work involves the following contributions:

- A literature study of the application of propane in the internal combustion engine as an alternative fuel.
- A study on combustion and emission of dual direct injection fuel engines fueled with propane-diesel blends using various propane injection timing strategies.
- Performance and emission of propane direct injection fuel on compression ignition engine fueled with 10-100% propane and diesel as the ignition assistance.
- Autoignition characteristics of propane applied on compression ignition engine using 17 and 19 compression ratio
- A study of optimum operating parameter optimization of propane on dual direct injection strategy applied on compression ignition engine

## REFERENCES

- [1] G. Ergen, "Comprehensive analysis of the effects of alternative fuels on diesel engine performance combustion and exhaust emissions: Role of biodiesel, diethyl ether, and EGR," *Therm. Sci. Eng. Prog.*, vol. 47, p. 102307, 2024, doi: <https://doi.org/10.1016/j.tsep.2023.102307>.
- [2] D. B. Lata, A. Misra, and S. Medhekar, "Investigations on the combustion parameters of a dual fuel diesel engine with hydrogen and LPG as secondary fuels," *Int. J. Hydrogen Energy*, vol. 36, no. 21, pp. 13808–13819, 2011.
- [3] M. Almazrouei and I. Janajreh, "Thermogravimetric study of the combustion characteristics of biodiesel and petroleum diesel," *J. Therm. Anal. Calorim.*, vol. 136, pp. 925–935, 2019.
- [4] R. Datla, R. K. Puli, C. Velayudhan Parvathy, and E. G. Varuvel, "Effect of start of main injection timing on performance, emission, and combustion characteristics of a VGT CI engine fueled with neem biodiesel," *Environ. Sci. Pollut. Res.*, vol. 28, pp. 11942–11953, 2021.
- [5] T. Y. Kim and S. H. Lee, "Combustion and emission characteristics of wood pyrolysis oil-butanol blended fuels in a DI diesel engine," *Int. J. Automot. Technol.*, vol. 16, pp. 903–912, 2015.
- [6] S. C. Anenberg *et al.*, "Impacts and mitigation of excess diesel-related NO<sub>x</sub> emissions in 11 major vehicle markets," *Nature*, vol. 545, no. 7655, pp. 467–471, 2017.
- [7] L. Zhang, Z. Huang, T. Wang, N. Zhao, H. Cheng, and W. Chen, "Lean combustion and emission performance of a gasoline direct injection engine with active pre-chamber," *Adv. Mech. Eng.*, vol. 14, no. 7, p. 16878132221113452, Jul. 2022, doi: 10.1177/16878132221113453.
- [8] J. B. Heywood, *Internal Combustion Engine Fundamentals*, 2nd Editio. New York: McGraw-Hill Education, 2018.
- [9] A. Parivar, A. Bouquet, J. Neumeister, N. Ajami, and H. Fajri, *Effects of Using CNG Direct Injection on Performance of a 3 Cylinder Naturally Aspirated Engine*. 2018.
- [10] H. L. Yip *et al.*, "A review of hydrogen direct injection for internal combustion engines: towards carbon-free combustion," *Appl. Sci.*, vol. 9, no. 22, p. 4842, 2019.
- [11] Z. Li *et al.*, "Dual fuel intelligent charge compression ignition (ICCI) combustion: Efficient and clean combustion technology for compression ignition engines," *Fuel*, vol. 279, p. 118565, 2020.
- [12] N. Sharma and A. K. Agarwal, "Particulate emission reduction by fuel injection timing optimization in a gasoline direct injection engine," *J. Energy Resour. Technol.*, vol. 144, no. 3, p. 32302, 2022.
- [13] Q. Peng, T. Rockstroh, and C. Hall, "The impact of fuel and injection strategy on combustion characteristics, emissions and efficiency in gasoline compression ignition operation," *Fuel*, vol. 318, p. 123548, 2022.
- [14] J. Dernotte, J. Dec, and C. Ji, "Efficiency improvement of boosted low-temperature gasoline combustion engines (LTGC) using a double direct-injection strategy," SAE Technical Paper, 2017.
- [15] V. Hariram and R. V. Shangar, "Influence of compression ratio on combustion and performance characteristics of direct injection compression ignition engine," *Alexandria Eng. J.*, vol. 54, no. 4, pp. 807–814, 2015.

- [16] B. Mohan, W. Yang, and S. Kiang Chou, "Fuel injection strategies for performance improvement and emissions reduction in compression ignition engines—A review," *Renew. Sustain. Energy Rev.*, vol. 28, pp. 664–676, 2013.
- [17] J. Lee, S. Chu, J. Kang, and K. Min, "Experimental Research on the Carbon Dioxides Reduction Potential by Substitution Gasoline with Ethanol and Propane Under Reactivity Controlled Compression Ignition in a Single Cylinder Engine," *Int. J. Automot. Technol.*, vol. 25, no. 2, pp. 321–330, 2024, doi: 10.1007/s12239-024-00026-6.
- [18] P. Price, S. Guo, and M. Hirschmann, "Performance of an evaporator for a LPG powered vehicle," *Appl. Therm. Eng.*, vol. 24, no. 8–9, pp. 1179–1194, 2004.
- [19] D. G. Snelgrove, P. Dupont, and R. Bonetto, "An investigation into the influence of LPG (autogas) composition on the exhaust emissions and fuel consumption of 3 bi-fuelled Renault vehicles," SAE Technical Paper, 1996.
- [20] I. Schifter, L. Díaz, E. López-Salinas, R. Rodríguez, S. Avalos, and V. Guerrero, "An evaluation of the LPG vehicles program in the metropolitan area of Mexico City," *J. Air Waste Manage. Assoc.*, vol. 50, no. 2, pp. 301–309, 2000.
- [21] K. Kim, J. Kim, S. Oh, C. Kim, and Y. Lee, "Lower particulate matter emissions with a stoichiometric LPG direct injection engine," *Fuel*, vol. 187, pp. 197–210, 2017, doi: <https://doi.org/10.1016/j.fuel.2016.09.058>.
- [22] S. Baek, K. Kim, J. Cho, C.-L. Myung, and S. Park, "Assessment of gaseous, particulate, and unregulated emissions from diesel compression ignition and LPG direct injection spark ignition minibus vehicles under the world harmonized vehicle cycle on a chassis dynamometer," *Fuel*, vol. 294, p. 120392, 2021, doi: <https://doi.org/10.1016/j.fuel.2021.120392>.
- [23] C. Windarto and O. Lim, "A comprehensive study of the effects of spark discharge duration on low-carbon combustion of high-pressure direct-injection propane: Factors affecting combustion, in-cylinder performance, and emissions," *Int. J. Hydrogen Energy*, vol. 49, pp. 796–815, 2024, doi: <https://doi.org/10.1016/j.ijhydene.2023.09.090>.
- [24] T. F. Stocker *et al.*, "Climate Change 2013: The physical science basis. contribution of working group I to the fifth assessment report of IPCC the intergovernmental panel on climate change," 2014.
- [25] R. B. T.-A. D. H. and C. (DHC) S. Wiltshire, Ed., "Woodhead Publishing Series in Energy," in *Woodhead Publishing Series in Energy*, Oxford: Woodhead Publishing, 2016, pp. xiii–xvii.
- [26] J. Cho, K. Kim, S. Baek, C.-L. Myung, and S. Park, "Abatement potential analysis on CO<sub>2</sub> and size-resolved particle emissions from a downsized LPG direct injection engine for passenger car," *Atmos. Pollut. Res.*, vol. 10, no. 6, pp. 1711–1722, 2019.
- [27] M. Lu, X. Wang, and Y. Cang, "Carbon Productivity: Findings from Industry Case Studies in Beijing," *Energies*, vol. 11, no. 10, 2018, doi: 10.3390/en11102796.
- [28] J. D. Ampah, A. A. Yusuf, S. Afrane, C. Jin, and H. Liu, "Reviewing two decades of cleaner alternative marine fuels: Towards IMO's decarbonization of the maritime transport sector," *J. Clean. Prod.*, vol. 320, p. 128871, 2021.
- [29] M. A. N. E. Solutions, "Cost and benefits of alternative fuels for an LR1 product tanker; 2015." .



- [30] M. A. N. E. Solutions, “MAN B&W ME-LGIP dual-fuel engines,” *man-es. com:[caŷm]*.—URL: <https://www.man-es.com/marine/products/planning-tools-and-downloads/technical-papers/2> (дата обращения: 22.03. 2021), 2018.
- [31] “Fuel price comparison | European Alternative Fuels Observatory.” [Online]. Available: <https://alternative-fuels-observatory.ec.europa.eu/consumer-portal/fuel-price-comparison>.
- [32] M. A. Burnett and M. S. Wooldridge, “An experimental investigation of flame and autoignition behavior of propane,” *Combust. Flame*, vol. 224, pp. 24–32, 2021.
- [33] C. Windarto, A. Setiawan, N. H. X. Duy, and O. Lim, “Investigation of propane direct injection performance in a rapid compression and expansion machine: Pathways to diesel marine engine efficiency parity with spark discharge duration strategies,” *Int. J. Hydrogen Energy*, vol. 48, no. 87, pp. 33960–33980, 2023, doi: <https://doi.org/10.1016/j.ijhydene.2023.05.131>.
- [34] M. Izadi Najafabadi and N. Abdul Aziz, “Homogeneous charge compression ignition combustion: challenges and proposed solutions,” *J. Combust.*, vol. 2013, 2013.
- [35] D. Splitter, V. Boronat, F. D. F. Chuahy, and J. Storey, “Performance of direct injected propane and gasoline in a high stroke-to-bore ratio SI engine: Pathways to diesel efficiency parity with ultra low soot,” *Int. J. Engine Res.*, vol. 22, no. 12, pp. 3475–3488, 2021.
- [36] C. Bae and J. Kim, “Alternative fuels for internal combustion engines,” *Proc. Combust. Inst.*, vol. 36, no. 3, pp. 3389–3413, Jan. 2017, doi: 10.1016/J.PROCI.2016.09.009.
- [37] R. D. Reitz *et al.*, “IJER editorial: The future of the internal combustion engine,” *International Journal of Engine Research*, vol. 21, no. 1. SAGE Publications Ltd, pp. 3–10, Jan. 2020, doi: 10.1177/1468087419877990.
- [38] A. T. Hoang, “Combustion behavior, performance and emission characteristics of diesel engine fuelled with biodiesel containing cerium oxide nanoparticles: A review,” *Fuel Process. Technol.*, vol. 218, p. 106840, Jul. 2021, doi: 10.1016/J.FUPROC.2021.106840.
- [39] R. Rajasegar and A. Srna, “Effect of Spray Collapse on Mixture Preparation and Combustion Characteristics of a Spark-Ignition Heavy-Duty Diesel Optical Engine Fueled with Direct-Injected Liquefied Petroleum Gas (LPG),” Apr. 2023, doi: 10.4271/2023-01-0323.
- [40] J. Shin and S. Park, “Numerical analysis for optimizing combustion strategy in an ammonia-diesel dual-fuel engine,” *Energy Convers. Manag.*, vol. 284, p. 116980, May 2023, doi: 10.1016/J.ENCONMAN.2023.116980.
- [41] X. Zhen and Y. Wang, “An overview of methanol as an internal combustion engine fuel,” *Renew. Sustain. Energy Rev.*, vol. 52, pp. 477–493, Dec. 2015, doi: 10.1016/J.RSER.2015.07.083.
- [42] D. Splitter, V. Boronat, F. D. F. Chuahy, and J. Storey, “Performance of direct injected propane and gasoline in a high stroke-to-bore ratio SI engine: Pathways to diesel efficiency parity with ultra low soot,” *Int. J. Engine Res.*, vol. 22, no. 12, pp. 3475–3488, Dec. 2021, doi: 10.1177/14680874211006981/ASSET/IMAGES/LARGE/10.1177\_14680874211006981-FIG2.JPEG.
- [43] K. J. Morganti, T. M. Foong, M. J. Brear, G. Da Silva, Y. Yang, and F. L. Dryer, “The Research and Motor octane numbers of Liquefied Petroleum Gas (LPG),” *Fuel*, vol. 108, pp. 797–811, Jun. 2013, doi: 10.1016/J.FUEL.2013.01.072.

- [44] D. F. Chuahy, D. Splitter, V. Boronat, and S. W. Wagnon, "Enabling high compression ratio in boosted spark ignition engines: Thermodynamic trajectory and fuel chemistry effects on knock," *Combust. Flame*, vol. 222, pp. 446–459, Dec. 2020, doi: 10.1016/J.COMBUSTFLAME.2020.09.010.
- [45] Y. Seo, J. Kim, E. Park, J. Lee, M. Cho, and S. Han, "Analysis of Energy Consumption of Novel Re-Liquefaction System Integrated with Fuel Supply System (FSS) for LPG-Fuelled LPG Carrier to Conventional Systems," *Energies*, vol. 15, no. 24, 2022, doi: 10.3390/en15249384.
- [46] T. Kar, T. Fosudo, A. Marchese, B. Windom, and D. Olsen, "Effect of fuel composition and EGR on spark-ignited engine combustion with LPG fueling: Experimental and numerical investigation," *Fuel*, vol. 327, no. July, p. 125221, 2022, doi: 10.1016/j.fuel.2022.125221.
- [47] L. Bilgili, "A systematic review on the acceptance of alternative marine fuels," *Renew. Sustain. Energy Rev.*, vol. 182, p. 113367, Aug. 2023, doi: 10.1016/J.RSER.2023.113367.
- [48] K. Kim, J. Kim, S. Oh, C. Kim, and Y. Lee, "Lower particulate matter emissions with a stoichiometric LPG direct injection engine," *Fuel*, vol. 187, pp. 197–210, Jan. 2017, doi: 10.1016/J.FUEL.2016.09.058.
- [49] A. K. Ramalingam, M. Kriek, S. Pischinger, and K. A. Heufer, "Understanding the Oxidation Behavior of Automotive Liquefied Petroleum Gas Fuels: Experimental and Kinetic Analyses," *Energy and Fuels*, vol. 34, no. 2, pp. 2323–2333, Feb. 2020, doi: 10.1021/ACS.ENERGYFUELS.9B03695/ASSET/IMAGES/LARGE/EF9B03695\_0010.JPEG.
- [50] D. A. DelVescovo, J. Li, D. A. Splitter, F. D. F. Chuahy, and P. Zhao, "Genetic algorithm optimization of a chemical kinetic mechanism for propane at engine relevant conditions," *Fuel*, vol. 338, p. 127371, Apr. 2023, doi: 10.1016/J.FUEL.2022.127371.
- [51] A. Vardhan, R. S. Rajput, A. C. Tiwari, and R. Randa, "Performance and Emission Analysis of Modified Compression Ignition Engine from Diesel Engine to Variable Load using Petrol and LPG Fuel," *Chem. Eng. Process. - Process Intensif.*, vol. 181, p. 109115, Nov. 2022, doi: 10.1016/J.CEP.2022.109115.
- [52] H. Kokabi, M. Najafi, S. A. Jazayeri, and O. Jahanian, "Hydrogen and propane implications for reactivity controlled compression ignition combustion engine running on landfill gas and diesel fuel," *Int. J. Hydrogen Energy*, vol. 46, no. 62, pp. 31903–31915, Sep. 2021, doi: 10.1016/J.IJHYDENE.2021.07.050.
- [53] E. Arslan and N. Kahraman, "Comparison of natural gas and propane addition to combustion air in terms of engine performance in compression ignition engine," *Fuel*, vol. 312, p. 122952, Mar. 2022, doi: 10.1016/J.FUEL.2021.122952.
- [54] S. Baek, K. Kim, J. Cho, C. L. Myung, and S. Park, "Assessment of gaseous, particulate, and unregulated emissions from diesel compression ignition and LPG direct injection spark ignition minibus vehicles under the world harmonized vehicle cycle on a chassis dynamometer," *Fuel*, vol. 294, p. 120392, Jun. 2021, doi: 10.1016/J.FUEL.2021.120392.
- [55] C. Windarto, A. Setiawan, N. H. X. Duy, and O. Lim, "Investigation of propane direct injection performance in a rapid compression and expansion machine: Pathways to diesel marine engine efficiency parity with spark discharge duration strategies," *Int. J. Hydrogen Energy*, Jun. 2023, doi: 10.1016/J.IJHYDENE.2023.05.131.

- [56] K. A. Hodges, A. Aniello, S. R. Krishnan, and K. K. Srinivasan, "Impact of propane energy fraction on diesel-ignited propane dual fuel low temperature combustion," *Fuel*, vol. 209, no. April, pp. 769–775, 2017, doi: 10.1016/j.fuel.2017.07.096.
- [57] E. Elnajjar, M. Y. E. Selim, and M. O. Hamdan, "Experimental study of dual fuel engine performance using variable LPG composition and engine parameters," *Energy Convers. Manag.*, vol. 76, pp. 32–42, Dec. 2013, doi: 10.1016/J.ENCONMAN.2013.06.050.
- [58] A. Chakraborty, S. Biswas, S. Meitei, A. Sengupta, D. Kakati, and R. Banerjee, "Examining the significance of the ignition characteristics of hydrogen and liquefied-petroleum-gas on the reactivity controlled compression ignition and its interspersed profiles induced in an existing diesel engine: A comparative perspective," *Energy Convers. Manag.*, vol. 268, p. 115976, Sep. 2022, doi: 10.1016/J.ENCONMAN.2022.115976.
- [59] M. Aydin, A. Irgin, and M. B. Çelik, "The impact of diesel/LPG dual fuel on performance and emissions in a single cylinder diesel generator," *Appl. Sci.*, vol. 8, no. 5, pp. 1–14, 2018, doi: 10.3390/app8050825.
- [60] R. Daniel, G. Tian, H. Xu, M. L. Wyszynski, X. Wu, and Z. Huang, "Effect of spark timing and load on a DISI engine fuelled with 2, 5-dimethylfuran," *Fuel*, vol. 90, no. 2, pp. 449–458, 2011.
- [61] M. C. Drake, T. D. Fansler, and A. M. Lippert, "Stratified-charge combustion: modeling and imaging of a spray-guided direct-injection spark-ignition engine," *Proc. Combust. Inst.*, vol. 30, no. 2, pp. 2683–2691, 2005.
- [62] P. Whitaker, P. Kapus, M. Ogris, and P. Hollerer, "Measures to reduce particulate emissions from gasoline DI engines," *SAE Int. J. Engines*, vol. 4, no. 1, pp. 1498–1512, 2011.
- [63] S. Zhang and W. McMahon, "Particulate emissions for LEV II light-duty gasoline direct injection vehicles," *SAE Int. J. Fuels Lubr.*, vol. 5, no. 2, pp. 637–646, 2012.
- [64] X. He, M. A. Ratcliff, and B. T. Zigler, "Effects of gasoline direct injection engine operating parameters on particle number emissions," *Energy & Fuels*, vol. 26, no. 4, pp. 2014–2027, 2012.
- [65] X. Q. Li, L. K. Yang, M. Pang, and X. J. Liang, "Effect of LPG injection methods on engine performance," *Adv. Mater. Res.*, vol. 97, pp. 2279–2282, 2010.
- [66] S. Oh, S. Lee, Y. Choi, K.-Y. Kang, J. Cho, and K. Cha, "Combustion and emission characteristics in a direct injection LPG/gasoline spark ignition engine," SAE Technical Paper, 2010.
- [67] I. G. Hwang, K. Choi, J. Kim, C. L. Myung, and S. Park, "Experimental evaluation of combustion phenomena in and nanoparticle emissions from a side-mounted direct-injection engine with gasoline and liquid-phase liquefied petroleum gas fuel," *Proc. Inst. Mech. Eng. Part D J. Automob. Eng.*, vol. 226, no. 1, pp. 112–122, 2012.
- [68] G. Talib Hashem, M. F. Al-Dawody, and I. E. Sarris, "The characteristics of gasoline engines with the use of LPG: An experimental and numerical study," *Int. J. Thermofluids*, vol. 18, p. 100316, 2023, doi: <https://doi.org/10.1016/j.ijft.2023.100316>.
- [69] K. Kim, J. Kim, S. Oh, C. Kim, and Y. Lee, "Evaluation of injection and ignition schemes for the ultra-lean combustion direct-injection LPG engine to control particulate emissions," *Appl. Energy*, vol. 194, pp. 123–135, 2017.

- [70] J. Li, C. Gong, Y. Su, H. Dou, and X. Liu, "Performance and hydrocarbon (HC) emissions from a spark-ignition liquefied petroleum gas (LPG) engine during cold start," *Energy & fuels*, vol. 23, no. 9, pp. 4337–4342, 2009.
- [71] S. Woo, J. Lee, and K. Lee, "Investigation of injection characteristics for optimization of liquefied petroleum gas applied to a direct-injection engine," *Energy Reports*, vol. 9, pp. 2130–2139, Dec. 2023, doi: 10.1016/j.egy.2023.01.022.
- [72] Y. Putrasari and O. LIM, "A study of a GCI engine fueled with gasoline-biodiesel blends under pilot and main injection strategies," *Fuel*, vol. 221, pp. 269–282, Jun. 2018, doi: 10.1016/J.FUEL.2018.01.063.
- [73] S. R. Krishnan, K. K. Srinivasan, and M. S. Raihan, "The effect of injection parameters and boost pressure on diesel-propane dual fuel low temperature combustion in a single-cylinder research engine," *Fuel*, vol. 184, pp. 490–502, Nov. 2016, doi: 10.1016/J.FUEL.2016.07.042.
- [74] M. Elkelawy *et al.*, "Influence of lean premixed ratio of PCCI-DI engine fueled by diesel/biodiesel blends on combustion, performance, and emission attributes; a comparison study," *Energy Convers. Manag.* X, vol. 10, p. 100066, Jun. 2021, doi: 10.1016/J.ECMX.2020.100066.
- [75] Z. Ahmad, O. Kaario, C. Qiang, and M. Larmi, "Effect of pilot fuel properties on lean dual-fuel combustion and emission characteristics in a heavy-duty engine," *Appl. Energy*, vol. 282, p. 116134, Jan. 2021, doi: 10.1016/J.APENERGY.2020.116134.
- [76] G. T. Kalghatgi, P. Risberg, and H. E. Ångström, "Advantages of Fuels with High Resistance to Auto-ignition in Late-injection, Low-temperature, Compression Ignition Combustion," *SAE Tech. Pap.*, Oct. 2006, doi: 10.4271/2006-01-3385.
- [77] J. Lee *et al.*, "A study of emissions reduction through dual-fuel combustion with propane in a compression ignition engine," *SAE Tech. Pap.*, vol. 11, 2013, doi: 10.4271/2013-01-2669.
- [78] R. Ianniello, G. Di Blasio, R. Marialto, C. Beatrice, and M. Cardone, "Assessment of direct injected liquefied petroleum gas-diesel blends for ultra-low soot combustion engine application," *Appl. Sci.*, vol. 10, no. 14, 2020, doi: 10.3390/app10144949.
- [79] A. C. Polk, C. D. Carpenter, K. K. Srinivasan, and S. R. Krishnan, "An investigation of diesel-ignited propane dual fuel combustion in a heavy-duty diesel engine," *Fuel*, vol. 132, pp. 135–148, 2014, doi: 10.1016/j.fuel.2014.04.069.
- [80] U. Oester and J. S. Wallace, "Liquid propane injection for diesel engines," *SAE Tech. Pap.*, 1987, doi: 10.4271/872095.
- [81] A. Boretti, "Advances in Diesel-LNG Internal Combustion Engines," *Appl. Sci.* 2020, Vol. 10, Page 1296, vol. 10, no. 4, p. 1296, Feb. 2020, doi: 10.3390/APP10041296.
- [82] L. P. Wyszynski, C. R. Stone, and G. T. Kalghatgi, "The volumetric efficiency of direct and port injection gasoline engines with different fuels," *SAE Tech. Pap.*, 2002, doi: 10.4271/2002-01-0839.
- [83] C. Park *et al.*, "Emission characteristics of gasoline and LPG in a spray-guided-type direct injection engine," SAE Technical Paper, 2013.
- [84] M. Walls, M. Joo, and M. Ross, "Impact of the Direct Injection of Liquid Propane on the Efficiency of a Light-Duty, Spark-Ignited Engine," SAE Technical Paper, 2017.

- [85] R. Ryskamp, "Emissions and Performance of Liquefied Petroleum Gas as a Transportation Fuel: A Review," *Cent. Altern. Fuels, Engines Emiss. West Virginia Univ.*, 2017.
- [86] Z. Yang *et al.*, "Effects of Spark Discharge Energy Scheduling on Flame Kernel Formation under Quiescent and Flow Conditions." SAE International , 2019, doi: 10.4271/2019-01-0727.
- [87] S. Tsuboi, S. Miyokawa, M. Matsuda, T. Yokomori, and N. Iida, "Influence of spark discharge characteristics on ignition and combustion process and the lean operation limit in a spark ignition engine," *Appl. Energy*, vol. 250, no. April, pp. 617–632, 2019, doi: 10.1016/j.apenergy.2019.05.036.
- [88] T. Badawy, X. C. Bao, and H. Xu, "Impact of spark plug gap on flame kernel propagation and engine performance," *Appl. Energy*, vol. 191, pp. 311–327, Apr. 2017, doi: 10.1016/J.APENERGY.2017.01.059.
- [89] Z. Yang *et al.*, "Impacts of Spark Discharge Current and Duration on Flame Development of Lean Mixtures Under Flow Conditions," *ASME 2018 Intern. Combust. Engine Div. Fall Tech. Conf. ICEF 2018*, vol. 1, Jan. 2019, doi: 10.1115/ICEF2018-9771.
- [90] S. V. Channapattana, A. A. Pawar, and P. G. Kamble, "Optimisation of operating parameters of DI- CI engine fueled with second generation Bio-fuel and development of ANN based prediction model," *Appl. Energy*, vol. 187, pp. 84–95, 2017, doi: 10.1016/j.apenergy.2016.11.030.
- [91] J. Liu, B. Ma, and H. Zhao, "Combustion parameters optimization of a diesel/natural gas dual fuel engine using genetic algorithm," *Fuel*, vol. 260, p. 116365, Jan. 2020, doi: 10.1016/J.FUEL.2019.116365.
- [92] Y. Li, M. Jia, X. Han, and X. S. Bai, "Towards a comprehensive optimization of engine efficiency and emissions by coupling artificial neural network (ANN) with genetic algorithm (GA)," *Energy*, vol. 225, p. 120331, Jun. 2021, doi: 10.1016/J.ENERGY.2021.120331.
- [93] C. Windarto and O. Lim, "A neural network approach on forecasting spark duration effect on in-cylinder performance of a large bore compression ignition engine fueled with propane direct injection," *Fuel Process. Technol.*, vol. 257, p. 108088, 2024, doi: <https://doi.org/10.1016/j.fuproc.2024.108088>.
- [94] M. S. P, G. V, P. P, G. A, and D. G, "Prediction efficiency of artificial neural network for CRDI engine output parameters," *Transp. Eng.*, vol. 3, p. 100041, Mar. 2021, doi: 10.1016/J.TRENG.2020.100041.
- [95] D. Babu, V. Thangarasu, and A. Ramanathan, "Artificial neural network approach on forecasting diesel engine characteristics fuelled with waste frying oil biodiesel," *Appl. Energy*, vol. 263, p. 114612, 2020.
- [96] J. Seo, B. Yun, J. Kim, M. Shin, and S. Park, "Development of a cold-start emission model for diesel vehicles using an artificial neural network trained with real-world driving data," *Sci. Total Environ.*, vol. 806, p. 151347, 2022, doi: 10.1016/j.scitotenv.2021.151347.
- [97] A. T. Le, D. Q. Tran, T. T. Tran, A. T. Hoang, and V. V. Pham, "Performance and combustion characteristics of a retrofitted CNG engine under various piston-top shapes and compression ratios," *Energy Sources, Part A Recover. Util. Environ. Eff.*, pp. 1–17, Aug. 2020, doi: 10.1080/15567036.2020.1804016.

- [98] S. Foroutani, G. Salehi, H. Fallahsohi, K. Lary, and A. M. Arasteh, "Artificial Neural Network Modeling and Numerical Simulation of Syngas Fuel and Injection Timing Effects on the Performance and Emissions of a Heavy-Duty Compression Ignition Engine," *ACS Omega*, vol. 6, no. 48, pp. 32379–32394, Dec. 2021, doi: 10.1021/ACSOMEGA.1C02829/ASSET/IMAGES/LARGE/AO1C02829\_0016.JPEG.
- [99] F. Jaliliantabar, B. Ghobadian, G. Najafi, and T. Yusaf, "Artificial neural network modeling and sensitivity analysis of performance and emissions in a compression ignition engine using biodiesel fuel," *Energies*, vol. 11, no. 9, 2018, doi: 10.3390/en11092410.
- [100] X. H. Fang, N. Papaioannou, F. Leach, and M. H. Davy, "On the application of artificial neural networks for the prediction of NOx emissions from a high-speed direct injection diesel engine," *Int. J. Engine Res.*, vol. 22, no. 6, pp. 1808–1824, Jun. 2021, doi: 10.1177/1468087420929768/ASSET/IMAGES/LARGE/10.1177\_1468087420929768-FIG20.JPEG.
- [101] A. S. El-Shafay, U. F. Alqsair, S. M. Abdel Razek, and M. S. Gad, "Artificial neural network prediction of performance and emissions of a diesel engine fueled with palm biodiesel," *Sci. Rep.*, vol. 12, no. 1, pp. 1–15, 2022, doi: 10.1038/s41598-022-13413-9.
- [102] X. Niu, C. Yang, H. Wang, and Y. Wang, "Investigation of ANN and SVM based on limited samples for performance and emissions prediction of a CRDI-assisted marine diesel engine," *Appl. Therm. Eng.*, vol. 111, pp. 1353–1364, Jan. 2017, doi: 10.1016/J.APPLTHERMALENG.2016.10.042.
- [103] H. Taghavifar and L. P. Perera, "Data-driven modeling of energy-exergy in marine engines by supervised ANNs based on fuel type and injection angle classification," *Process Saf. Environ. Prot.*, vol. 172, pp. 546–561, Apr. 2023, doi: 10.1016/J.PSEP.2023.02.034.
- [104] S. S. Goldsborough, S. Hochgreb, G. Vanhove, M. S. Wooldridge, H. J. Curran, and C.-J. Sung, "Advances in rapid compression machine studies of low-and intermediate-temperature autoignition phenomena," *Prog. Energy Combust. Sci.*, vol. 63, pp. 1–78, 2017.
- [105] C.-J. Sung and H. J. Curran, "Using rapid compression machines for chemical kinetics studies," *Prog. Energy Combust. Sci.*, vol. 44, pp. 1–18, 2014.
- [106] D. H. Qi, B. Chen, and D. Zhang, "Combustion and Exhaust Emissions Characteristics of a Dual-Fuel Compression Ignition Engine Operated with Diesel Fuel and Liquefied Petroleum Gas," *J. Energy Eng.*, vol. 142, p. 4016017, Apr. 2016, doi: 10.1061/(ASCE)EY.1943-7897.0000359.
- [107] J. P. Holman, *Experimental Methods for Engineers*, Eighth Edi., vol. s1-VIII, no. 193. New York: McGraw-Hill Education, 1853.
- [108] A. Gharehghani, A. Kakoe, A. M. Andwari, T. Megaritis, and A. Pesyridis, "Numerical investigation of an RCCI engine fueled with natural gas/dimethyl-ether in various injection strategies," *Energies*, vol. 14, no. 6, 2021, doi: 10.3390/en14061638.
- [109] Z. Han and R. D. Reitz, "Turbulence modeling of internal combustion engines using RNG  $k-\epsilon$  models," *Combust. Sci. Technol.*, vol. 106, no. 4–6, pp. 267–295, 1995.
- [110] B. S. de Lima, K. C. Fagundes, G. R. C. Faria, M. H. B. Sandoval, and C. E. C. Alvarez, "ENCIT2018-0458 ANALYSIS OF THE COMBUSTION PROCESS IN AN ENGINE ADAPTED WITH PRE-CHAMBER USING A ZERO DIMENSIONAL NUMERICAL MODEL AND A THREE-DIMENSIONAL MODEL."
- [111] R. D. Reitz, "Mechanism of breakup of round liquid jets," *Encycl. fluid Mech.*, vol. 10, 1986.



- [112] D. P. Schmidt and C. J. Rutland, "A new droplet collision algorithm," *J. Comput. Phys.*, vol. 164, no. 1, pp. 62–80, 2000.
- [113] A. A. Amsden, P. J. O'Rourke, and T. D. Butler, "KIVA-II: A computer program for chemically reactive flows with sprays," Los Alamos National Lab.(LANL), Los Alamos, NM (United States), 1989.
- [114] C. Windarto and O. Lim, "Spark discharge energy effect on in-cylinder characteristics performance of rapid compression and expansion machine with spark ignition direct injection strategy," *Fuel*, vol. 337, p. 127165, 2023.
- [115] S.-J. Jeong, W.-S. Kim, J.-K. Park, H.-K. Lee, and H.-H. Chun, *An Experimental Study on the Clutch-Type Water Pump of Diesel Passenger Vehicle for Reducing Fuel Consumption and CO<sub>2</sub> Emission*. 2011.
- [116] J. Luecke, M. J. Rahimi, B. T. Zigler, and R. W. Grout, "Experimental and numerical investigation of the Advanced Fuel Ignition Delay Analyzer (AFIDA) constant-volume combustion chamber as a research platform for fuel chemical kinetic mechanism validation," *Fuel*, vol. 265, p. 116929, 2020, doi: <https://doi.org/10.1016/j.fuel.2019.116929>.
- [117] K. S. Varde, "Ignition delay and emissions characteristics of a methanol-diesel fueled engine at low charge temperatures," SAE Technical Paper, 1992.
- [118] S. H. Park, H. J. Kim, and C. S. Lee, "Comparison of experimental and predicted atomization characteristics of high-pressure diesel spray under various fuel and ambient temperature," *J. Mech. Sci. Technol.*, vol. 24, pp. 1491–1499, 2010.
- [119] S. Chu, J. Lee, J. Kang, Y. Lee, and K. Min, "High load expansion with low emissions and the pressure rise rate by dual-fuel combustion," *Appl. Therm. Eng.*, vol. 144, pp. 437–443, 2018, doi: <https://doi.org/10.1016/j.applthermaleng.2018.08.027>.
- [120] M. R. Aosaf, Y. Wang, and K. Du, "Comparison of the emission factors of air pollutants from gasoline, CNG, LPG and diesel fueled vehicles at idle speed," *Environ. Pollut.*, vol. 305, p. 119296, 2022, doi: <https://doi.org/10.1016/j.envpol.2022.119296>.
- [121] A. S. Huzayyin, H. A. Moneib, M. S. Shehatta, and A. M. A. Attia, "Laminar burning velocity and explosion index of LPG–air and propane–air mixtures," *Fuel*, vol. 87, no. 1, pp. 39–57, 2008, doi: <https://doi.org/10.1016/j.fuel.2007.04.001>.
- [122] Y. Zhang, H. Zhao, M. Ojapah, and A. B. T.-I. C. E. I. P. Cairns Fuel Economy and Emission, "Analysis of CAI/HCCI combustion in a 2-stroke poppet valve engine," Woodhead Publishing, 2011, pp. 127–134.
- [123] Z. Zhang *et al.*, "Effect of wall surface temperature on ignition and combustion characteristics of diesel fuel spray impingement," *Appl. Therm. Eng.*, vol. 137, pp. 47–53, 2018.
- [124] S. Wadekar, A. Yamaguchi, and M. Oevermann, "Large-Eddy Simulation Study of Ultra-High Fuel Injection Pressure on Gasoline Sprays," *Flow, Turbul. Combust.*, vol. 107, no. 1, pp. 149–174, 2021, doi: [10.1007/s10494-020-00231-0](https://doi.org/10.1007/s10494-020-00231-0).
- [125] P. K. Kundu, I. M. Cohen, and D. R. Dowling, "Chapter 13 - Geophysical Fluid Dynamics," P. K. Kundu, I. M. Cohen, and D. R. B. T.-F. M. (Sixth E. Dowling, Eds. Boston: Academic Press, 2016, pp. 699–771.



- [126] A. MOHAMMADI and F. Ommi, "Numerical and experimental study of twin-fluid two-phase internal-mixing atomizer to develop maximum entropy method," *Chinese J. Aeronaut.*, vol. 33, pp. 2281–2294, Sep. 2020, doi: 10.1016/j.cja.2020.03.001.
- [127] K. Jwa, A. Setiawan, and O. Lim, "Effect of Pilot Injection with Various Starts of Second Injection Command (SOIC2) and Fuel Injection Pressures on Gasoline Compression Ignition Combustion," *Int. J. Energy Res.*, vol. 2023, p. 2402918, 2023, doi: 10.1155/2023/2402918.
- [128] A. Makino and C. K. Law, "Quasi-steady and transient combustion of a carbon particle: Theory and experimental comparisons," in *Symposium (International) on Combustion*, 1988, vol. 21, no. 1, pp. 183–191.
- [129] J. Woo Jeong, S. Baek, Y. Kim, S. Woo, Y. Lim, and K. Lee, "Investigation of CO<sub>2</sub> and PN emission characteristics according to the propane content for a LPG engine," *Fuel*, vol. 357, p. 129877, 2024, doi: <https://doi.org/10.1016/j.fuel.2023.129877>.
- [130] S. Tavakoli, M. V. Jensen, E. Pedersen, and J. Schramm, "Unburned hydrocarbon formation in a natural gas engine under sea wave load conditions," *J. Mar. Sci. Technol.*, vol. 26, pp. 128–140, 2021.
- [131] H. E. Saleh, "Effect of variation in LPG composition on emissions and performance in a dual fuel diesel engine," *Fuel*, vol. 87, no. 13–14, pp. 3031–3039, 2008.
- [132] S. Ramalingam and S. Rajendran, "14 - Assessment of performance, combustion, and emission behavior of novel annona biodiesel-operated diesel engine," in *Woodhead Publishing Series in Energy*, K. B. T.-A. in E.-F. for a S. E. Azad, Ed. Woodhead Publishing, 2019, pp. 391–405.
- [133] Y. Ikeda, T. Nakajima, and E. Sher, "Chapter 13 - Air Pollution from Small Two-Stroke Engines and Technologies to Control It," E. B. T.-H. of A. P. F. I. C. E. Sher, Ed. San Diego: Academic Press, 1998, pp. 441–476.
- [134] J. E *et al.*, "Soot formation mechanism of modern automobile engines and methods of reducing soot emissions: A review," *Fuel Process. Technol.*, vol. 235, p. 107373, 2022, doi: <https://doi.org/10.1016/j.fuproc.2022.107373>.
- [135] J. Song, C. Song, Y. Tao, G. Lv, and S. Dong, "Diesel soot oxidation during the late combustion phase," *Combust. Flame*, vol. 158, no. 3, pp. 446–451, 2011, doi: <https://doi.org/10.1016/j.combustflame.2010.09.017>.
- [136] H. K. Aasi and M. Mishra, "Experimental investigation and ANN modelling on thermo-hydraulic efficacy of cross-flow three-fluid plate-fin heat exchanger," *Int. J. Therm. Sci.*, vol. 164, p. 106870, 2021.
- [137] M. Aydın, S. Uslu, and M. B. Çelik, "Performance and emission prediction of a compression ignition engine fueled with biodiesel-diesel blends: A combined application of ANN and RSM based optimization," *Fuel*, vol. 269, p. 117472, 2020.
- [138] S. Bhowmik, R. Panua, D. Debroy, and A. Paul, "Artificial neural network prediction of diesel engine performance and emission fueled with diesel–kerosene–ethanol blends: a fuzzy-based optimization," *J. energy Resour. Technol.*, vol. 139, no. 4, p. 42201, 2017.
- [139] H. Taghavifar, H. Taghavifar, A. Mardani, A. Mohebbi, and S. Khalilarya, "A numerical investigation on the wall heat flux in a DI diesel engine fueled with n-heptane using a coupled

CFD and ANN approach," *Fuel*, vol. 140, pp. 227–236, 2015, doi:  
<https://doi.org/10.1016/j.fuel.2014.09.092>.